USGS
science for a changing world

Prepared in cooperation with the Missouri Geological Survey

Petrology and Geochronology of 1.48 to 1.45 Ga Igneous Rocks in the St. Francois Mountains Terrane, Southeast Missouri

Professional Paper 1866

U.S. Department of the Interior
U.S. Geological Survey

Cover. Prominent exposures of the 1.47 Ga Granite of Castor River Shut-Ins at the Castor River Shut-Ins, Missouri (photograph by John N. Aleinikoff, U.S. Geological Survey, March 2017).

Petrology and Geochronology of 1.48 to 1.45 Ga Igneous Rocks in the St. Francois Mountains Terrane, Southeast Missouri

By Edward A. du Bray, John N. Aleinikoff, Warren C. Day, Leonid A. Neymark, and Seth D. Burgess

Prepared in cooperation with the Missouri Geological Survey

Professional Paper 1866

U.S. Department of the Interior
U.S. Geological Survey

U.S. Geological Survey, Reston, Virginia: 2021

Suggested citation:
du Bray, E.A., Aleinikoff, J.N., Day, W.C., Neymark, L.A., Burgess, S.D., 2021, Petrology and geochronology of 1.48 to 1.45 Ga igneous rocks in the St. Francois Mountains terrane, southeast Missouri: U.S. Geological Survey Professional Paper 1866, 88 p., https://doi.org/10.3133/pp1866.

Associated data for this publication:
Aleinikoff, J.N., 2021, SHRIMP U-Pb geochronologic data for zircon and titanite from Mesoproterozoic rocks of the St. Francois Mountains terrane, southeast Missouri, U.S.A.: U.S. Geological Survey data release, https://doi.org/10.5066/P95Q3QC4.
Granitto, M., du Bray, E.A., Day, W.C., Meighan, C.J., Slack, J.F., and Ayuso, R.A., 2018, Geochemical and modal data for Mesoproterozoic igneous rocks of the St. Francois Mountains, southeast Missouri: U.S. Geological Survey data release, https://doi.org/10.5066/F79W0DSN.

ISSN 2330-7102 (online)

Acknowledgments

This study was undertaken as part of the Iron oxide-copper-cobalt-gold-rare earth element deposits of southeast Missouri project funded by the U.S. Geological Survey Mineral Resources Program. Thanks are due to C.M. Seeger, M.A. Starkey, and Lisa Lori at the Missouri Geological Survey, Rolla, Mo for their collaborative insights and making their knowledge and facilities available to this investigation. Thanks to R.M. Pillers for help with mineral separations, scanning electron microscope work, and sensitive high resolution ion microprobe analysis. Thanks also to J.D. Horton who determined areal extents of individual igneous rock types. Constructive reviews by K.E. Watts and A.K. Gilmer are much appreciated and helped clarify data presentation and interpretation.

Contents

Figures

Tables

Conversion Factors

International System of Units to U.S. customary units

Multiply	By	To obtain
	Length	
millimeter (mm)	0.03937	inch (in.)
meter (m)	3.281	foot (ft)
kilometer (km)	0.6214	mile (mi)

U.S. customary units to International System of Units

Multiply	By	To obtain
	Mass	
ounce, avoirdupois (oz)	28.35	gram (g)

Temperature in degrees Celsius (°C) may be converted to degrees Fahrenheit (°F) as follows:

$°F = (1.8 \times °C) + 32.$

Ages are expressed in Ga, for giga-annum (billion years), Ma for mega-annum (million years), and time intervals are in m.y. for million years.

Abbreviations and Acronyms

HFSE	High-field-strength element
HREE	Heavy rare earth element
LREE	Light rare earth element
LILE	Large-ion lithophile element
REE	Rare earth element
USGS	U.S. Geological Survey
MSWD	mean square of weighted deviates
NIST	National Institute of Standards and Technology
ppm	parts per million

Chemical Compounds

Al_2O_3	Aluminum oxide
CaO	Calcium oxide
FeO*	Total iron expressed as ferrous oxide
K_2O	Potassium oxide
MgO	Magnesium oxide
MnO	Manganese oxide
Na_2O	Sodium oxide

N_2	Nitrogen
P_2O_5	Phosphorus pentoxide
SiO_2	Silicon dioxide
TiO_2	Titanium dioxide
UO	Uranium oxide
UO_2	Uranium dioxide

Elements

Ag	Silver
Ar	Argon
As	Arsenic
Au	Gold
Ba	Barium
Ca	Calcium
Ce	Cerium
Co	Cobalt
Cr	Chromium
Cs	Cesium
Cu	Copper
Eu	Europium
Fe	Iron
He	Helium
Hg	Mercury
La	Lanthanum
Nb	Niobium
Nd	Neodymium
Ni	Nickel
O	Oxygen
Pb	Lead
Rb	Rubidium
Sc	Scandium
Sn	Tin
Sr	Strontium
Ta	Tantalum
Th	Thorium
U	Uranium
V	Vanadium
Y	Yttrium
Zr	Zirconium

Petrology and Geochronology of 1.48 to 1.45 Ga Igneous Rocks in the St. Francois Mountains Terrane, Southeast Missouri

By Edward A. du Bray, John N. Aleinikoff, Warren C. Day, Leonid A. Neymark, and Seth D. Burgess

Abstract

The igneous geology of the St. Francois Mountains terrane in southeast Missouri is dominated by the products of 1.48 to 1.45 billion year old volcanic and plutonic magmatism but also includes volumetrically minor, compositionally bimodal contributions added during plutonism between 1.34 and 1.27 billion years ago. The 1.48 to 1.45 billion year old igneous rocks in the St. Francois Mountains terrane are bimodally distributed between volumetrically dominant felsic rocks and volumetrically minor rocks with mafic to intermediate compositions. All of these rocks are ferroan, which like most of their trace element abundances, suggests a genesis associated with farfield intraplate extensional tectonism and decompression-related magmatism. The diversity of compositions among 1.48 to 1.45 billion year old igneous rocks in the St. Francois Mountains terrane probably reflects mixtures of mantle-derived mafic inputs and low-degree partial melting of more evolved crustal protoliths. Newly determined ages define essentially continuous magmatism during the 30-million-year period between 1.48 and 1.45 billion years ago. The products of this magmatism are essentially coeval, whether intrusive or extrusive or having mafic, intermediate, or felsic compositions. In addition, the iron oxide-apatite (for example, Pea Ridge) and likely the iron oxide-copper gold (Boss) deposits in the St. Francois Mountains terrane have ages coincident with this magmatic episode. Spatial and temporal relations between 1.48 to 1.45 billion year old igneous rocks in the St. Francois Mountains terrane and the mineral deposits they host suggest the associated magmatic and mineralization processes are also genetically related.

Geochemical, petrographic, geochronologic, and terrane-wide physical characteristics of the 1.48 to 1.45 billion year old igneous rocks in the St. Francois Mountains terrane are consistent with an origin involving extension well inboard from the margin of the Laurentian craton, associated mantle upwelling, lower crustal melting in response to mantle-derived thermal inputs, and mixing of mantle- and juvenile lower crustal-derived melts. Significant major and trace element compositional dispersion characteristics of these rocks likely reflect midcrustal magma reservoir fractionation of their principal rock-forming minerals. The resultant magmas constitute a series of variably hybridized reservoirs, emplaced at upper levels in the crust, that form a series of plutonic and associated eruptive products.

Introduction

Mesoproterozoic igneous rocks (fig. 1) constitute the basement beneath a relatively thick (greater than 400 meters [m]) Paleozoic sedimentary rock sequence in the southern midcontinent region of the United States in the St. Francois Mountains terrane of southeast Missouri (Kisvarsanyi, 1981; Tolman and Robertson, 1969). The 1.48 to 1.45 giga-annum (Ga) rocks of southeast Missouri are unique in hosting coeval and cospatial iron oxide-apatite ± rare earth element (IOA) and iron oxide-copper ± gold ± cobalt (IOCG) mineral deposits. These igneous rocks represent a significant component of a broadly early Mesoproterozoic igneous terrane, intruded by a middle Mesoproterozoic bimodal sequence of granite and gabbro at about 1.3 Ga in southeast Missouri, that crops out extensively in North America (Anderson and Bender 1989; Bickford and others, 2015; du Bray and others, 2018a). The petrogenesis and tectonic regime that prevailed during Mesoproterozoic magmatism in the United States remain elusive.

Our study focuses on the characteristics of early Mesoproterozoic igneous rocks in the St. Francois Mountains terrane in order to establish their petrogenesis and potential role in formation of associated IOA and IOCG deposits of the Missouri metallogenic province (Kisvarsanyi and Proctor, 1967). Recent investigations by Bickford and others (2015), du Bray and others (2018a), and Frost and Frost (2008, 2011) define the conditions favorable for ferroan granitoid, broadly within-plate magmatism that extends across the North American craton and Ayuso and others (2016) and Day and others (2016) review the factors that fostered approximately 1.4 Ga magmatism specifically in the St. Francois Mountains terrane. However, the tectonic setting that prevailed during Mesoproterozoic magmatism in the St. Francois Mountains terrane is uncertain and relations between

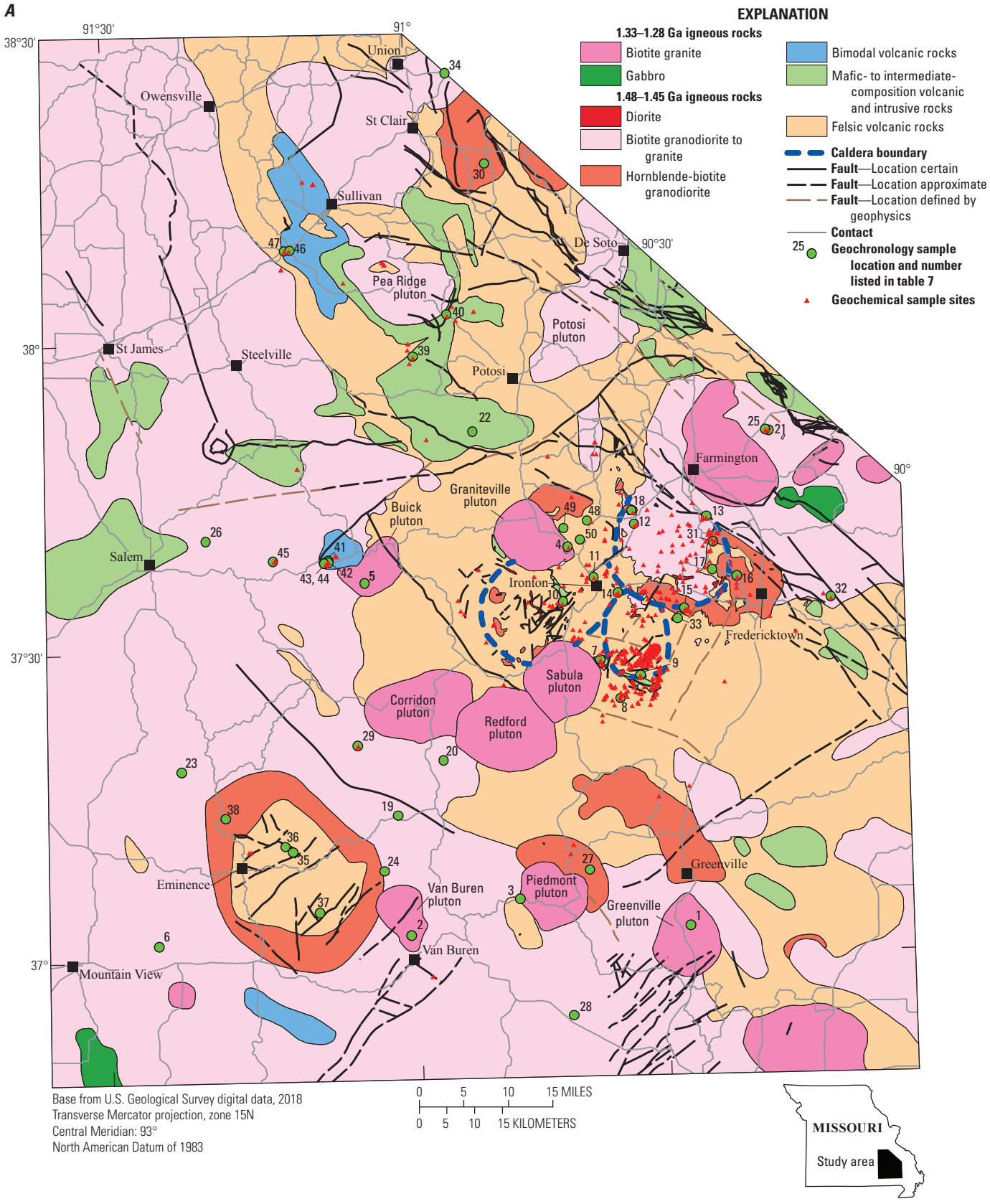

Figure 1. Map showing the spatial distribution of Mesoproterozoic igneous rocks in the St. Francois Mountains terrane, southeast Missouri. *A*, Geochemical and geochronologic sample sites. *B*, Locations and names of mines and prospects. [Ga, giga-annum (billion year old)]

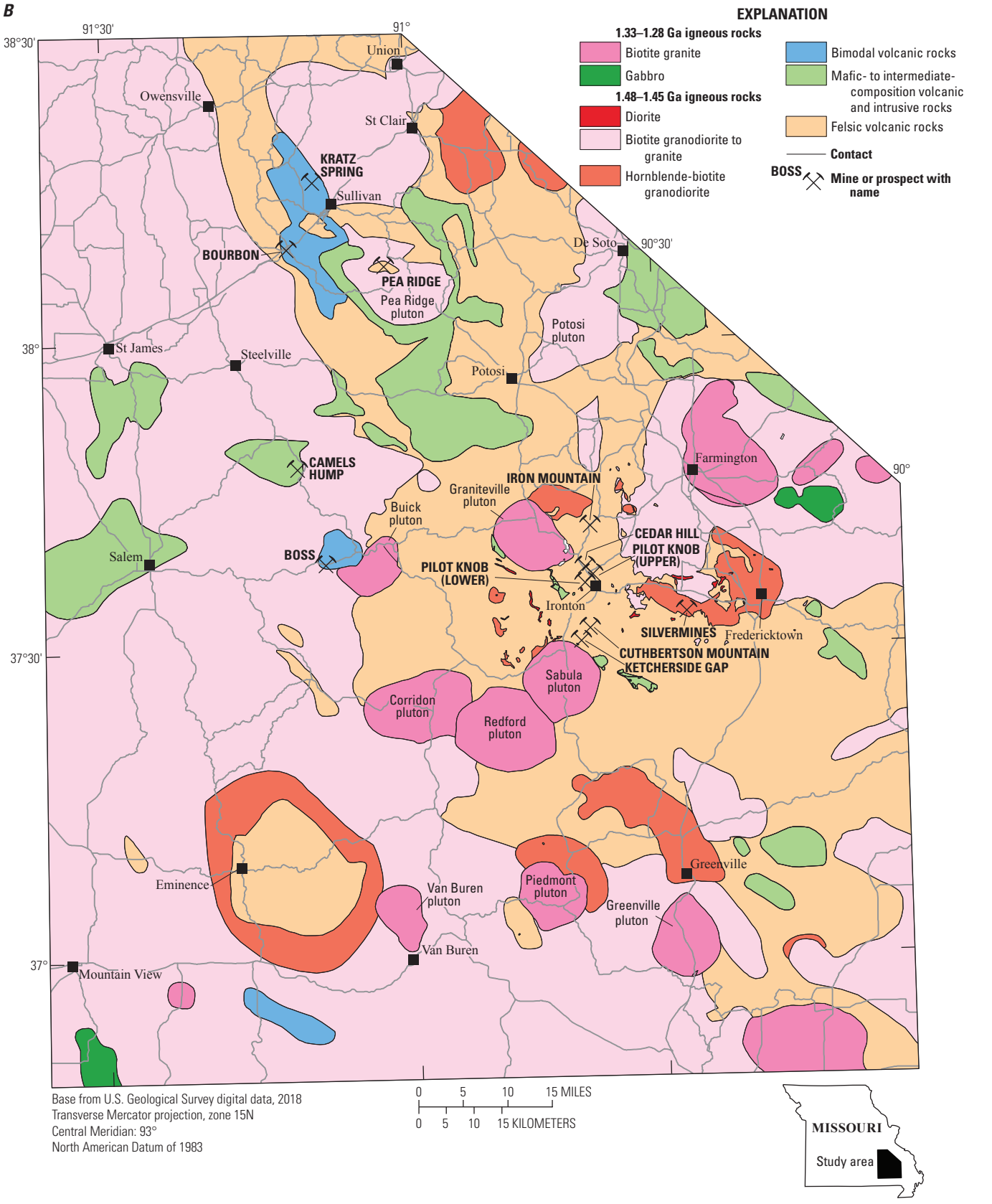

Figure 1. Map showing the spatial distribution of Mesoproterozoic igneous rocks in the St. Francois Mountains terrane, southeast Missouri. *A*, Geochemical and geochronologic sample sites. *B*, Locations and names of mines and prospects. [Ga, giga-annum (billion year old)] —Continued

the resulting igneous rocks and analogous but more widely distributed 1.4 Ga Mesoproterozoic igneous rocks across the United States are not well established.

Many relatively specific studies of Mesoproterozoic igneous rocks in the St. Francois Mountains terrane contributed to presently available knowledge about the character and petrogenesis of these rocks (Bickford and others, 1981; Cullers and others, 1981; Day and others, 2016; Lowell, 1991; Menuge and others, 2002; Sides and others, 1981; Walker and others, 2002). Ultimately, these studies constrain the geologic framework prevailing during magma genesis. Pioneering work by Anderson (1962) established the presence of widely distributed, voluminous rhyolitic ash-flow tuffs, and identified and defined the areal extent of calderas from which the associated volcanic rocks erupted. Similar studies by Berry (1970) and Brown (1988) added considerable detail concerning the character and distribution of igneous, principally volcanic rocks, exposed in the St. Francois Mountains terrane. The conceptual synthesis by Kisvarsanyi (1981) and systematic compilation efforts (Day and others, 2016; Pratt and others, 1979; Sides and others, 1981) considerably refined the distribution and character of these rocks; these investigations are critical to defining the geologic architecture prevailing during magmatism. The recently completed (2016), exhaustive study of the Pea Ridge IOA deposit, in particular, and igneous rocks and mineral deposits in the St. Francois Mountains terrane, in general, produced a significant volume of modern, high-quality whole-rock geochemical, radiogenic isotope tracer, and geochronologic data (Slack and others, 2016, and references therein). Similarly, Bickford and others (2015) have produced important new hafnium-in-zircon isotope data applicable to the study of these rocks. With completion of the compilation of whole-rock geochemical data for broadly 1.4 Ga igneous rocks in the conterminous United States (du Bray and others, 2015), including those in the St. Francois Mountains terrane, additional data compilation, and acquisition of data for newly collected samples (du Bray and others, 2018b; Granitto and others, 2018), the data necessary to better define the petrogenetic and tectonic processes responsible for 1.48 to 1.45 Ga magmatism in the St. Francois Mountains terrane are now available.

Rock unit names used throughout this report correspond to formal and informal stratigraphic nomenclature developed by Anderson (1962), Berry (1970), Brown (1988), Pippin (1996), Sides (1981), and Sylvester (1984). Mafic extrusive and hypabyssal intrusive units include the Lake Four Winds basalt, basalt in the Cope Hollow Formation, Boss basaltic trachyandesite, basalt of Kratz Spring, Silver Mines basaltic andesite, lower andesite of Marble Creek campground, Bourbon basalt, upper andesite of Marble Creek campground, trachyte host of Camels Hump IOA deposit, Boss trachyandesite, and trachyte of Kratz Spring. The sole recognized mafic intrusive unit is the diorite host of the Boss IOCG deposit. Intermediate composition extrusive and hypabyssal intrusive units include the trachyandesite of Floyd Tower/Indian Creek, trachyte of South Crane Mountain, Bourbon trachydacite, and trachyte of Kratz Spring. The sole intermediate composition intrusive unit is the Tiemann quartz diorite. Felsic extrusive and hypabyssal intrusive rocks include the Iron Mountain Lake rhyolite, Ironton Rhyolite, rhyolite at South Crane Mountain, Little Rock Creek rhyolite, Boss rhyolite, Russell Mountain Rhyolite, Shepherd Mountain Rhyolite, Upper Ridge rhyolite, Pond Ridge Rhyolite, Lower Ridge rhyolite, Tile Red ash-flow tuff, Pea Ridge 1825 rhyolite porphyry, Bourbon rhyolite, Ketcherside Mountain rhyolite, Grassy Mountain Ignimbrite, Royal Gorge Rhyolite, Lake Killarney Formation, Ironton Hollow-Cedar Bluff Rhyolite, lower campground tuff at Marble Creek campground, Taum Sauk Rhyolite, and Cuthbertson Mountain rhyolite. Felsic intrusive units include the Big Spring granite, Boss granite, Breadtray Granite, Brown Mountain granite porphyry, Bunker granite, Butler Hill Granite, Knoblick Granite, Silvermine Granite—fine grained, Silvermine Granite—medium grained, Slabtown Granite, and Stono Granite.

Nature of Mesoproterozoic Igneous Rocks in the St. Francois Mountains Terrane

Igneous rocks in the St. Francois Mountains terrane define two distinct episodes of Mesoproterozoic magmatism: (1) about 1.48 to 1.45 Ga, and (2) about 1.34 to 1.28 (Aleinikoff and others, 2016; Bickford and Mose, 1975; du Bray and others, 2018a; Thomas and others, 2012; and Van Schmus and others 1996). The St. Francois Mountains terrane is a Mesoproterozoic large felsic igneous province. The extent of the earlier (Calymmian) episode is dramatically greater than that of the later (Ectasian) episode (Kisvarsanyi, 1981; Pratt and others, 1979). The older magmatic episode consists of dominantly felsic volcanic and volcaniclastic rocks and associated intrusions with volumetrically lesser amounts of basalt, basaltic andesite, and andesite and their associated hypabyssal intrusions (for example, the Silver Mines mafic suite of Sylvester, 1984). The younger magmatic episode consists of a compositionally bimodal assemblage of volumetrically relatively minor mafic intrusions epitomized by the Skrainka suite (Sylvester, 1984) and its equivalents and a volumetrically more significant assemblage, exemplified by the Graniteville Granite, of mostly hypersolvus granites, most of which are concealed by overlying Paleozoic sedimentary rocks (Kisvarsanyi, 1981). All known magmatic-associated IOA and IOCG mineral deposits in the St. Francois Mountains terrane are coeval and cospatial with the products of and hosted in volcanic rocks of the older magmatic episode. Consequently, we focus on the petrogenesis and tectonic setting of the older Mesoproterozoic igneous rock assemblage in the St. Francois Mountains terrane. However, we present limited new geochronologic data for several plutons representative of the younger magmatic episode.

Mafic through felsic rocks, manifest as intrusive and extrusive masses, are represented among 1.48 to 1.45 Ga igneous rocks in the St. Francois Mountains terrane. However,

relative proportions of each of these various igneous rock types are quite dissimilar. The two most complete and useful regional-scale maps portraying the relative distribution of various igneous rock types in the St. Francois Mountains terrane were produced by Kisvarsanyi (1981) and Pratt and others (1979). Kisvarsanyi (1981) produced an interpretive map, based on geologic and geophysical data, portraying presumed continuous bedrock geologic relations beneath Paleozoic sedimentary rocks exposed throughout much of the St. Francois Mountains terrane. In contrast, Pratt and others (1979) produced a map that portrays the observed distribution and character of exposed Mesoproterozoic igneous rocks. For this study and following the guidance of Hildreth (2007), we classify mafic, intermediate, and felsic igneous rocks as those consisting of basalt through basaltic andesite, andesite through dacite, and rhyodacite through rhyolite, respectively. Accordingly, approximations of the relative areal extents of various igneous rock types in the St. Francois Mountains terrane were determined in a geographic information system context by applying these classification criteria to the maps of Kisvarsanyi (1981) and Pratt and others (1979) (table 1). Although results derived from the two maps are not identical, 1.48 to 1.45 Ga magmatism in the St. Francois Mountains terrane is dominated (95 to 99 percent) by felsic magmatism; the relative proportions of mafic and intermediate composition igneous rocks are minor (table 1). A similar classification of rock geochemistry verifies that the igneous rock population is dominated by felsic compositions but also reveals the compositions of these rocks are bimodally distributed, with respect to silica content, between a dominant felsic population and a much smaller mafic- to intermediate-composition population.

Several intrinsic features of igneous rocks in the St. Francois Mountains terrane further characterize these rocks. Importantly, except for outcrops in the Hawn State Park area (Lowell, 1976), none of the Mesoproterozoic igneous rocks in the St. Francois Mountains terrane exhibit deformation that resulted in penetrative fabrics. Rather, brittle deformation, as exemplified by fracture cleavage and brittle faulting, dominates throughout the terrane (Day and others, 2016). Most noticeably, felsic igneous rocks are much more abundant than either intermediate or mafic igneous rocks in this area (table 1). Although both the outcrop map of Pratt and others (1979) and the conceptual map of Kisvarsanyi (1981) indicate that the extent of felsic extrusive rocks is more than twice that of their intrusive equivalents (table 1) our updated compilation of St. Francois Mountains terrrane geology (fig. 1) suggests the opposite. Also, many of the felsic Mesoproterozoic intrusions in the St. Francois Mountains terrane form large, essentially circular plutons. These intrusions, principally the Breadtray and Butler Hill Granites but also including the Bunker and Big Spring granites, constitute the massif-type intrusions of Kisvarsanyi (1981). In contrast, the Stono, Knoblick, Silvermine, and Slabtown Granites constitute the ring-type intrusions of Kisvarsanyi (1981), many of which form broadly annular bodies surrounding the massif-type intrusions. Finally, most of the mafic and intermediate igneous rocks in this area consist of small subvolcanic or hypabyssal intrusions, although some formed lava flows. The diorite that hosts the Boss IOCG deposit is the best documented example of a volumetrically significant mafic 1.48 to 1.45 Ga intrusion in the St. Francois Mountains terrane. Similarly, the Tiemann quartz diorite, an intrusion in the east-central part of the St. Francois Mountains terrane, constitutes the sole known example of a volumetrically significant intermediate composition 1.48 to 1.45 Ga intrusion in the St. Francois Mountains terrane.

Detailed geologic mapping by Anderson (1962), Berry (1970), Brown (1988), and Sides (1981) first characterized the eruptive styles and types of volcanoes that dominated the Mesoproterozoic geologic landscape in the St. Francois Mountains terrane. Caldera-derived rhyolite ash-flow tuffs constitute the vast majority of volcanic units mapped in the St. Francois Mountains terrane (Day and others, 2016); their exceedingly large distribution and volumes markedly surpass the minor volume of rhyolite erupted as rhyolite flow dome complexes. The mafic and intermediate composition volcanic rocks, including the upper and lower andesites of Marble Creek

Table 1. Relative abundances, delineated from geologic maps of 1.48 to 1.45 Ga igneous rock types in the St. Francois Mountains terrane, southeast Missouri and corresponding sample abundances aggregated by geochemical composition; all data in percent.

[—, not present]

Rock type	Outcrop map[1]	Conceptual map[2]	This study (fig. 1)	Geochemistry samples[3]
Felsic volcanic rocks	71.0	65.3	31.3	56.1
Felsic intrusive rocks	27.9	29.3	61.6	22.2
Mafic and intermediate igneous rocks	—	5.3	—	—
Mafic-intermediate volcanic rocks	—	—	0.1	—
Mafic-intermediate intrusive rocks	—	—	6.3	—
Intermediate volcanic rocks	0.6	—	—	7.0
Mafic volcanic rocks	0.6	—	0.7	14.7

[1]Pratt and others (1979).

[2]Kisvarsanyi (1981).

[3]du Bray and others (2018b).

campground (Brown, 1988), Bourbon basalt, basalt in the Cope Hollow Formation, basalt of Kratz Spring, the trachyandesite of Floyd Tower/Indian Creek, Silver Mines basaltic andesite, and the Lake Four Winds basalt are dominantly composed of relatively isolated, volumetrically minor lava flows and lesser hypabyssal intrusive rocks for which preserved evidence of eruption from a significant volcanic edifice is absent. Some of these mafic to intermediate units include dikes and sills.

Geochronology of 1.48 to 1.45 Ga Igneous Rocks in the St. Francois Mountains Terrane

Forty-nine samples of zircon and two samples (table 2) of titanite (CLT-1-13; ICM-1-13) from Mesoproterozoic igneous rocks in the St. Francois Mountains terrane of southeast Missouri were analyzed using the U.S. Geological Survey (USGS)-Stanford sensitive high resolution ion microprobe-reverse geometry (SHRIMP-RG). In addition, titanite sample CLT-1-13 was analyzed using the USGS laser ablation-inductively coupled plasma mass spectrometery (LA-ICPMS) technique in Denver, Colo. The ages of two additional samples were determined by uranium-lead (U-Pb) surface analysis using the SHRIMP-RG. Uranium and lead ages for these two samples were also determined by chemical abrasion-isotope dilution-thermal ionization mass spectrometry (CA-ID-TIMS) at the W.M. Keck Isotope Laboratory at the University of California, Santa Cruz.

Methods

The procedures used to prepare samples for analysis are described in the following sections.

Sample Preparation

Samples for dating were collected either at outcrops or from drill core archived at the McCracken Core Library and Research Center, Rolla, Mo. At outcrop sample sites, about 4–6 kilogram (kg) samples were collected, whereas drill core samples consist of 0.5–2 m of half-split drill core. Zircon was extracted using standard mineral separation techniques including crushing, pulverizing, processing over a Wilfley table, and passing the heavy mineral suite through a Frantz Isodynamic Magnetic Separator. Nonmagnetic grains were then poured into methylene iodide (density of 3.3 grams per cubic centimeter) for density separation. Zircon (plus titanite and pyrite, if present) sunk, whereas apatite (plus quartz and feldspar, if present) floated.

For SHRIMP analyses, individual grains of zircon and titanite were handpicked under a binocular microscope. Selected grains were placed onto double-sided tape, mounted in epoxy, ground to about half thickness using 2,500-grit wet-dry sandpaper, and polished sequentially using 6 micrometer (μm) and 1 μm diamond suspensions. All grains were imaged in reflected and transmitted light on a petrographic microscope. Using the USGS JEOL 5800LV scanning electron microscope (SEM) in Lakewood, Colo., zircon was imaged in cathodoluminescence (CL), whereas titanite was imaged using backscattered electrons (BSE) (fig. 2).

For the U-Pb surface analyses, individual euhedral crystals were adhered to a glass slide coated with a thin (<10 μm) film of agave nectar. After the [010] crystal faces were oriented in the plane of the glass slide, the slide was flipped to press all crystals into indium metal containing pre-polished standard grains, resulting in flat, non-polished zircon surfaces exposed parallel to the mount surface (Matthews and others, 2015). All grains were imaged with reflected light on a petrographic microscope to identify inclusions and physical defects such as fractured crystal faces. Prior to introduction into the SHRIMP-RG, the indium-mounted zircons were soaked in soapy water, followed by a 10 percent ethylenediaminetetraacetic acid wash for about 2 minutes each, thoroughly rinsed in distilled water, and dried at 50 degrees Celsius (°C) in a vacuum oven. The sample surface was coated with about 100 nanometers of gold prior to analysis.

For LA-ICPMS analyses, fragments or single crystals of titanite from sample CLT-1-13 were handpicked, mounted in epoxy, and imaged in transmitted and (or) reflected light on a petrographic microscope. BSE imaging on the USGS FEI Quanta FEG 450 SEM in Lakewood, Colo revealed internal textures (core-rim structures) and inclusions in individual grains.

For CA-ID-TIMS analyses, zircon crystals were plucked from indium grain mounts and thermally annealed in a quartz crucible at 900 °C for 60 hours. Following thermal annealing, each zircon crystal was placed into a 200 microliter Teflon® microcapsule and leached in 29 M (molar) hydrofluoric acid inside a high-pressure Parr® vessel held at 220 °C for 12 hours, a procedure modified after the chemical abrasion partial-dissolution procedure of Mattinson (2005). Grains were then transferred to 3 mL Savillex® perfluoroalkoxy beakers and rinsed with 16 M nitric acid and 6 M hydrochloric acid, fluxed in the acid at 80 °C, followed by an approximately 30-minute ultrasonic bath. Between acid washes, grains were rinsed three times with Milli-Q® water. Single zircon crystals were loaded with clean water into Teflon® microcapsules and spiked with the EARTHTIME ^{205}Pb-^{233}U-^{235}U (ET535) tracer solution and dissolved in 29 M hydrofluoric acid at 220 °C for 48 hours. Upon dissolution, aliquots were dried down on a hotplate and redissolved under pressure in 6 M hydrochloric acid overnight at 180 °C. Sample solutions were then dried and redissolved at 180 °C in 3 N (normal) hydrochloric acid. Lead and uranium were separated using a miniaturized hydrochloric acid-based ion-exchange chromatography

procedure modified from Krogh (1973) with 40 microliter columns of AG1x8 resin. Eluted uranium and lead were dried down with phosphoric acid, redissolved in a silica gel emitter solution following Gerstenberger and Haase (1997), and loaded onto a zone-refined, outgassed rhenium filament.

SHRIMP U-Pb Analysis

Zircon and titanite from the St. Francois Mountains terrane were analyzed using the USGS-Stanford SHRIMP-RG ion microprobe following methods described in Ireland (1995) and Williams (1998). The primary ion beam was operated at about 4–6 nA with an analytical spot size of about 20–25 µm in diameter. The magnet was cycled through the appropriate mass stations five times. Measured $^{206}Pb/^{238}U$ for zircon was normalized to the accepted value for zircon standard R33 (419 Ma; Black and others, 2004). For samples dated during 2013–2014, zircon standards FC-1 (1099 Ma; Paces and Miller 1993) or OG-1 (3441 Ma; Stern and others, 2009) were run as secondary standards to verify accuracy of $^{207}Pb/^{206}Pb$ ages. For samples run after 2014, zircon standard Z1242 (2679 ± 1 Ma; Davis and others, 2018) was analyzed on all mounts with unknowns; any divergence from the accepted $^{207}Pb/^{206}Pb$ age of the standard was used to normalize measured values of $^{207}Pb/^{206}Pb$ for unknowns. Titanite was dated using titanite standard BLR-1 (1047 ± 1 Ma; Aleinikoff and others, 2007) to normalize measured $^{206}Pb/^{238}U$ ages.

Measured SHRIMP U-Pb data (Aleinikoff, 2021) were reduced using Squid 2 (Ludwig, 2009) and plotted using Isoplot 3 (Ludwig, 2003) (fig. 2). Ages of these Mesoproterozoic zircon samples were determined using one of two methods: (1) for discordant data (mostly less than 10 percent discordant), the weighted mean of selected $^{207}Pb/^{206}Pb$ ages was calculated; or (2) for concordant data, a Concordia Age (CA) (Ludwig, 1980; 2003) was calculated. Unless otherwise noted, ages were calculated by method (1). Concentrations of uranium and thorium (Th), determined by analysis of zircon standard MADDER, are believed to be accurate to about ± 20 percent (Ireland, 1995).

SHRIMP U-Pb Surface Analysis

Uranium and Pb isotopic measurements (table 3) were performed on the Stanford-USGS SHRIMP-RG using an O_2- primary beam with an intensity ranging from 6.0 to 7.2 nanoamps and spot dimension of approximately 35 x 32 x 2 µm (length x width x depth). Calculated U/Pb dates (fig. 3) are standardized relative to zircon standard 91500 (1065 million years old [Ma]; Wiedenbeck and others, 1995) calibrated from the ratio of uranium oxide to uranium (UO/U) (Schmitt and Zack, 2012), which was determined repeatedly throughout the duration of the analytical session. Ion intensities were measured on a single ETP® discrete-dynode electron multiplier operated in pulse counting mode and corrected for deadtime. Measurements were performed at mass resolutions of 6,500–7,500 (10 percent peak height), which eliminates interfering molecular species at lead, thorium, and uranium peaks. Data reduction for geochronology follows the methods described by Ireland and Williams (2003) using the spreadsheet add-in program Squid 2.51 (Ludwig, 2009, 2012). Individual spots are reported as $^{206}Pb/^{238}U$ dates that were corrected for common Pb using ^{207}Pb and with application of an age-appropriate-modeled Pb composition from Stacey and Kramers (1975), and for initial ^{230}Th disequilibrium using the method of Scharer (2002). Uranium and thorium concentrations were calculated relative to MAD-559 zircon (uranium = 3940; Coble and others, 2018). Some analyses were omitted from the final dataset based on common Pb concentration (greater than 5 percent ^{207}Pb-corrected for sample MO16-015, greater than 2 percent for sample MO16-001), and run quality, which varied depending on the degree of surface contamination, grain size, surface topography (cracks or significant undulation), secondary ion yield, and uranium concentration.

LA-ICPMS Analysis

Titanite from sample CLT-1-13 was analyzed using a LA-ICPMS method because this titanite has an unusual composition (resulting in matrix effect problems for SHRIMP analysis) and low concentrations of uranium and high common lead contents, also problematic for SHRIMP analysis.

We used an LA-ICPMS system that includes a Teledyne Photon Machines Excite-Analyte™ 193 nm excimer ArF (argon fluoride) laser and a Nu Instruments AttoM ES™ high resolution-sector field ICPMS to acquire U-Th-Pb isotopic data. Prior to analysis, the system was optimized using NIST (National Institute of Standards and Technology) 610 glass (National Institute of Standards and Technology, 1992) ablated in raster mode to achieve maximum signal intensity, optimal peak shape at mass 238, and low interelement fractionation monitored by Th/U (typically approximately 0.8). Approximate uranium and thorium concentrations (table 4) were obtained using the Iolite™ U-Pb geochronology data reduction scheme (U_Pb_Geochronology3; Paton and others, 2011), using NIST 610 glass as the primary standard reference material (461.5 parts per million [ppm] uranium and 457.2 ppm thorium). NIST glasses can exhibit substantially different elemental fractionation behavior than many common geological matrices, resulting in degraded precision and accuracy for concentrations of some elements (Jackson, 2008; Sylvester, 2008). Because of the matrix difference between the NIST 610 glass and titanite, we assume an accuracy of uranium and thorium concentrations in titanite to be ±20 percent based on results by Jochum and others (2011). We used the Pb/U isotopic values in NIST 610 from Baker and others (2004) and Stern and Amelin (2003). Additional instrumental and data acquisition parameters are defined in table 5.

Raw data were reduced using a combination of Iolite™ and spreadsheet calculations using Isoplot software (Ludwig, 2012). We used NIST 610 glass as a primary matrix-mismatched standard and titanite standard BLR-1 (1047 Ma; Aleinikoff and others, 2002) as a secondary matrix-matched standard. Normalization to the primary standard was done using Iolite™, which calculates accurate titanite lead-isotope ratios and biased U/Pb values because the matrix-mismatched primary standard was used. Biased $^{206}Pb/^{238}U$ age for the BLR-1 standard was calculated by Isoplot using Stacey-Kramers 1.05 Ga common lead correction (Stacey and Kramers, 1974) and Tera-Wasserburg isochron diagram (Tera and Wasserburg, 1972). Measured U/Pb for titanite sample CLT-1-13 were corrected for instrumental bias by applying a correction factor F calculated from the difference between the measured biased age and known "true" age for the BLR-1 matrix-matched standard. Two-sigma uncertainties were appropriately propagated. The validity of this approach was verified by analyzing secondary titanite standards Khan (approximately 520 Ma; Heaman, 2009) and OLT-1 (approximately 1015 Ma; Kennedy and others, 2010). More details on the analytical techniques and data reduction protocols are described by Neymark and others (2018).

CA-ID-TIMS Analysis

Measurement of isotopic ratios of uranium and lead was done on an IsotopX X62 thermal ionization mass spectrometer at the W.M. Keck Isotope Laboratory at the University of California at Santa Cruz. Isotopes of lead were measured by peak-hopping on a single Daly/photomultiplier detector system (table 6). Isotopes of uranium were measured as uranium dioxide (UO_2) on Faraday detectors in static mode. Isotope ratios of lead were corrected for mass dependent fractionation by empirically determining alpha-lead based on long-term measurements of the NBS−981 common-lead standard. Isotopes of uranium were corrected for mass fractionation during analysis using the ET535 tracer solution. Data reduction was done using the Tripoli and U/Pb Redux software packages (Bowring and others, 2011; McLean and others, 2011). Zircon analyses were corrected for initial thorium diseqilibrium by using the measured ^{208}Pb for the Th/U of the zircon crystal and assuming a Th/U of the magma of 4.

Results

For each of the analyzed samples, we compiled the data (table 7), including source of the rock sample, age (including 2-sigma uncertainty), and method of age calculation (Concordia Age or $^{207}Pb/^{206}Pb$ weighted mean age); also, we present a representative CL or BSE image and concordia plot, pertinent to each geochronologic age determination. All of the previously published, high precision ages for Mesoproterozoic igneous rocks in southeast Missouri are given in table 8.

Fifty samples, regionally distributed throughout the St. Francois Mountains terrane, were dated as part of this study. Of these, 25 are samples from drill core obtained from the McCracken Core Library, whereas 25 samples were collected at outcrops (table 7). Unless otherwise noted, zircon grains from Mesoproterozoic igneous rocks in the St. Francois Mountains terrane are euhedral, prismatic, doubly terminated, and display concentric oscillatory zoning (see representative CL images in figure 2*A*–*S*).

Samples are grouped by geographic location and geologic association and by age. As shown by Van Schmus and others (1996) and confirmed by Thomas and others (2012), Mesoproterozoic rocks of the St. Francois Mountains terrane define two broad age groups, approximately 1.46 Ga and approximately 1.32 Ga. Our new data, discussed from youngest to oldest (table 7), define these same two magmatic episodes.

1.34–1.27 Ga Bimodal Plutonic Rocks

Six samples of granitic rocks (five from drill core and one collected from outcrop) from the middle Mesoproterozoic bimodal plutonic rock group (Day and others, 2016) were dated. The three youngest plutonic rocks of this age group in the study area are the Greenville pluton (sample 63W20; weighted mean age 1275 ± 13 Ma, mean square of weighted deviates (MSWD) = 1.6), Van Buren pluton (sample CT-5; weighted mean age 1278 ± 10 Ma, MSWD = 0.65) and Piedmont pluton (sample 82MO-8; weighted mean age 1290 ± 15 Ma, MSWD = 1.2) (fig. 2*A*1–2*A*6). All of these granites are in the southern part of the study area (fig. 1). Slightly older granitic rocks, the Graniteville Granite (sample GVG-1-13; weighted mean age 1311 ± 13 Ma, MSWD = 1.2) and the Buick pluton (sample FED3; 1317 ± 8; Concordia Age) (fig. 2*B*1–2*B*4), are in the central part of the study area. An alkali-feldspar granite sample (sample 124-14A; weighted mean age 1338 ± 10 Ma, MSWD = 1.12) (fig. 2*B*5, 2*B*6) was collected from core derived from a hole drilled southwest of the study area, in the area coincident with the regional Missouri gravity low (Guiness and others, 1982; Hildenbrand and others, 1996).

The Graniteville Granite had previously been dated by two studies. Our SHRIMP age of 1311 ± 13 Ma is within uncertainty of the 1317 ± 2 Ma age determined by CA-ID-TIMS (Thomas and others, 2012). Multigrain TIMS data (Van Schmus and others, 1996) yielded an older and less precise age of 1358 ± 25 Ma.

The alkali-feldspar granite sample was dated as part of an investigation of the Missouri gravity low (MGL), which forms a belt about 125 kilometers wide and about 600 kilometers long across the Mesoproterozoic eastern granite-rhyolite province and the Central Plains orogen. Historically, the MGL has been most commonly and plausibly attributed to either (1) an approximately 1.3 Ga granite batholith related to a mantle plume (Hildenbrand and others, 1996), or (2) a failed Precambrian rift (Guiness and others, 1982). An age was also determined for a second granite intrusion coincident with the MGL (see text in the Regional Granitoids and Rhyolite section of this report; table 7).

Table 2. Samples of igneous rocks in the St. Francois Mountains terrane, southeast Missouri for which ages were determined by SHRIMP U-Th-Pb analysis of zircon and titanite.

[Aleinikoff (2021) presents SHRIMP U-Pb geochronologic data for the analyzed samples]

Map number (fig. 1)	Sample number	Geologic unit	North latitude	West longitude
1	63W20	Greenville pluton	37.0424	−90.4524
2	CT-5	Van Buren pluton	37.0359	−91.0179
3	82MO-8	Piedmont pluton	37.0913	−90.7964
4	GVG-1-13	Graniteville Granite	37.6619	−90.6833
5	FED3	Buick pluton	37.6087	−91.0977
6	124-14A	Alkali-feldspar granite	37.0242	−91.5299
7	CLT-1-13	Rhyolite of South Crane Mountain	37.4770	−90.6219
8	MO14-053	Tuff at Crane Pond	37.4135	−90.5830
9	MO14-043	Lower campground tuff at Marble Creek campground	37.4500	−90.5418
10	RGR-1-13	Royal Gorge Rhyolite	37.5723	−90.6949
11	MO15-008	Shepherd Mountain Rhyolite	37.6112	−90.6311
12	BTG-1-13	Breadtray Granite	37.6946	−90.5455
13	BHG-1-13	Butler Hill Granite	37.7045	−90.3993
14	GMI-2-13	Grassy Mountain Ignimbrite	37.5853	−90.5829
15	SMG-1-13	Silvermine Granite	37.5571	−90.4481
16	STG-1-13	Slabtown Granite	37.6069	−90.3392
17	KLG-1-13	Knoblick Granite	37.6189	−90.3885
18	MO17-013	Stono Granite	37.7167	−90.5499
19	RE060	Massif-type granite	37.2310	−91.0399
20	RE037	Granite near Redford pluton	37.3191	−90.9445
21	MO17-002	Biotite granite	37.8419	−90.2660
22	MR-3-1556	Rhyolite tuff	37.8518	−90.8722
23	SV-5	Massif-type granite	37.3067	−91.4780
24	VB-23-2153	Biotite granite	37.1401	−91.0697
25	MO17-001	Quartz-alkali feldspar andesite dike	37.8436	−90.2730
26	M-DT-3-1	Massif-type biotite granite	37.6807	−91.4208
27	WY032	Granite near Piedmont pluton	37.1353	−90.6532
28	W-6-2578	Megacrystic granite	36.9007	−90.6937
29	RE05	Massif-type granite	37.3459	−91.1201
30	MH-1	Massif-type biotite granite	38.2848	−90.8341
31	GMI-1-13	Stouts Creek Rhyolite	37.6634	−90.3854
32	MO17-006	Granite of Castor River Shut-Ins	37.5688	−90.1497
33	OZ-5	Rhyolite near Silver Mines	37.5405	−90.4632
34	M-FK-1-1	Biotite granite	38.4336	−90.9115
35	MO14-007	Upper unit of Coot Mountain	37.1744	−91.2547
36	MO14-009	Lower unit Coot Mountain	37.1826	−91.2694
37	MO14-003	Rhyolite of Stegall Mountain	37.0754	−91.2030
38	SV-3	Biotite-hornblende granodiorite	37.2291	−91.3906
39	MO13-006	Trachyandesite at Floyd Tower	37.9750	−90.9913
40	ICM-1-13	Trachyandesite of Indian Creek mine	38.0414	−90.9194
41	USA-50	Rhyolite host at Boss deposit	37.6473	−91.1730
42	J-22-1541-1562	Trachyte host at Boss deposit	37.6500	−91.2800
43	S5	Post-mineralization diorite at Boss deposit	37.6427	−91.1791
44	S5-gr	Granite dike at Boss deposit	37.6427	−91.1791
45	J-15	Biotite granite dike at Boss deposit	37.6473	−91.2835
46	Bourb-435	Bourbon rhyolite	38.1516	−91.2431
47	Bourb-204	Trachydacite	38.1511	−91.2505
48	PcF-075	Trachyandesite at Iron Mountain	37.7006	−90.6412
49	PcF-076	Trachyandesite at Buford Mountain	37.6887	−90.6907
50	PcF-077	Rhyolite at Middlebrook Hill	37.6703	−90.6567

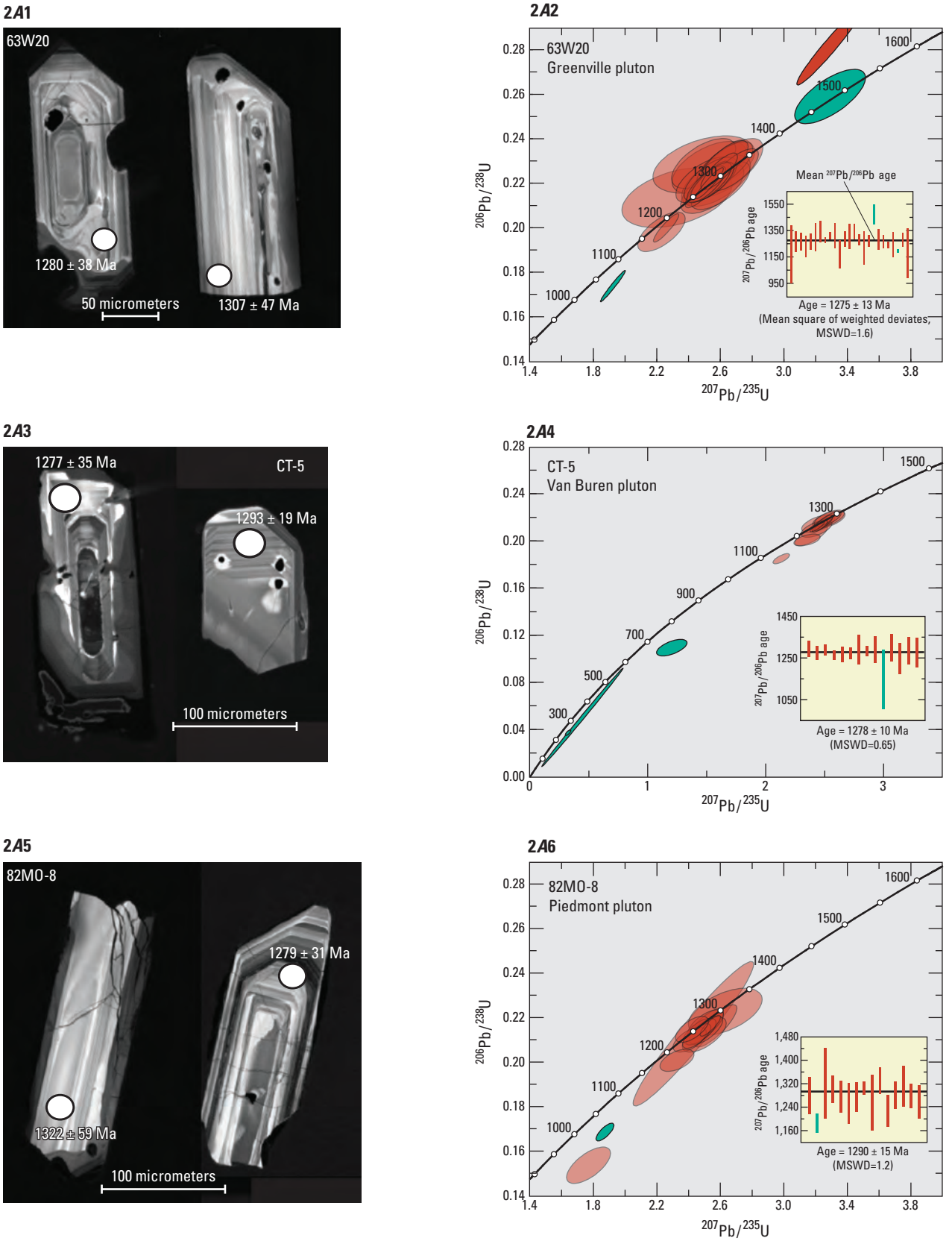

Figure 2. Representative cathodoluminescence images of zircon and backscattered electron images of titanite from igneous rocks in the St. Francois Mountains terrane, southeast Missouri. Zircon uranium-lead isotope data are plotted on Wetherill (1956) concordia curves, whereas titanite uranium-lead isotope data are plotted on Tera-Wasserburg (1972) concordia curves. Insets show weighted means of selected $^{207}Pb/^{206}Pb$ ages. [Ma, million years; Ga, billion years]

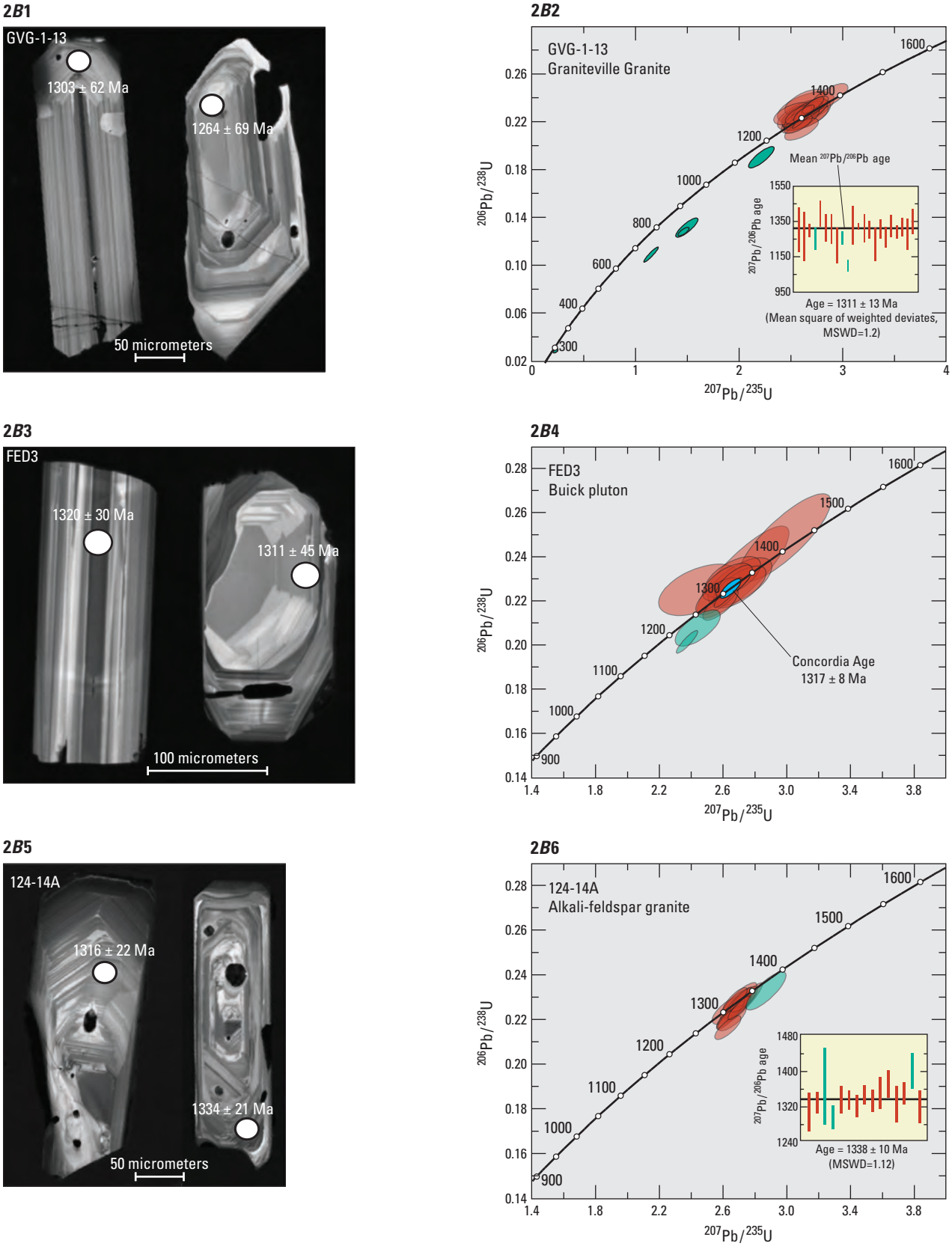

Figure 2. Representative cathodoluminescence images of zircon and backscattered electron images of titanite from igneous rocks in the St. Francois Mountains terrane, southeast Missouri. Zircon uranium-lead isotope data are plotted on Wetherill (1956) concordia curves, whereas titanite uranium-lead isotope data are plotted on Tera-Wasserburg (1972) concordia curves. Insets show weighted means of selected $^{207}Pb/^{206}Pb$ ages. [Ma, million years; Ga, billion years]—Continued

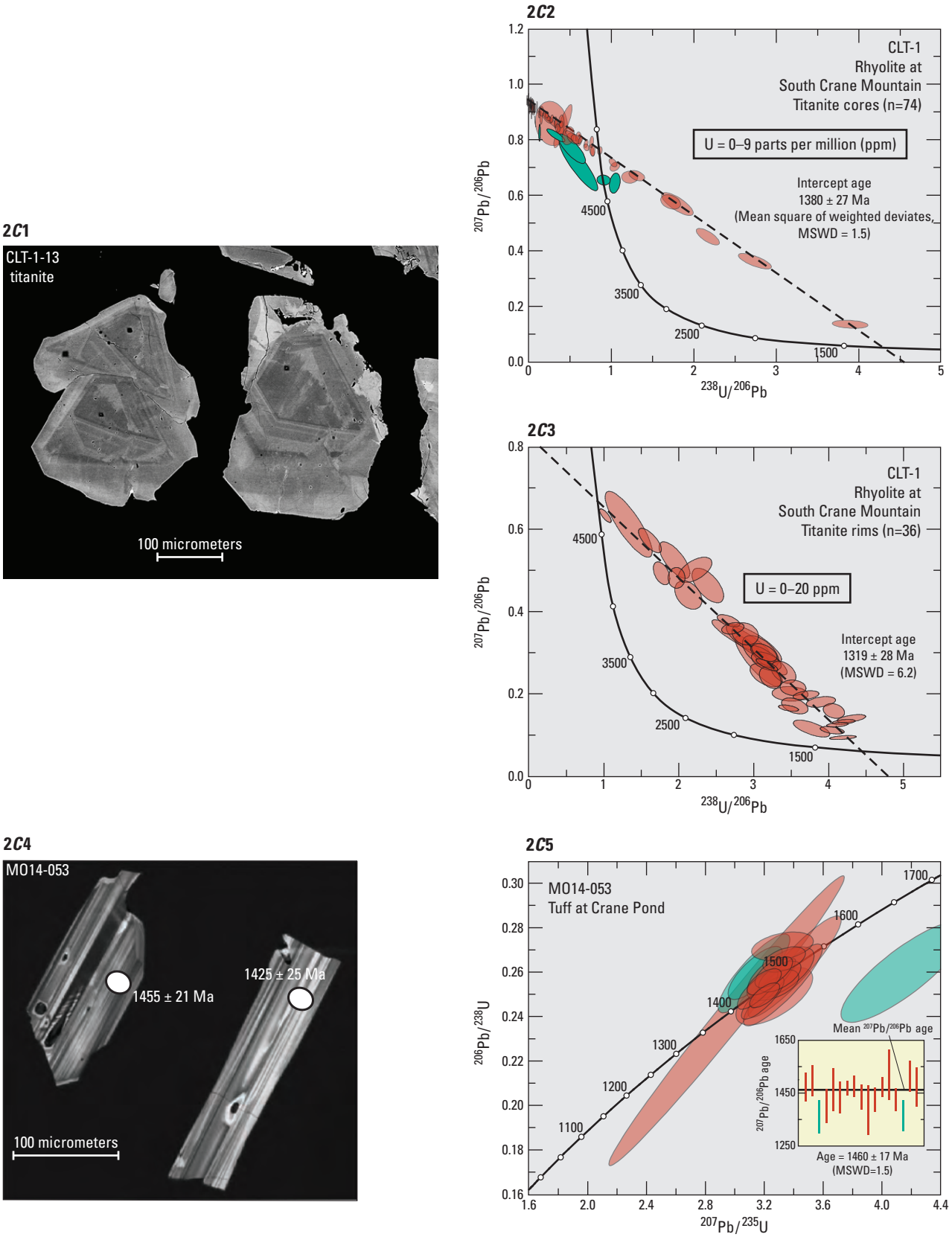

Figure 2. Representative cathodoluminescence images of zircon and backscattered electron images of titanite from igneous rocks in the St. Francois Mountains terrane, southeast Missouri. Zircon uranium-lead isotope data are plotted on Wetherill (1956) concordia curves, whereas titanite uranium-lead isotope data are plotted on Tera-Wasserburg (1972) concordia curves. Insets show weighted means of selected $^{207}Pb/^{206}Pb$ ages. [Ma, million years; Ga, billion years]—Continued

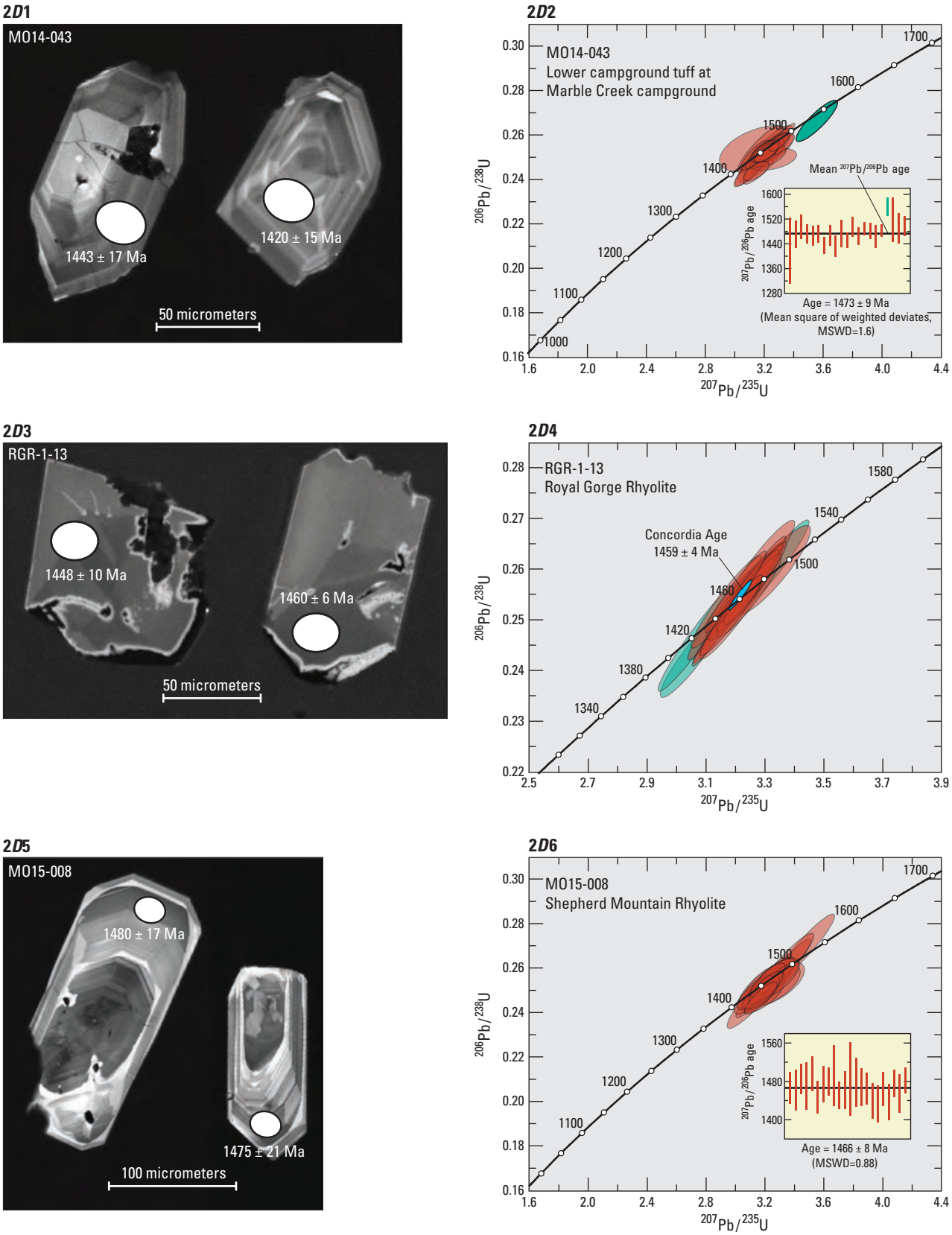

Figure 2. Representative cathodoluminescence images of zircon and backscattered electron images of titanite from igneous rocks in the St. Francois Mountains terrane, southeast Missouri. Zircon uranium-lead isotope data are plotted on Wetherill (1956) concordia curves, whereas titanite uranium-lead isotope data are plotted on Tera-Wasserburg (1972) concordia curves. Insets show weighted means of selected $^{207}Pb/^{206}Pb$ ages. [Ma, million years; Ga, billion years]—Continued

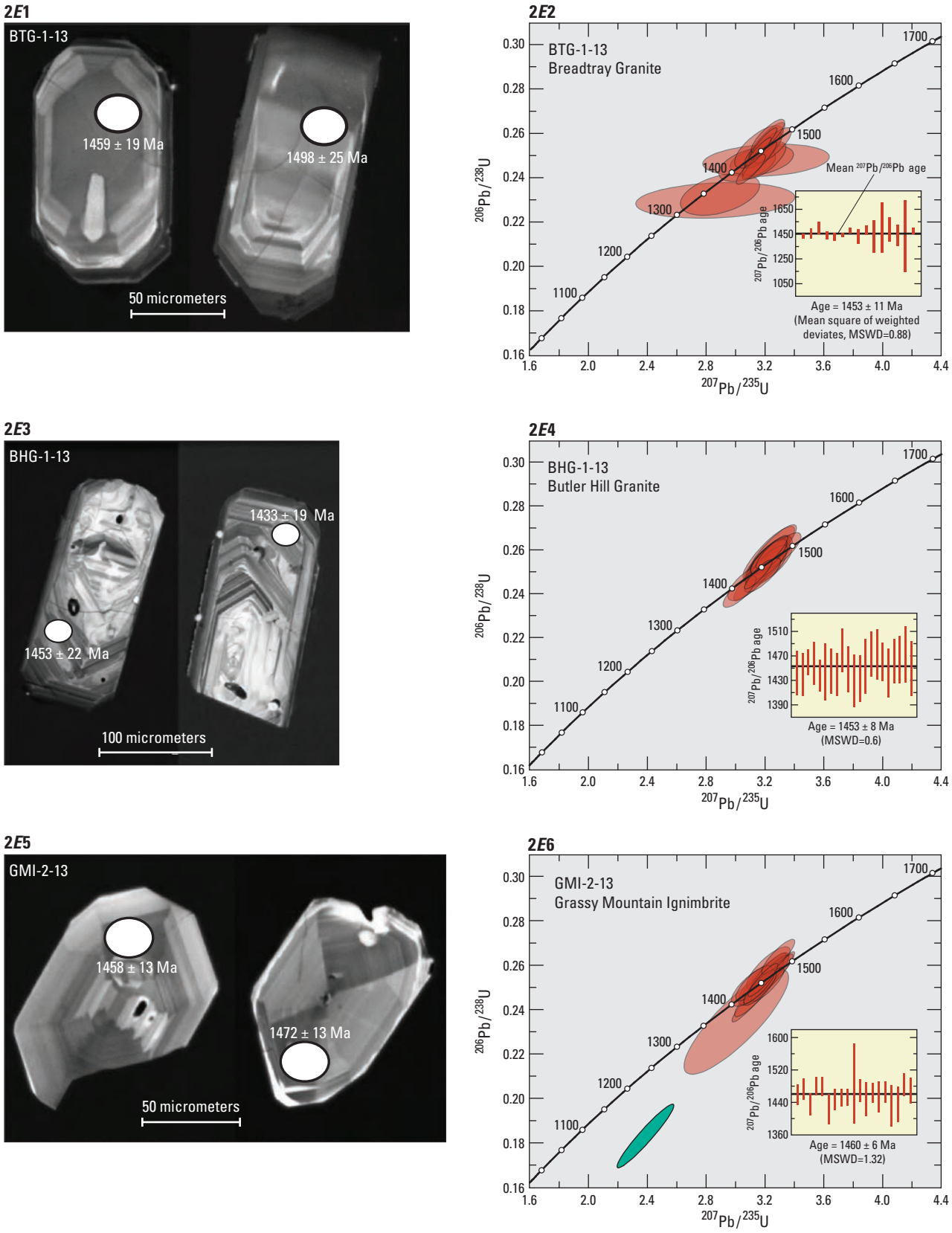

Figure 2. Representative cathodoluminescence images of zircon and backscattered electron images of titanite from igneous rocks in the St. Francois Mountains terrane, southeast Missouri. Zircon uranium-lead isotope data are plotted on Wetherill (1956) concordia curves, whereas titanite uranium-lead isotope data are plotted on Tera-Wasserburg (1972) concordia curves. Insets show weighted means of selected $^{207}Pb/^{206}Pb$ ages. [Ma, million years; Ga, billion years]—Continued

2*F*1

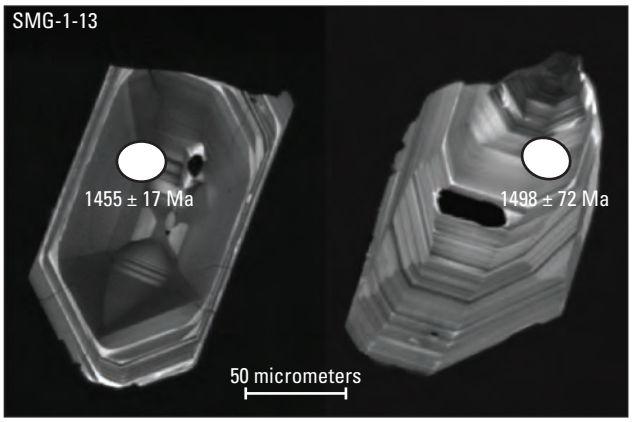

2*F*2

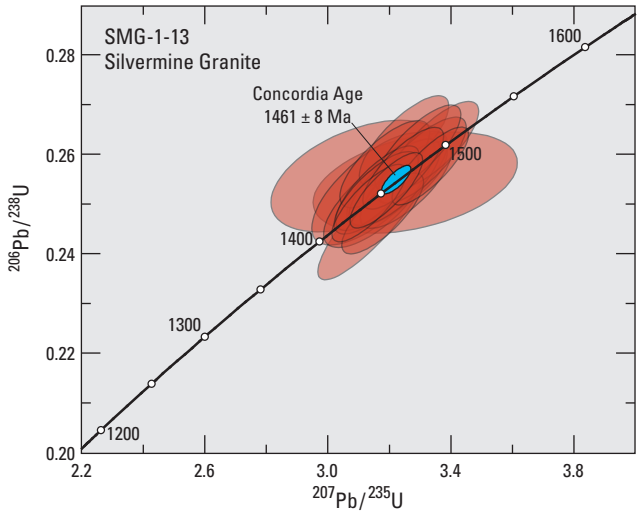

2*F*3

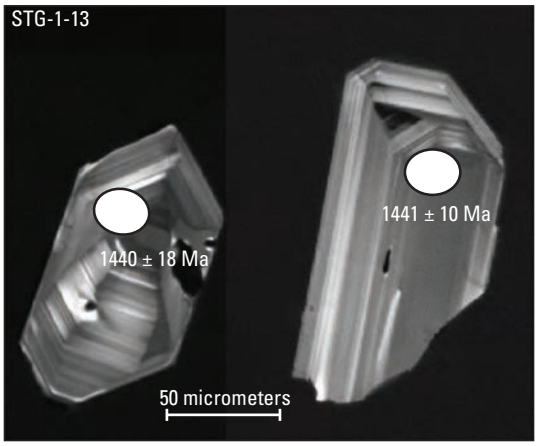

2*F*4

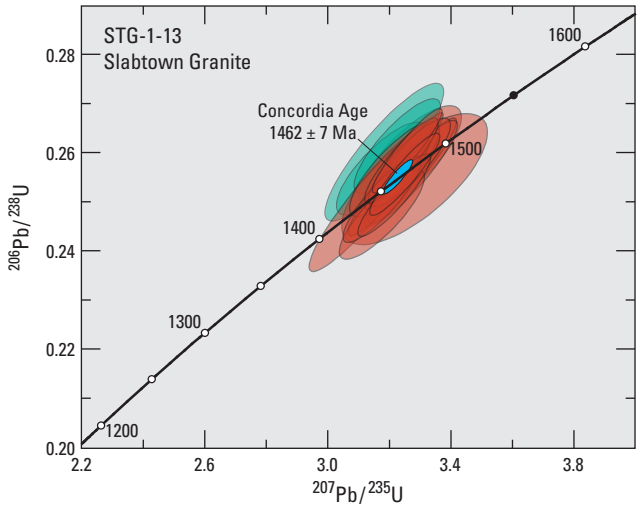

2*F*5

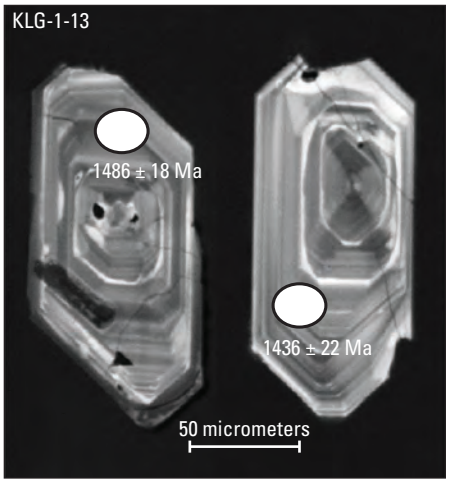

2*F*6

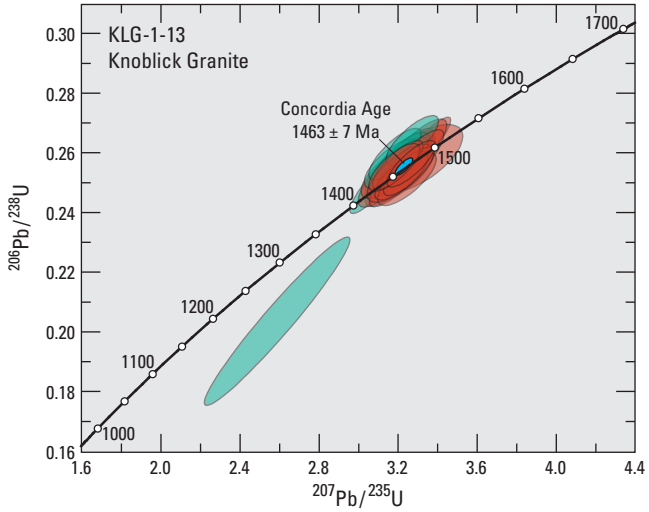

Figure 2. Representative cathodoluminescence images of zircon and backscattered electron images of titanite from igneous rocks in the St. Francois Mountains terrane, southeast Missouri. Zircon uranium-lead isotope data are plotted on Wetherill (1956) concordia curves, whereas titanite uranium-lead isotope data are plotted on Tera-Wasserburg (1972) concordia curves. Insets show weighted means of selected $^{207}Pb/^{206}Pb$ ages. [Ma, million years; Ga, billion years]—Continued

2*G*1

2*G*2

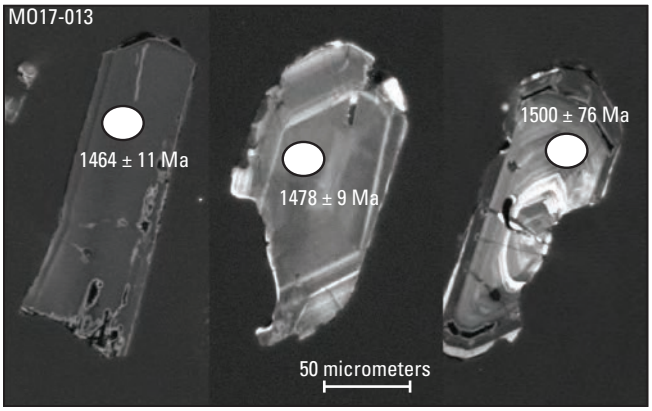

2*G*3

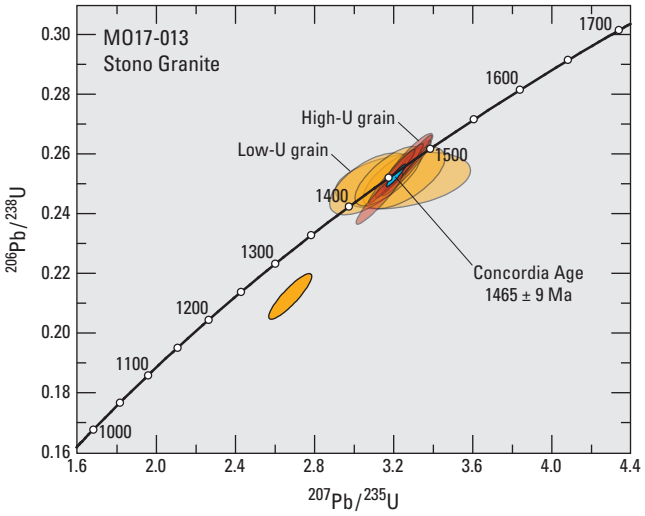

Figure 2. Representative cathodoluminescence images of zircon and backscattered electron images of titanite from igneous rocks in the St. Francois Mountains terrane, southeast Missouri. Zircon uranium-lead isotope data are plotted on Wetherill (1956) concordia curves, whereas titanite uranium-lead isotope data are plotted on Tera-Wasserburg (1972) concordia curves. Insets show weighted means of selected $^{207}Pb/^{206}Pb$ ages. [Ma, million years; Ga, billion years]—Continued

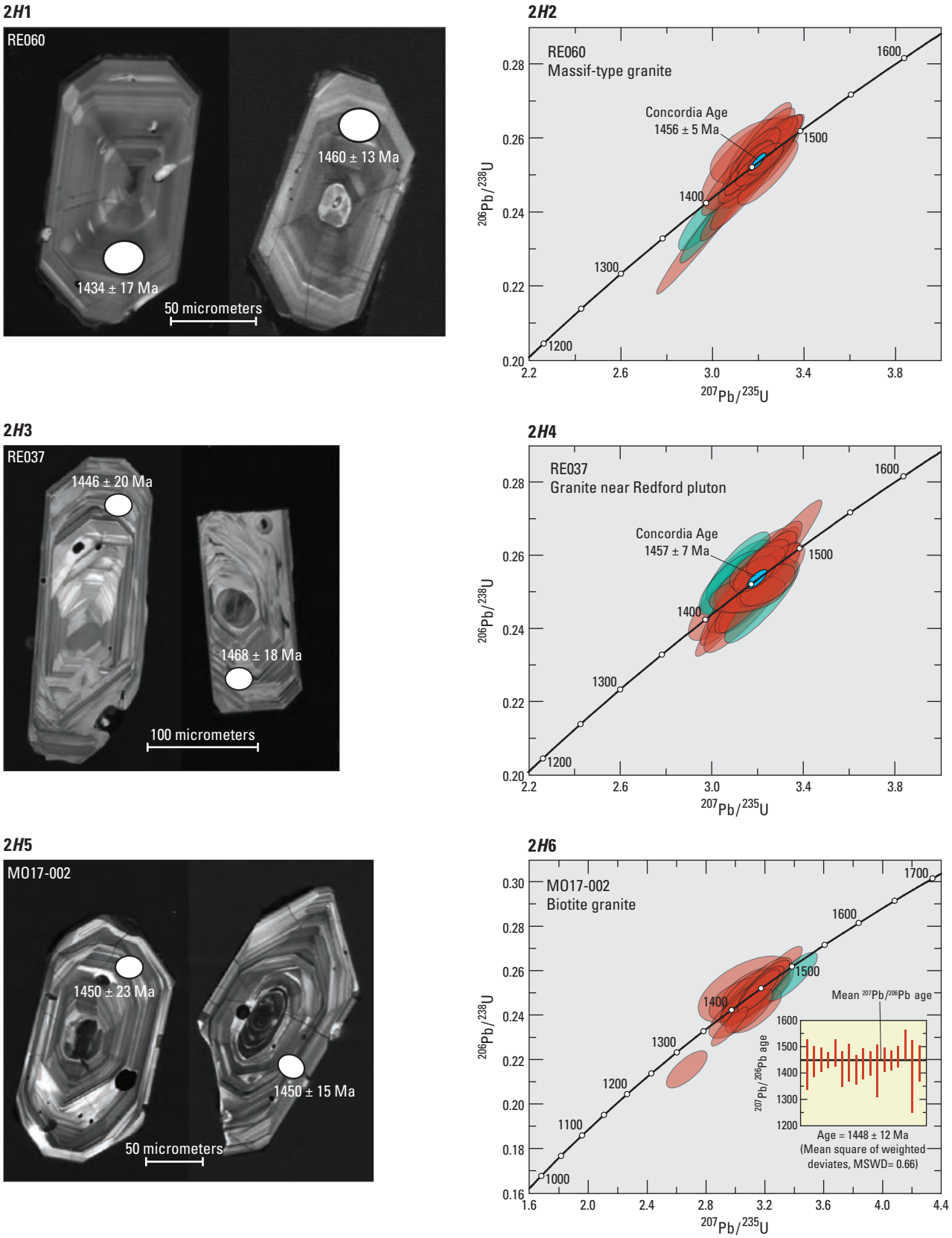

Figure 2. Representative cathodoluminescence images of zircon and backscattered electron images of titanite from igneous rocks in the St. Francois Mountains terrane, southeast Missouri. Zircon uranium-lead isotope data are plotted on Wetherill (1956) concordia curves, whereas titanite uranium-lead isotope data are plotted on Tera-Wasserburg (1972) concordia curves. Insets show weighted means of selected $^{207}Pb/^{206}Pb$ ages. [Ma, million years; Ga, billion years]—Continued

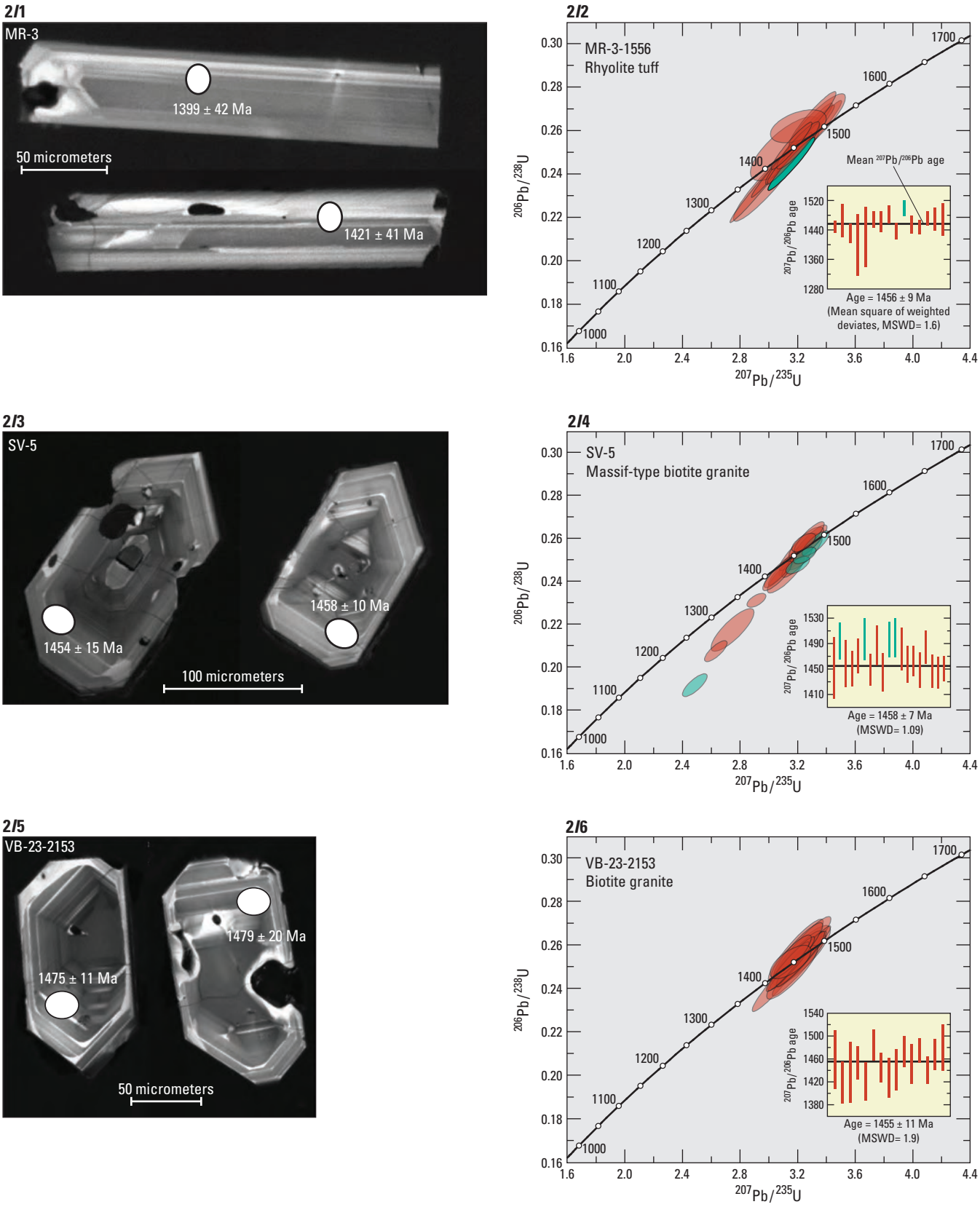

Figure 2. Representative cathodoluminescence images of zircon and backscattered electron images of titanite from igneous rocks in the St. Francois Mountains terrane, southeast Missouri. Zircon uranium-lead isotope data are plotted on Wetherill (1956) concordia curves, whereas titanite uranium-lead isotope data are plotted on Tera-Wasserburg (1972) concordia curves. Insets show weighted means of selected $^{207}Pb/^{206}Pb$ ages. [Ma, million years; Ga, billion years]—Continued

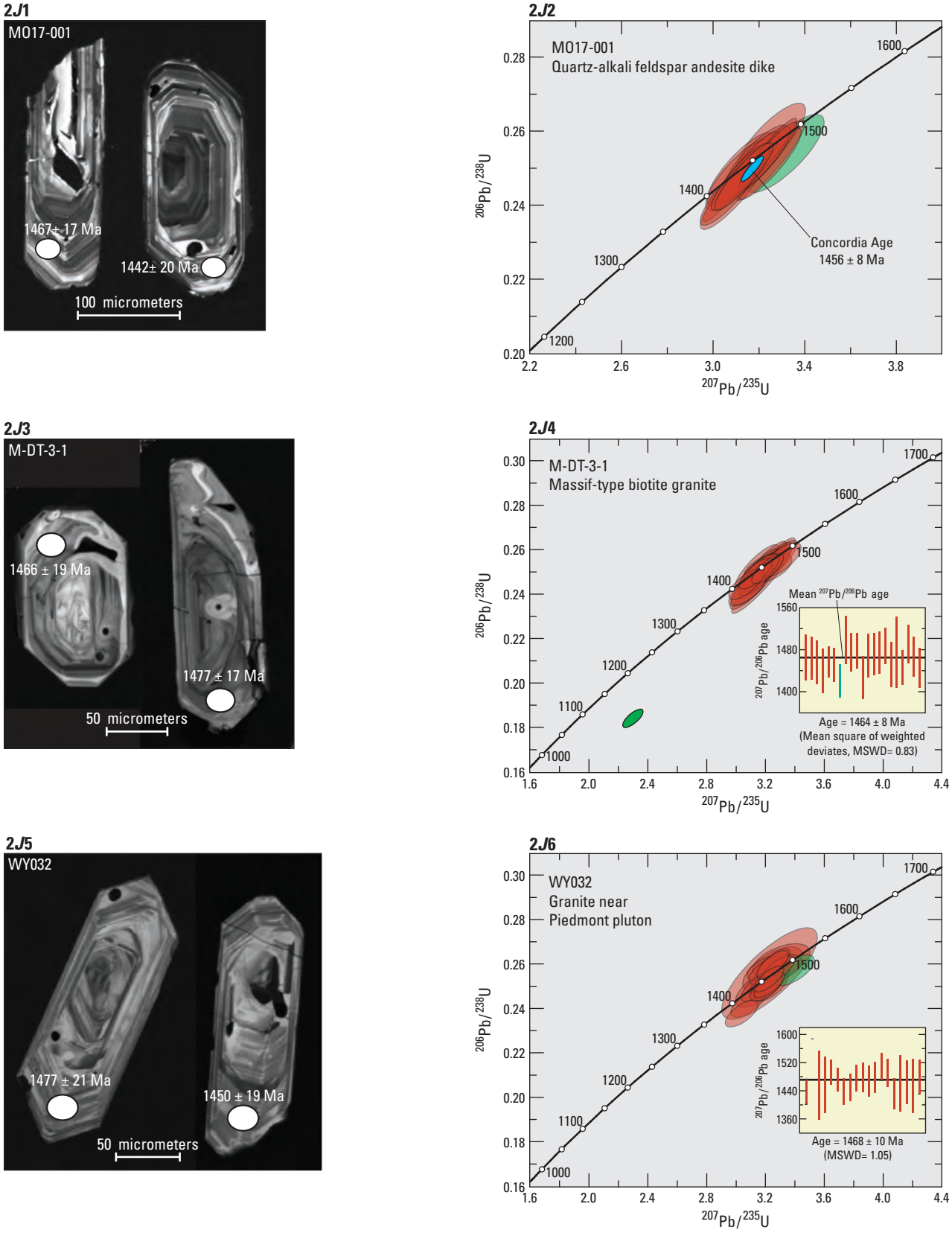

Figure 2. Representative cathodoluminescence images of zircon and backscattered electron images of titanite from igneous rocks in the St. Francois Mountains terrane, southeast Missouri. Zircon uranium-lead isotope data are plotted on Wetherill (1956) concordia curves, whereas titanite uranium-lead isotope data are plotted on Tera-Wasserburg (1972) concordia curves. Insets show weighted means of selected $^{207}Pb/^{206}Pb$ ages. [Ma, million years; Ga, billion years]—Continued

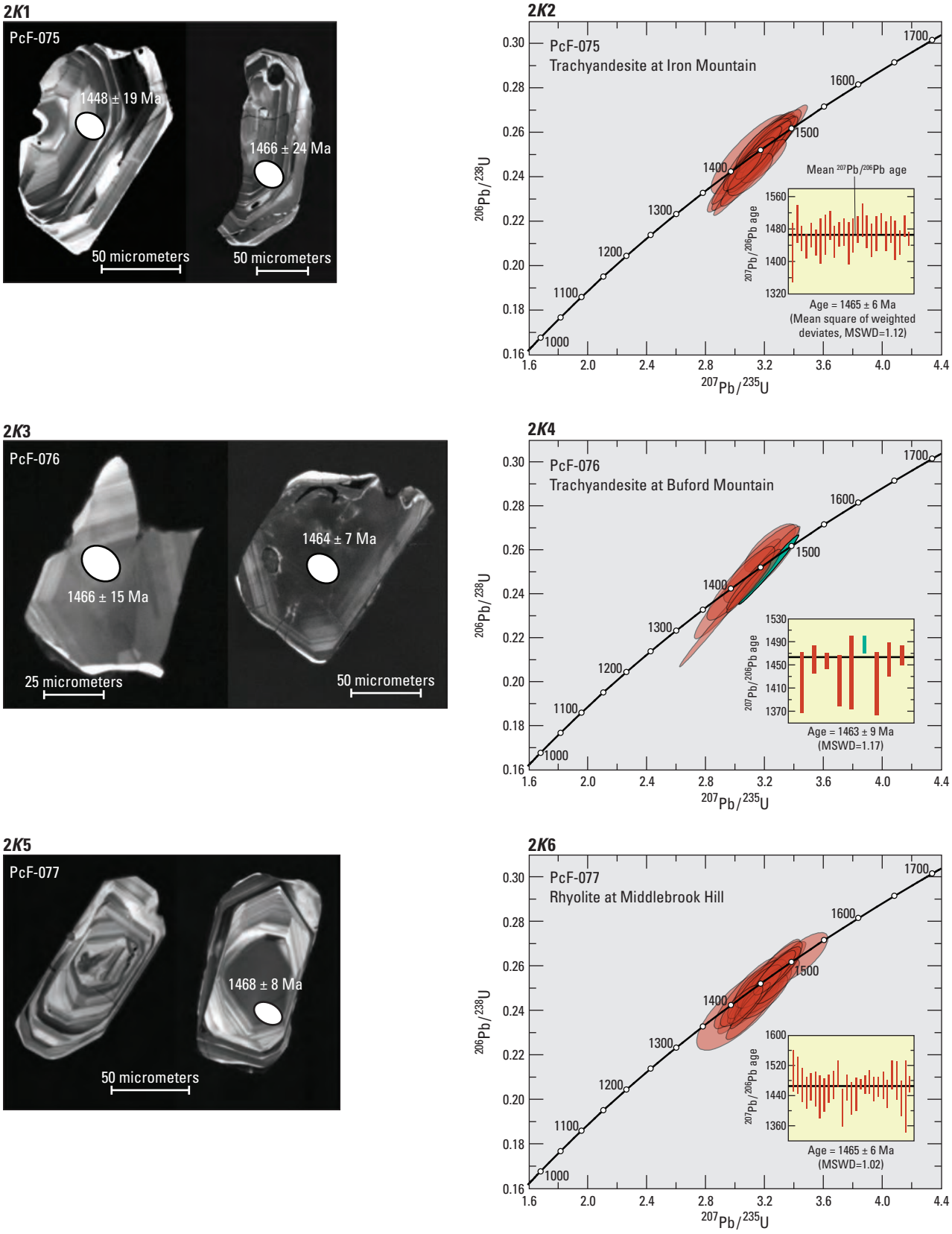

Figure 2. Representative cathodoluminescence images of zircon and backscattered electron images of titanite from igneous rocks in the St. Francois Mountains terrane, southeast Missouri. Zircon uranium-lead isotope data are plotted on Wetherill (1956) concordia curves, whereas titanite uranium-lead isotope data are plotted on Tera-Wasserburg (1972) concordia curves. Insets show weighted means of selected $^{207}Pb/^{206}Pb$ ages. [Ma, million years; Ga, billion years]—Continued

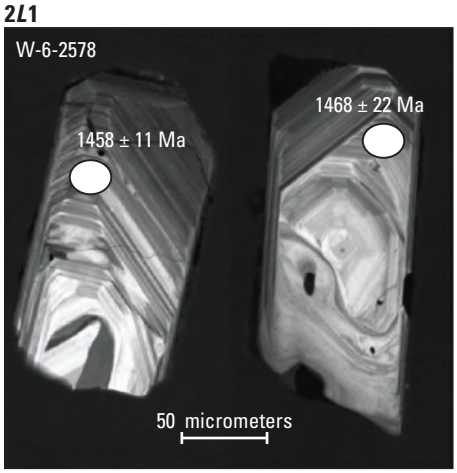

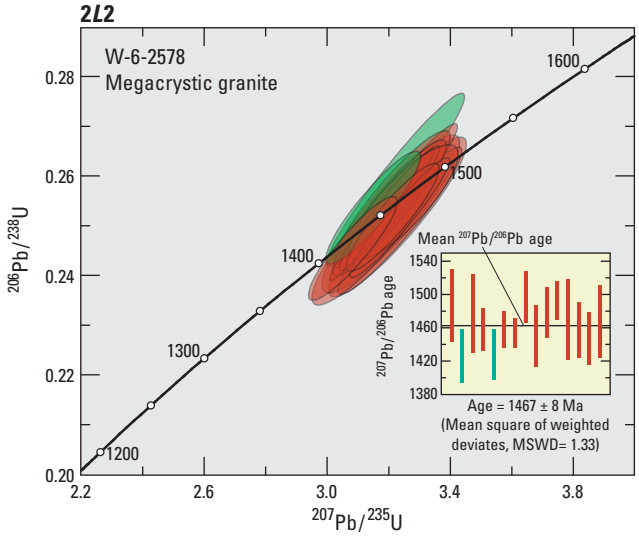

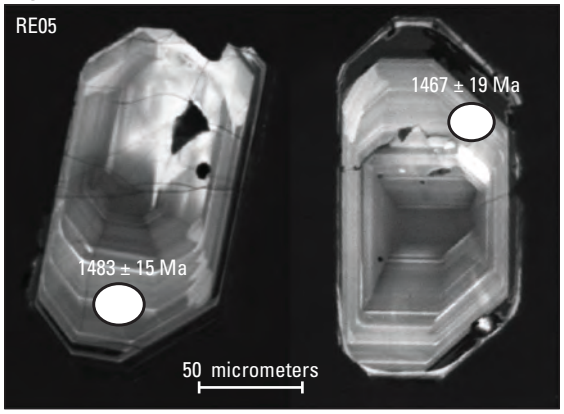

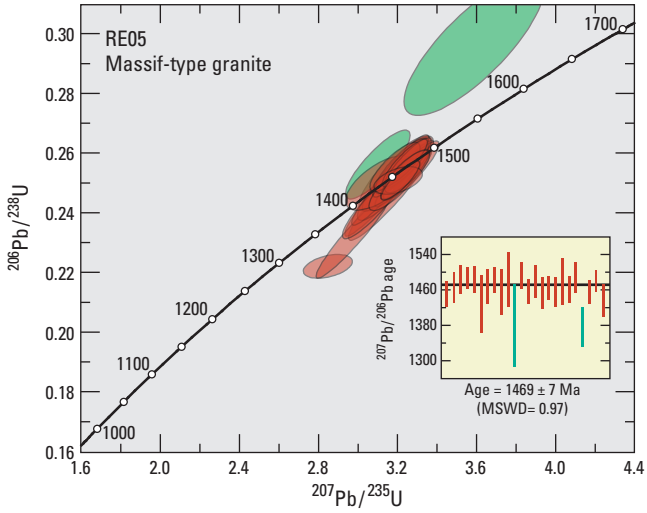

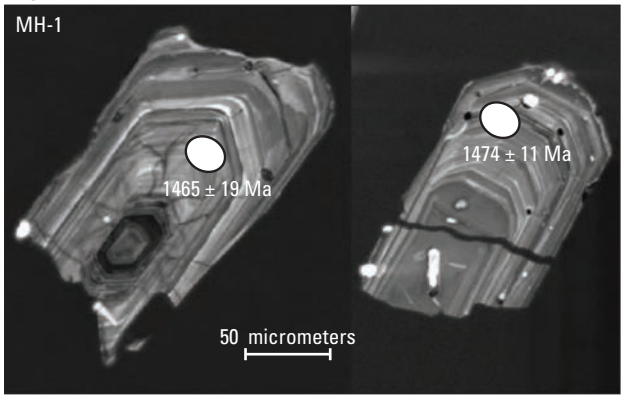

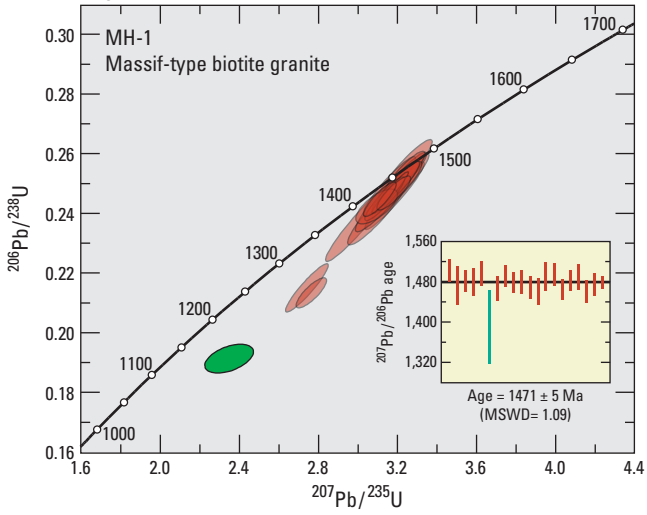

Figure 2. Representative cathodoluminescence images of zircon and backscattered electron images of titanite from igneous rocks in the St. Francois Mountains terrane, southeast Missouri. Zircon uranium-lead isotope data are plotted on Wetherill (1956) concordia curves, whereas titanite uranium-lead isotope data are plotted on Tera-Wasserburg (1972) concordia curves. Insets show weighted means of selected $^{207}Pb/^{206}Pb$ ages. [Ma, million years; Ga, billion years]—Continued

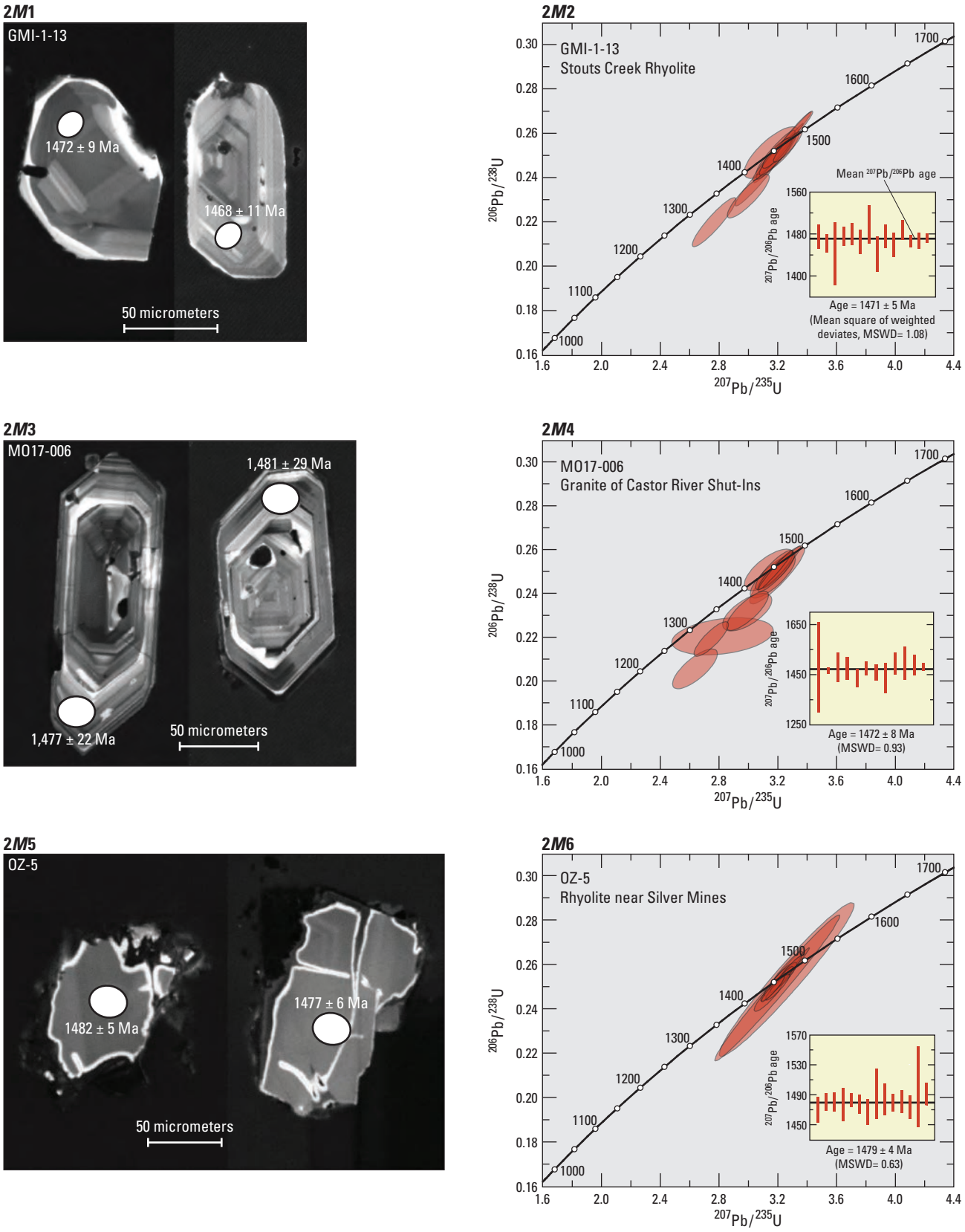

Figure 2. Representative cathodoluminescence images of zircon and backscattered electron images of titanite from igneous rocks in the St. Francois Mountains terrane, southeast Missouri. Zircon uranium-lead isotope data are plotted on Wetherill (1956) concordia curves, whereas titanite uranium-lead isotope data are plotted on Tera-Wasserburg (1972) concordia curves. Insets show weighted means of selected $^{207}Pb/^{206}Pb$ ages. [Ma, million years; Ga, billion years]—Continued

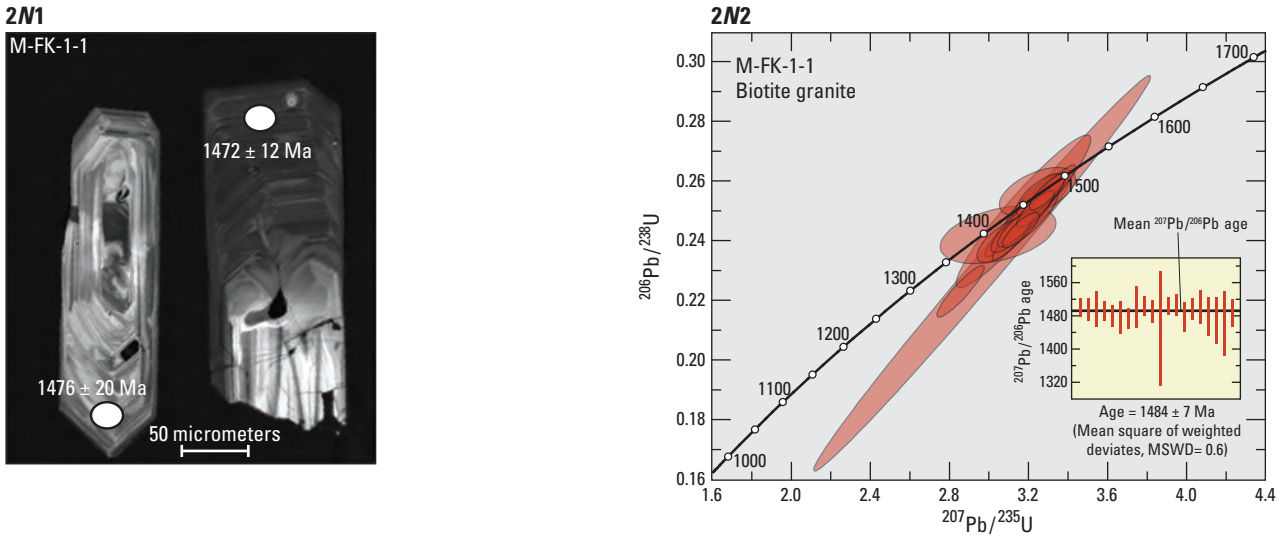

Figure 2. Representative cathodoluminescence images of zircon and backscattered electron images of titanite from igneous rocks in the St. Francois Mountains terrane, southeast Missouri. Zircon uranium-lead isotope data are plotted on Wetherill (1956) concordia curves, whereas titanite uranium-lead isotope data are plotted on Tera-Wasserburg (1972) concordia curves. Insets show weighted means of selected $^{207}Pb/^{206}Pb$ ages. [Ma, million years; Ga, billion years]—Continued

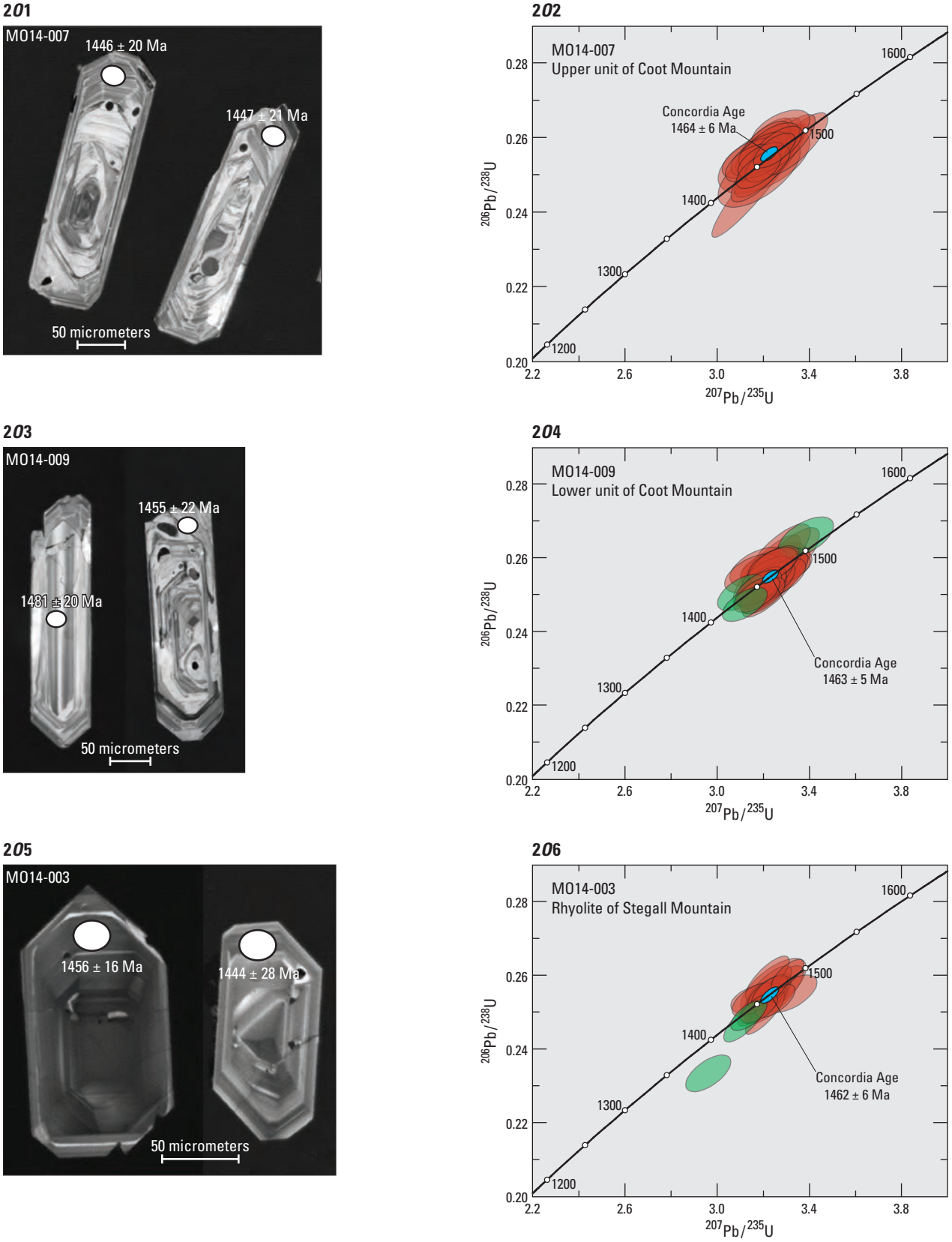

Figure 2. Representative cathodoluminescence images of zircon and backscattered electron images of titanite from igneous rocks in the St. Francois Mountains terrane, southeast Missouri. Zircon uranium-lead isotope data are plotted on Wetherill (1956) concordia curves, whereas titanite uranium-lead isotope data are plotted on Tera-Wasserburg (1972) concordia curves. Insets show weighted means of selected $^{207}Pb/^{206}Pb$ ages. [Ma, million years; Ga, billion years]—Continued

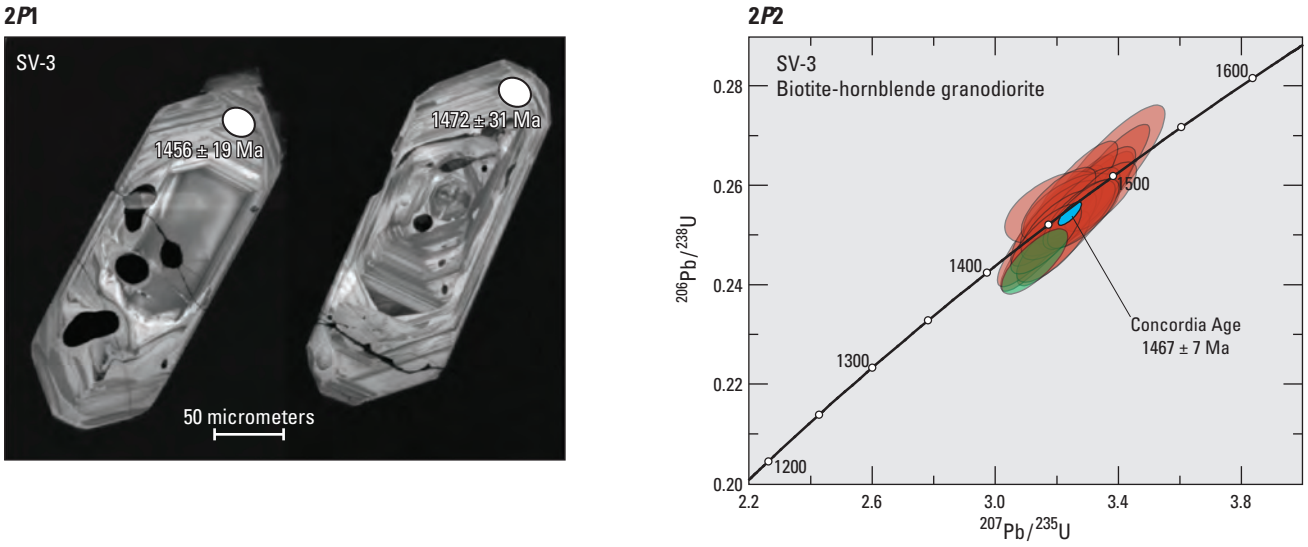

Figure 2. Representative cathodoluminescence images of zircon and backscattered electron images of titanite from igneous rocks in the St. Francois Mountains terrane, southeast Missouri. Zircon uranium-lead isotope data are plotted on Wetherill (1956) concordia curves, whereas titanite uranium-lead isotope data are plotted on Tera-Wasserburg (1972) concordia curves. Insets show weighted means of selected $^{207}Pb/^{206}Pb$ ages. [Ma, million years; Ga, billion years]—Continued

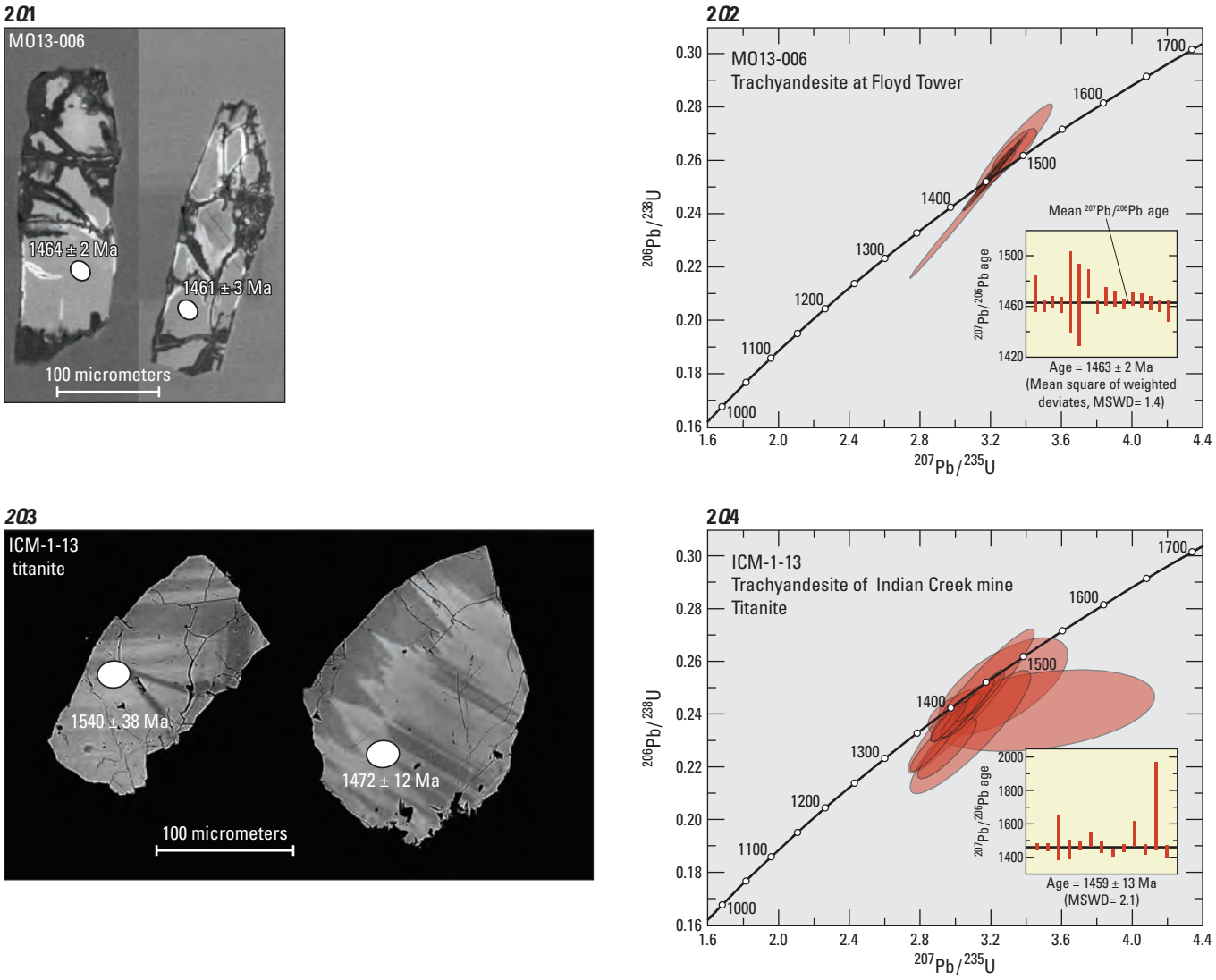

Figure 2. Representative cathodoluminescence images of zircon and backscattered electron images of titanite from igneous rocks in the St. Francois Mountains terrane, southeast Missouri. Zircon uranium-lead isotope data are plotted on Wetherill (1956) concordia curves, whereas titanite uranium-lead isotope data are plotted on Tera-Wasserburg (1972) concordia curves. Insets show weighted means of selected $^{207}Pb/^{206}Pb$ ages. [Ma, million years; Ga, billion years]—Continued

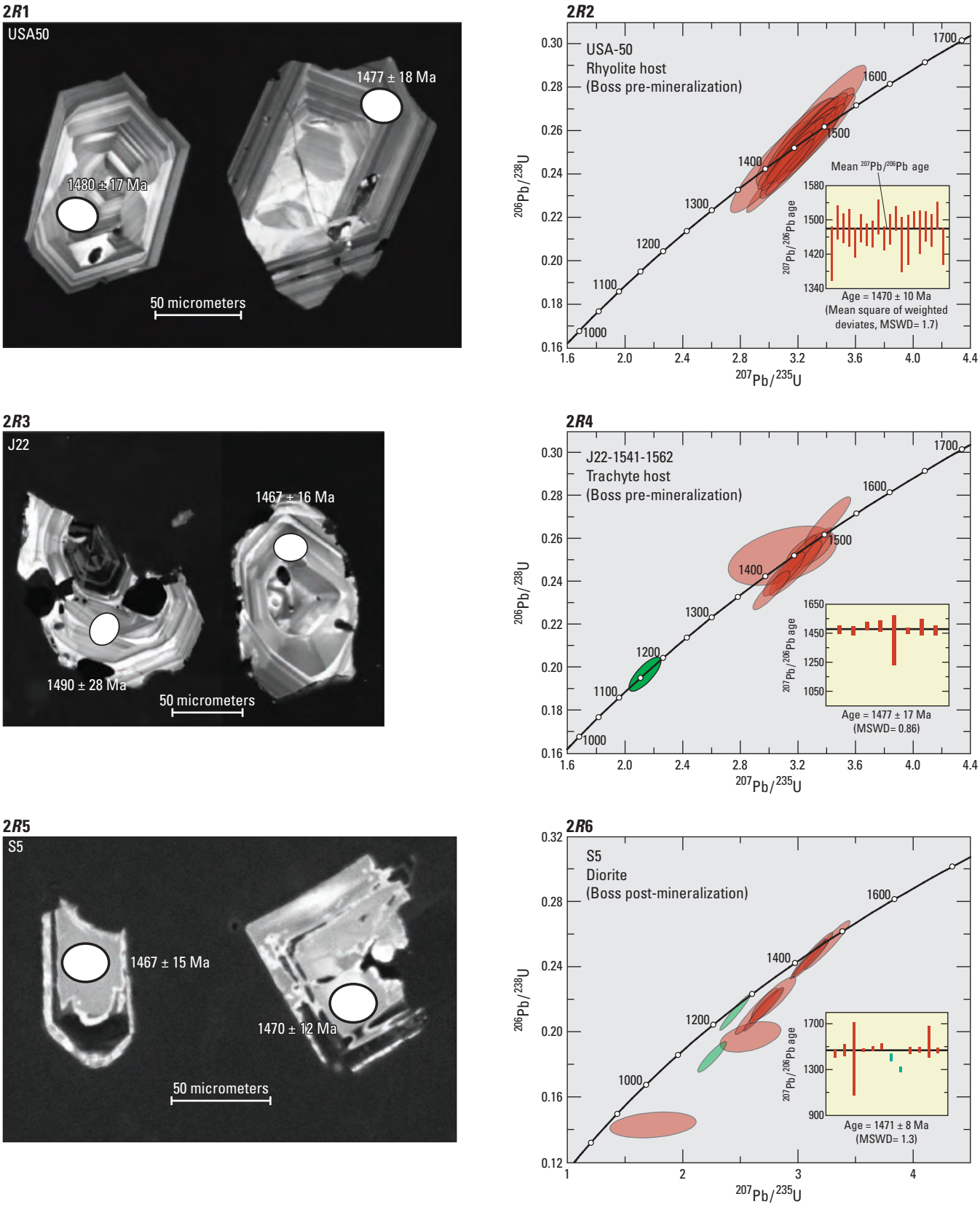

Figure 2. Representative cathodoluminescence images of zircon and backscattered electron images of titanite from igneous rocks in the St. Francois Mountains terrane, southeast Missouri. Zircon uranium-lead isotope data are plotted on Wetherill (1956) concordia curves, whereas titanite uranium-lead isotope data are plotted on Tera-Wasserburg (1972) concordia curves. Insets show weighted means of selected $^{207}Pb/^{206}Pb$ ages. [Ma, million years; Ga, billion years]—Continued

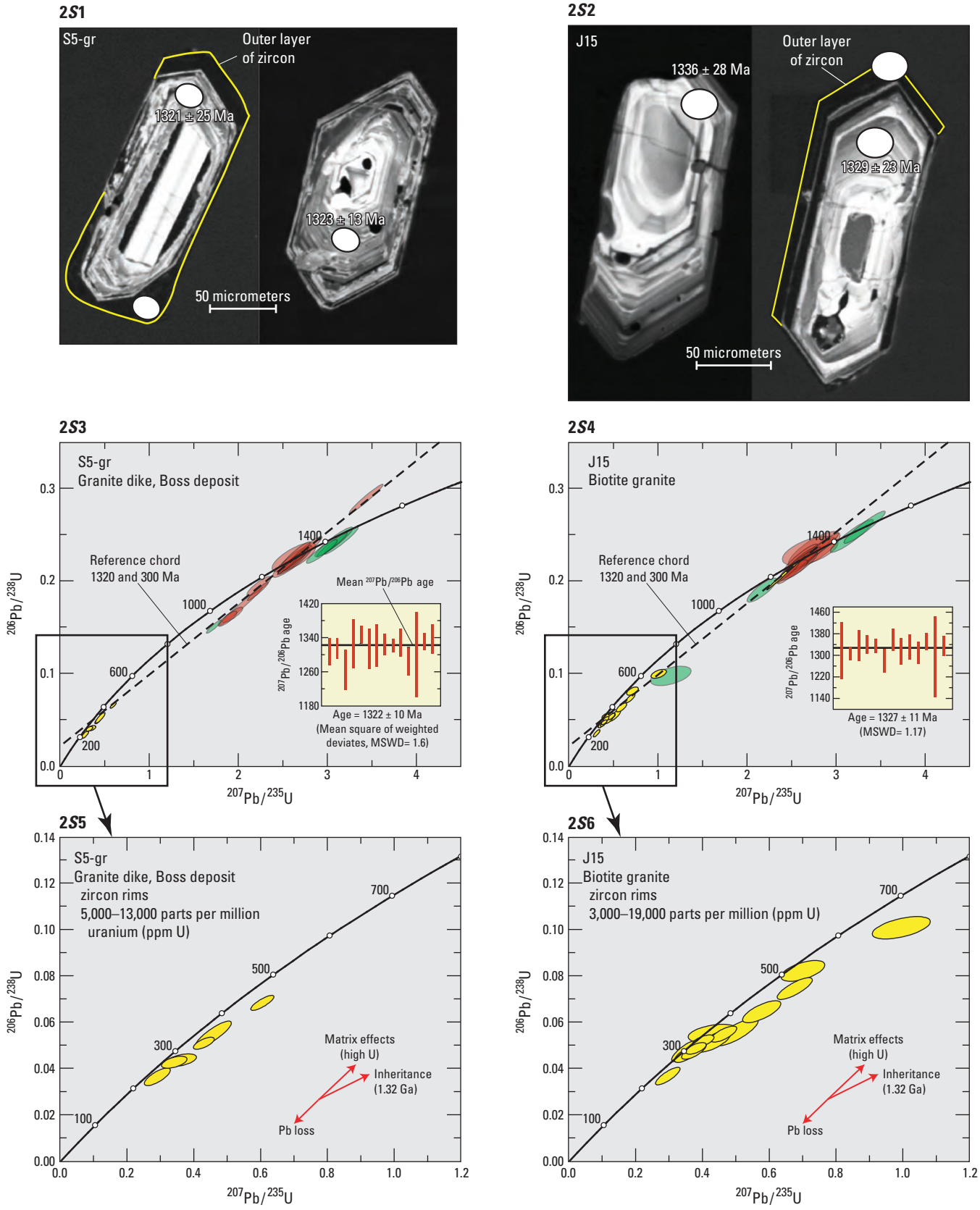

Figure 2. Representative cathodoluminescence images of zircon and backscattered electron images of titanite from igneous rocks in the St. Francois Mountains terrane, southeast Missouri. Zircon uranium-lead isotope data are plotted on Wetherill (1956) concordia curves, whereas titanite uranium-lead isotope data are plotted on Tera-Wasserburg (1972) concordia curves. Insets show weighted means of selected $^{207}Pb/^{206}Pb$ ages. [Ma, million years; Ga, billion years]—Continued

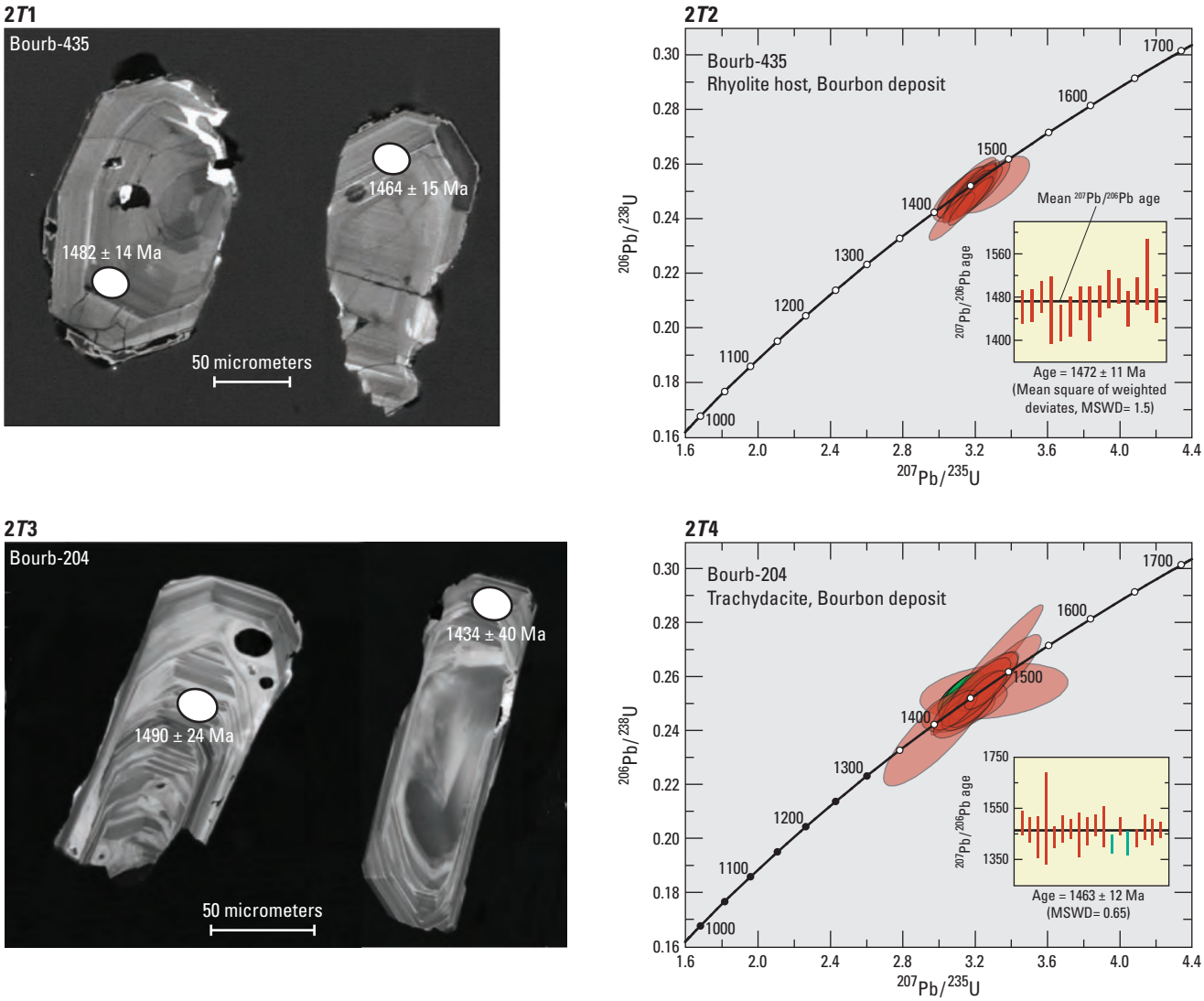

Figure 2. Representative cathodoluminescence images of zircon and backscattered electron images of titanite from igneous rocks in the St. Francois Mountains terrane, southeast Missouri. Zircon uranium-lead isotope data are plotted on Wetherill (1956) concordia curves, whereas titanite uranium-lead isotope data are plotted on Tera-Wasserburg (1972) concordia curves. Insets show weighted means of selected $^{207}Pb/^{206}Pb$ ages. [Ma, million years; Ga, billion years]—Continued

Table 3. SHRIMP-RG U-Th-Pb isotopic data and dates for two samples of Mesoproterozoic igneous rock from the St. Francois Mountains terrane, southeast Missouri.

[Errors are 1 sigma unless otherwise specified. Struckthrough data are omitted from the weighted mean based on percent common Pb. Pb* denotes radiogenic lead. $^{204}Pb/^{206}Pb$, ratio of the abundances of the mass 204 isotope of lead to that of the mass 206 isotope of lead; %, percent; $^{207}Pb/^{206}Pb$, ratio of the abundances of the mass 207 isotope of lead to that of the mass 206 isotope of lead; $^{208}Pb/^{206}Pb$, ratio of the abundances of the mass 208 isotope of lead to that of the mass 206 isotope of lead; $^{206}Pb/^{238}U$, ratio of the abundances of the mass 206 isotope of lead to that of the mass 238 isotope of uranium; ^{207}Pb, mass 207 isotope of lead; ^{206}Pb, mass 206 isotope of lead; U ppm, uranium abundance in parts per million; Th ppm, thorium abundance in parts per million; $^{232}Th/^{238}U$, ratio of the abundances of the mass 232 isotope of thorium to that of the mass 238 isotope of uranium; Ma, million years; $^{238}U/^{206}Pb$, ratio of the abundances of the mass 238 isotope of uranium to that of the mass 206 isotope of lead; $^{207}Pb/^{235}U$, ratio of the abundances of the mass 207 isotope of lead to that of the mass 235 isotope of uranium]

Spot Name	$^{204}Pb/^{206}Pb$	% error	$^{207}Pb/^{206}Pb$	% error	$^{208}Pb/^{206}Pb$	% error	$^{206}Pb/^{238}U$	% error	$^{206}Pb/^{238}U$ calibration constant	% error	^{207}Pb-corrected $^{204}Pb/^{206}Pb$	^{207}Pb-corrected common ^{206}Pb (%)	U ppm	Th ppm	^{207}Pb-corrected ^{206}Pb* ppm	$^{232}Th/^{238}U$	^{207}Pb corrected $^{206}Pb/^{238}U$ age, Ma
MO16-015-1	0.0020	9.0	0.1148	5.0	0.2362	~~10.3~~	~~0.4073~~	~~1.6~~	~~0.0118~~	~~5.5~~	~~0.0030~~	~~5.1~~	~~141.2~~	~~142.3~~	~~20.10~~	~~1.0410~~	~~988.49~~
MO16-015-2	0.0004	19.9	0.0959	0.6	0.2024	4.1	0.4532	1.5	0.0142	2.9	0.0011	1.8	231.5	167.4	41.00	0.7470	1,208.31
MO16-015-3	0.0003	22.9	0.0954	0.7	0.1967	5.0	0.4711	3.3	0.0137	1.8	0.0012	2.0	190.9	148.1	32.45	0.8015	1,163.85
MO16-015-4	0.0023	6.3	0.1202	4.2	0.2523	10.3	0.4850	4.0	0.0153	1.0	0.0027	4.4	192.9	99.8	35.88	0.5344	1,263.65
MO16-015-5	0.0006	16.6	0.0979	1.9	0.1803	8.7	0.5289	1.9	0.0149	2.5	0.0011	1.8	187.4	159.0	34.88	0.8765	1,264.24
MO16-015-6	0.0003	31.2	0.0968	0.8	0.1942	5.7	0.4495	0.4	0.0135	3.4	0.0013	2.2	172.3	137.4	28.93	0.8239	1,150.63
MO16-015-7	0.0006	17.7	0.0988	0.8	0.1945	7.1	0.4223	3.6	0.0147	1.1	0.0012	2.0	162.8	110.9	29.77	0.7040	1,244.48
MO16-015-8	~~0.0036~~	~~5.3~~	~~0.1335~~	~~9.5~~	~~0.3185~~	~~14.7~~	~~0.5319~~	~~3.3~~	~~0.0159~~	~~1.9~~	~~0.0035~~	~~5.8~~	~~185.7~~	~~152.4~~	~~35.39~~	~~0.8476~~	~~1,291.56~~
MO16-015−9	0.0002	41.2	0.0967	0.8	0.2116	10.1	0.4546	2.2	0.0147	1.8	0.0010	1.7	148.5	164.7	27.25	1.1455	1,247.84
MO16-015-10	0.0007	14.2	0.1021	0.7	0.1974	5.4	0.5534	3.3	0.0167	1.2	0.0009	1.5	193.4	103.2	40.35	0.5511	1,402.13
MO16-015-11	0.0110	3.0	0.1721	4.9	0.4486	~~9.8~~	~~0.4728~~	~~2.8~~	~~0.0115~~	~~1.4~~	~~0.0072~~	~~12.4~~	~~140.0~~	~~128.2~~	~~17.83~~	~~0.9459~~	~~891.14~~
MO16-015-12	0.0009	11.7	0.1020	1.4	0.2181	9.6	0.4812	2.7	0.0150	1.6	0.0014	2.3	189.7	183.5	35.29	0.9993	1,263.46
MO16-015-13	0.0025	6.0	0.1202	6.0	0.2628	8.6	0.4112	1.6	0.0132	3.5	0.0031	5.3	226.2	158.8	35.90	0.7253	1,093.00
~~MO16-015-14~~	0.0036	6.9	0.1314	2.9	0.2724	9.7	0.4011	2.8	0.0143	0.6	0.0037	~~6.3~~	~~108.4~~	~~137.0~~	~~18.37~~	~~1.3060~~	~~1,160.87~~
MO16-015-015	0.0010	11.7	0.1012	2.2	0.1888	5.9	0.4704	4.0	0.0155	1.3	0.0012	2.0	176.7	93.8	34.05	0.5484	1,304.61
MO16-015-16	0.0006	19.6	0.0958	1.6	0.1918	12.4	0.5360	1.7	0.0163	1.7	0.0006	0.9	168.4	132.7	34.62	0.8136	1,382.79
MO16-015-17	0.0007	10.3	0.0946	0.6	0.2198	8.1	0.4478	2.0	0.0130	3.7	0.0013	2.1	294.2	207.4	47.64	0.7283	1,113.07
MO16-015-18	0.0011	13.6	0.1058	3.0	0.1893	12.6	0.3564	3.5	0.0125	2.4	0.0022	3.7	106.8	121.1	16.33	1.1718	1,056.03
MO16-015-19	0.0003	27.6	0.0994	2.3	0.1597	1.5	0.5124	4.3	0.0162	1.7	0.0009	1.4	161.4	86.6	32.64	0.5545	1,362.77
MO16-015-20	0.0029	7.0	0.1213	~~4.5~~	~~0.2703~~	~~9.5~~	~~0.3461~~	~~5.2~~	~~0.0116~~	~~1.7~~	~~0.0035~~	~~6.0~~	~~134.3~~	~~129.1~~	~~18.60~~	~~0.9936~~	~~963.77~~
MO16-015-21	0.0003	23.5	0.0988	1.5	0.1936	1.2	0.4487	2.2	0.0136	1.4	0.0015	2.4	243.0	163.6	40.89	0.6955	1,153.16
MO16-015-22	0.0016	9.0	0.1134	2.0	0.2470	9.0	0.4888	5.5	0.0154	2.2	0.0021	3.5	133.5	145.3	25.20	1.1244	1,280.54
MO16-015-23	0.0001	65.0	0.0953	0.7	0.1730	1.4	0.5290	3.4	0.0165	1.5	0.0005	0.8	174.7	94.5	36.31	0.5590	1,397.00
MO16-015-24	0.0003	22.5	0.0971	0.7	0.1713	4.0	0.4476	4.3	0.0152	1.0	0.0009	1.5	171.6	163.7	32.67	0.9854	1,290.38
MO16-001-1	0.0002	29.8	0.0973	0.6	0.1658	1.1	0.4936	2.9	0.0157	0.8	0.0008	1.4	341.6	178.7	67.32	0.5404	1,331.42
MO16-001-2	0.0002	43.3	0.0989	0.7	0.1552	6.2	0.4866	2.3	0.0144	2.7	0.0013	2.1	192.3	89.2	~~34.44~~	~~0.4790~~	~~1,220.68~~
MO16-001-3	0.0000	89.7	0.0947	0.5	0.1531	4.2	0.4664	1.4	0.0161	1.4	0.0005	0.9	344.6	162.5	69.89	0.4869	1,366.32
MO16-001-4	0.0001	55.1	0.0937	0.6	0.1595	1.2	0.4549	3.5	0.0158	2.9	0.0005	0.9	287.5	169.6	57.25	0.6095	1,344.11
MO16-001-5	~~0.0005~~	~~13.5~~	~~0.0989~~	~~0.9~~	~~0.1794~~	~~9.1~~	~~0.4175~~	~~2.0~~	~~0.0139~~	~~0.8~~	~~0.0014~~	~~2.3~~	~~331.6~~	~~287.4~~	~~57.28~~	~~0.8954~~	~~1181.14~~
MO16-001-6	0.0001	45.5	0.0964	0.7	0.1538	1.3	0.5194	2.3	0.0162	2.7	0.0006	1.1	217.9	105.9	44.23	0.5019	1,367.50
MO16-001-7	0.0002	25.9	0.0957	1.2	0.1712	8.0	0.4294	2.4	0.0145	0.9	0.0010	1.7	301.1	155.9	54.64	0.5348	1,235.62
MO16-001-8	0.0001	94.4	0.0971	0.7	0.1436	9.9	0.4648	3.3	0.0152	0.6	0.0009	1.6	194.4	84.0	36.91	0.4467	1,287.65
MO16-001−9	0.0003	24.4	0.0943	0.7	0.1493	1.2	0.5536	1.9	0.0161	1.2	0.0005	0.8	285.7	128.4	58.06	0.4643	1,368.86
MO16-001-10	0.0002	48.2	0.0998	0.9	0.2137	10.5	0.4812	0.6	0.0140	0.7	~~0.0014~~	~~2.4~~	~~114.1~~	~~100.2~~	~~19.76~~	~~0.9071~~	~~1,183.75~~
MO16-001-12	0.0000	205	0.0932	0.7	0.1454	3.1	0.5002	3.5	0.0167	0.5	0.0003	0.4	230.0	111.3	48.47	0.4999	1,414.34
MO16-001-13	0.0002	24.3	0.0936	1.3	0.1743	7.8	0.4680	2.7	0.0149	2.0	0.0008	1.3	324.3	200.4	60.53	0.6385	1,267.58
MO16-001-14	0.0001	50.3	0.0937	1.4	0.1545	1.2	0.5189	2.4	0.0165	0.8	0.0003	0.6	366.0	210.4	76.38	0.5938	1,402.07
MO16-001-15	0.0000	130	0.0927	0.5	0.1557	3.0	0.4853	2.9	0.0159	0.7	0.0004	0.7	393.5	198.0	78.95	0.5199	1,353.11
MO16-001-16	0.0001	40.1	0.0917	1.9	0.1502	2.8	0.5218	2.5	0.0163	1.1	0.0002	0.4	306.6	151.3	63.29	0.5099	1,388.48

Table 3. SHRIMP-RG U-Th-Pb isotopic data and dates for two samples of Mesoproterozoic igneous rock from the St. Francois Mountains terrane, southeast Missouri.—Continued

[Errors are 1 sigma unless otherwise specified. Struckthrough data are omitted from the weighted mean based on percent common Pb. Pb* denotes radiogenic lead. $^{204}Pb/^{206}Pb$, ratio of the abundances of the mass 204 isotope of lead to that of the mass 206 isotope of lead; %, percent; $^{207}Pb/^{206}Pb$, ratio of the abundances of the mass 207 isotope of lead to that of the mass 206 isotope of lead; $^{208}Pb/^{206}Pb$, ratio of the abundances of the mass 208 isotope of lead to that of the mass 206 isotope of lead; $^{206}Pb/^{238}U$, ratio of the abundances of the mass 206 isotope of lead to that of the mass 238 isotope of uranium; ^{207}Pb, mass 207 isotope of lead; ^{206}Pb, mass 206 isotope of lead; U ppm, uranium abundance in parts per million; Th ppm, thorium abundance in parts per million; $^{232}Th/^{238}U$, ratio of the abundances of the mass 232 isotope of thorium to that of the mass 238 isotope of uranium; Ma, million years; $^{238}U/^{206}Pb$, ratio of the abundances of the mass 238 isotope of uranium to that of the mass 206 isotope of lead; $^{207}Pb/^{235}U$, ratio of the abundances of the mass 207 isotope of lead to that of the mass 235 isotope of uranium]

Spot Name	1-sigma error	^{204}Pb-corrected $^{207}Pb/^{206}Pb$ age, Ma	1-sigma error	^{207}Pb-corrected $^{206}Pb^*/^{238}U$	% error	Total $^{238}U/^{206}Pb$	% error	Total $^{207}Pb/^{206}Pb$	% error	^{204}Pb-corrected $^{238}U/^{206}Pb^*$	% error	^{204}Pb-corrected $^{207}Pb^*/^{206}Pb^*$	% error	^{204}Pb-corrected $^{207}Pb^*/^{235}U$	% error	^{204}Pb-corrected $^{206}Pb^*/^{238}U$	% error	error correlation
MO16-015-1	53.05	1,345.30	~~146.81~~	~~0.1657~~	~~1.8~~	~~5.7258~~	~~5.5~~	~~0.1148~~	~~5.0~~	~~5.9315~~	~~5.5~~	~~0.0863~~	~~7.6~~	~~2.0065~~	~~9.4~~	~~0.1686~~	~~5.5~~	~~0.59~~
MO16-015-2	33.88	1,442.72	25.03	0.2062	1.0	4.7621	2.9	0.0959	0.6	4.7913	2.9	0.0908	1.3	2.6134	3.2	0.2087	2.9	0.91
MO16-015-3	20.72	1,445.87	25.68	0.1979	0.6	4.9535	1.8	0.0954	0.7	4.9803	1.9	0.0910	1.3	2.5184	2.3	0.2008	1.9	0.81
MO16-015-4	15.89	1,371.49	123.66	0.2166	0.4	4.4142	1.2	0.1202	4.2	4.5920	1.2	0.0875	6.4	2.6272	6.5	0.2178	1.2	0.18
MO16-015-5	31.67	1,422.03	49.96	0.2167	0.9	4.5331	2.6	0.0979	1.9	4.5771	2.6	0.0898	2.6	2.7062	3.7	0.2185	2.6	0.70
MO16-015-6	38.02	1,491.41	27.45	0.1954	1.2	5.0044	3.4	0.0968	0.8	5.0262	3.4	0.0932	1.5	2.5560	3.7	0.1990	3.4	0.92
MO16-015-7	14.60	1,447.45	32.91	0.2129	0.4	4.6030	1.2	0.0988	0.8	4.6457	1.2	0.0910	1.7	2.7020	2.1	0.2153	1.2	0.58
MO16-015-8	31.85	1,268.95	325.71	0.2218	0.9	4.2450	2.0	0.1335	9.5	~~4.5130~~	~~2.0~~	~~0.0830~~	17	~~2.5354~~	~~16.8~~	~~0.2216~~	~~2.0~~	~~0.12~~
MO16-015−9	22.51	1,501.65	29.48	0.2136	0.6	4.6016	1.9	0.0967	0.8	4.6182	1.9	0.0937	1.6	2.7968	2.4	0.2165	1.9	0.77
MO16-015-10	17.46	1483.99	30.87	0.2430	0.4	4.0522	1.3	0.1021	0.7	4.0969	1.3	0.0928	1.6	3.1234	2.1	0.2441	1.3	0.62
MO16-015-11	16.27	na	na	0.1482	0.6	5.9063	1.5	0.1721	4.9	7.2912	1.6	0.0015	816	~~0.0284~~	~~816.7~~	~~0.1372~~	~~1.6~~	~~0.00~~
MO16-015-12	20.97	1,426.20	42.74	0.2165	0.6	4.5140	1.7	0.1020	1.4	4.5789	1.7	0.0900	2.2	2.7110	2.8	0.2184	1.7	0.61
MO16-015-13	38.17	1,330.54	177.69	0.1848	1.2	5.1269	3.5	0.1202	6.0	5.3493	3.5	0.0857	9.2	2.2079	9.8	0.1869	3.5	0.36
~~MO16-015-14~~	10.23	1,226.89	131.11	0.1973	0.3	4.7506	0.8	0.1314	2.9	5.0520	0.9	0.0812	6.7	2.2168	6.7	~~0.1979~~	~~0.9~~	~~0.13~~
MO16-015-15	18.37	1,374.19	61.73	0.2243	0.5	4.3709	1.4	0.1012	2.2	4.4419	1.4	0.0876	3.2	2.7199	3.5	0.2251	1.4	0.41
MO16-015-16	23.26	1,356.77	51.97	0.2392	0.6	4.1415	1.7	0.0958	1.6	4.1855	1.7	0.0868	2.7	2.8604	3.2	0.2389	1.7	0.54
MO16-015-17	40.20	1,308.73	27.31	0.1885	1.3	5.1927	3.7	0.0946	0.6	5.2554	3.8	0.0847	1.4	2.2222	4.0	0.1903	3.8	0.94
MO16-015-18	25.02	1,421.92	84.42	0.1780	0.8	5.4087	2.4	0.1058	3.0	5.5156	2.4	0.0898	4.4	2.2456	5.0	0.1813	2.4	0.48
MO16-015-19	23.50	1,536.13	51.08	0.2354	0.6	4.1867	1.8	0.0994	2.3	4.2066	1.8	0.0954	2.7	3.1272	3.2	0.2377	1.8	0.55
MO16-015-20	17.96	~~1,196.37~~	~~159.56~~	~~0.1613~~	~~0.6~~	~~5.8292~~	~~1.8~~	~~0.1213~~	~~4.5~~	~~6.1361~~	~~1.8~~	~~0.0800~~	~~8.1~~	~~1.7971~~	~~8.3~~	~~0.1630~~	~~1.8~~	~~0.22~~
MO16-015-21	17.06	1,531.09	33.38	0.1959	0.5	4.9806	1.5	0.0988	1.5	5.0028	1.5	0.0952	1.8	2.6224	2.3	0.1999	1.5	0.65
MO16-015-22	27.97	1,455.24	65.36	0.2197	0.8	4.3901	2.2	0.1134	2.0	4.5082	2.3	0.0914	3.4	2.7958	4.1	0.2218	2.3	0.55
MO16-015-23	20.99	1,504.73	23.44	0.2420	0.5	4.1004	1.6	0.0953	0.7	4.1075	1.6	0.0938	1.2	3.1497	2.0	0.2435	1.6	0.78
MO16-015-24	13.87	1,474.87	25.52	0.2216	0.4	4.4426	1.1	0.0971	0.7	4.4675	1.1	0.0924	1.3	2.8506	1.8	0.2238	1.1	0.64
MO16-001-1	12.35	1,526.31	17.75	0.2294	0.3	4.2997	1.0	0.0973	0.6	4.3118	1.0	0.0949	0.9	3.0350	1.3	0.2319	1.0	0.72
MO16-001-2	32.51	1,557.00	24.93	0.2085	0.9	4.6951	~~2.8~~	~~0.0989~~	~~0.7~~	~~4.7089~~	~~2.8~~	~~0.0965~~	~~1.3~~	~~2.8248~~	~~3.1~~	~~0.2124~~	~~2.8~~	~~0.90~~
MO16-001-3	19.10	1,511.43	14.71	0.2361	0.5	4.1986	1.4	0.0947	0.5	4.2015	1.5	0.0942	0.8	3.0902	1.6	0.2380	1.5	0.88
MO16-001-4	37.90	1,477.48	17.56	0.2318	1.0	4.2759	2.9	0.0937	0.6	4.2819	2.9	0.0925	0.9	2.9783	3.1	0.2335	2.9	0.95
MO16-001-5	11.26	1,468.06	26.79	0.2011	0.3	4.8582	1.0	0.0989	0.9	~~4.8984~~	~~1.0~~	~~0.0920~~	~~1.4~~	~~2.5905~~	~~1.7~~	~~0.2041~~	~~1.0~~	~~0.57~~
MO16-001-6	36.18	1,514.72	23.13	0.2363	0.9	4.1866	2.7	0.0964	0.7	4.1969	2.7	0.0943	1.2	3.0990	3.0	0.2383	2.7	0.91
MO16-001-7	11.97	1,486.54	28.32	0.2113	0.3	4.6543	1.0	0.0957	1.2	4.6697	1.0	0.0929	1.5	2.7440	1.8	0.2141	1.0	0.56
MO16-001-8	9.37	1,548.41	24.03	0.2211	0.3	4.4522	0.7	0.0971	0.7	4.4578	0.8	0.0960	1.3	2.9703	1.5	0.2243	0.8	0.51
MO16-001−9	17.63	1,441.53	22.51	0.2366	0.5	4.1928	1.3	0.0943	0.7	4.2103	1.3	0.0908	1.2	2.9722	1.8	0.2375	1.3	0.75
MO16-001-10	10.34	1,554.92	37.25	0.2016	0.3	4.8415	0.9	0.0998	0.9	4.8618	0.9	0.0964	2.0	2.7329	~~2.2~~	~~0.2057~~	~~0.9~~	~~0.42~~
MO16-001-12	9.94	1,483.38	21.81	0.2453	0.2	4.0585	0.7	0.0932	0.7	4.0604	0.7	0.0928	1.2	3.1505	1.4	0.2463	0.7	0.54
MO16-001-13	25.45	1,438.10	29.28	0.2173	0.7	4.5439	2.1	0.0936	1.3	4.5604	2.1	0.0906	1.5	2.7390	2.6	0.2193	2.1	0.80
MO16-001-14	13.18	1,478.71	29.66	0.2430	0.3	4.0926	1.0	0.0937	1.4	4.0983	1.0	0.0926	1.6	3.1137	1.8	0.2440	1.0	0.52
MO16-001-15	11.24	1,473.60	14.18	0.2336	0.3	4.2514	0.9	0.0927	0.5	4.2533	0.9	0.0923	0.7	2.9921	1.1	0.2351	0.9	0.76
MO16-001-16	16.99	1,426.95	39.40	0.2403	0.4	4.1438	1.3	0.0917	1.9	4.1520	1.3	0.0901	2.1	2.9910	2.4	0.2408	1.3	0.52

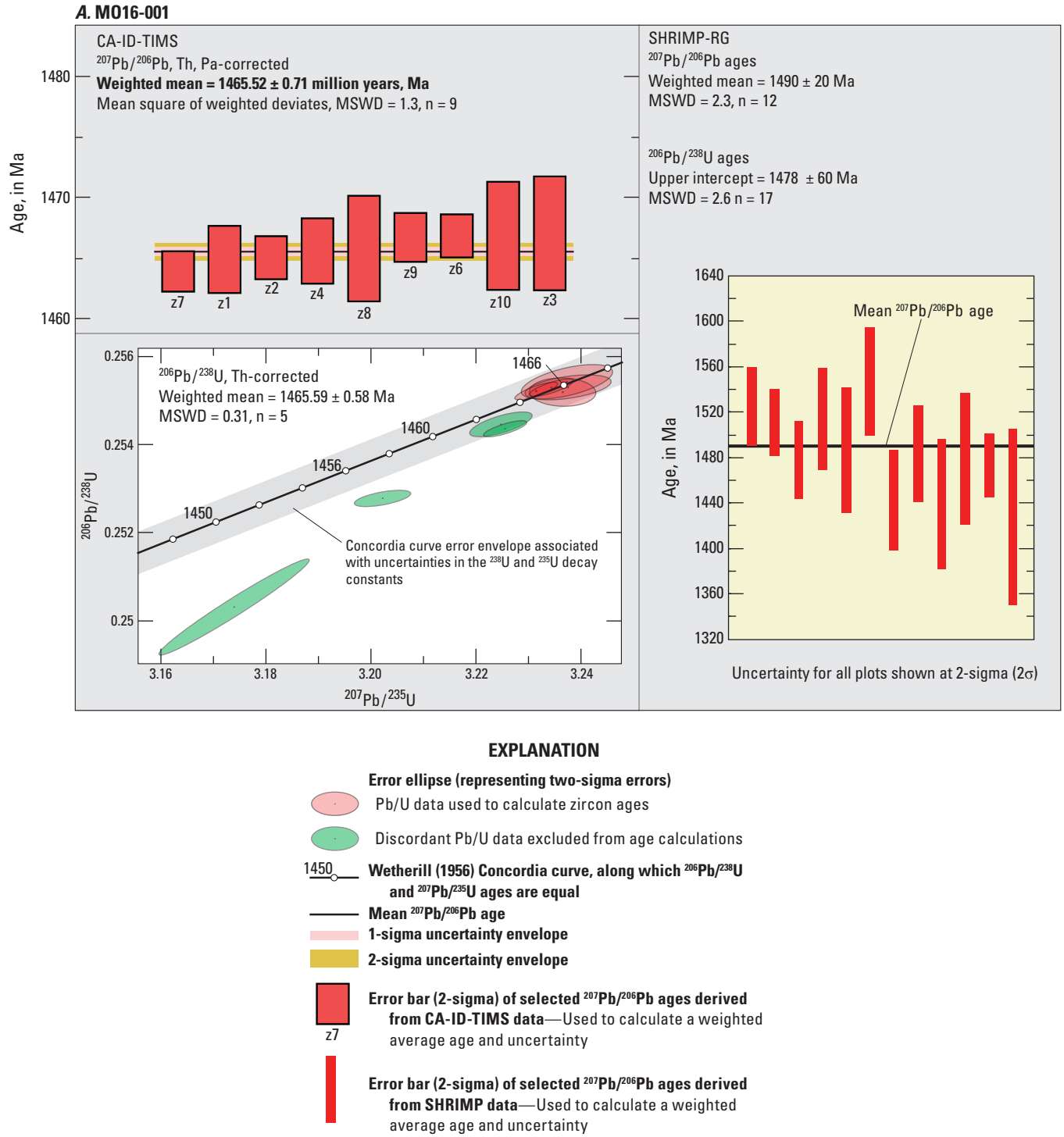

EXPLANATION

Error ellipse (representing two-sigma errors)

Pb/U data used to calculate zircon ages

Discordant Pb/U data excluded from age calculations

1450 **Wetherill (1956) Concordia curve, along which $^{206}Pb/^{238}U$ and $^{207}Pb/^{235}U$ ages are equal**

Mean $^{207}Pb/^{206}Pb$ age

1-sigma uncertainty envelope

2-sigma uncertainty envelope

z7 **Error bar (2-sigma) of selected $^{207}Pb/^{206}Pb$ ages derived from CA-ID-TIMS data**—Used to calculate a weighted average age and uncertainty

Error bar (2-sigma) of selected $^{207}Pb/^{206}Pb$ ages derived from SHRIMP data—Used to calculate a weighted average age and uncertainty

Figure 3. CA-ID-TIMS and SHRIMP-RG zircon Pb/Pb weighted mean and U/Pb concordia plots for two samples of Mesoproterozoic igneous rock from the St. Francois Mountains terrane, southeast Missouri. Preferred dates shown in bold type. [CA-ID-TIMS, chemical abrasion-isotope dilution-thermal ionization mass spectrometry; SHRIMP-RG, sensitive high resolution ion microprobe-reverse geometry; Pb, lead; U, uranium]

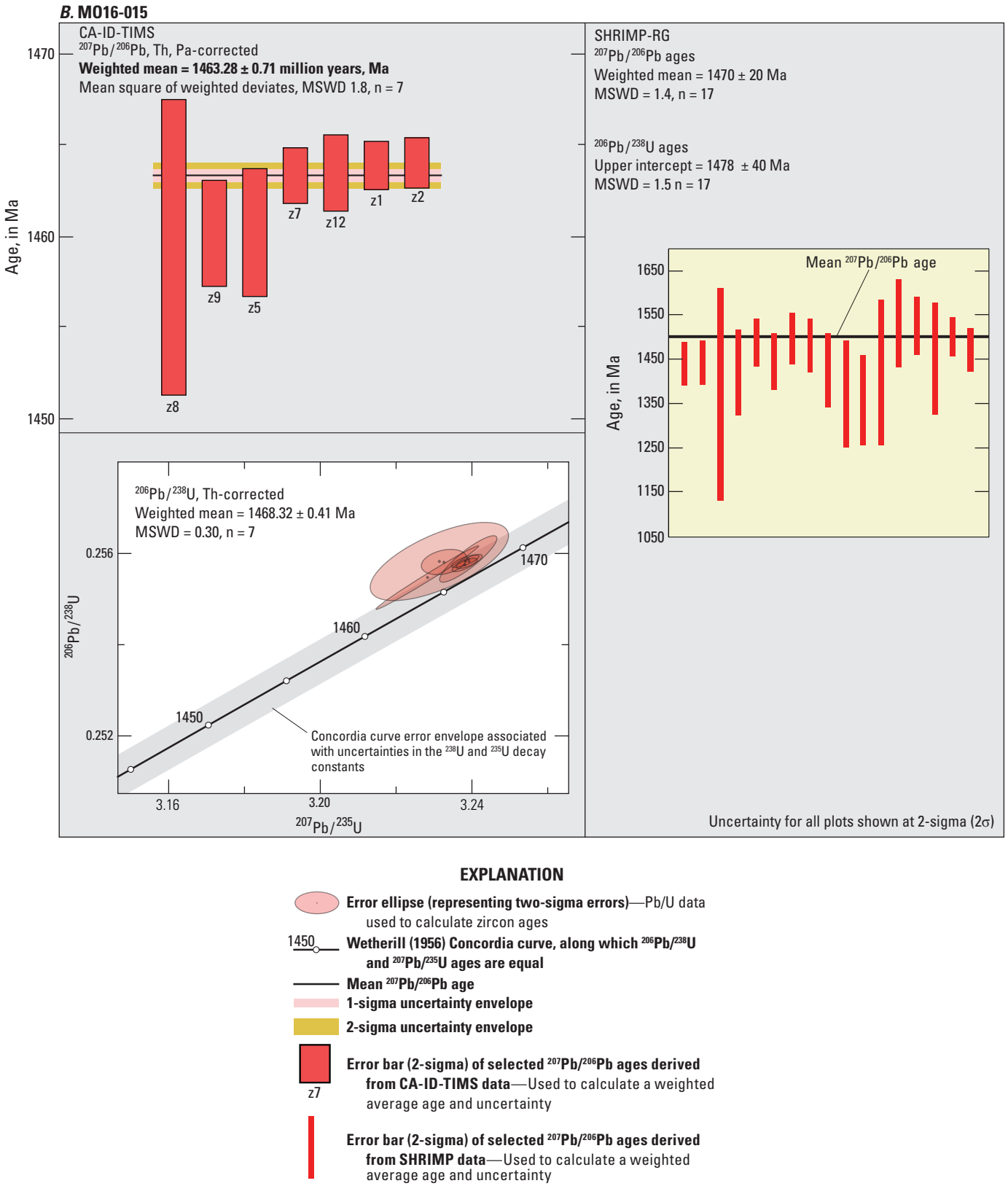

EXPLANATION

Error ellipse (representing two-sigma errors)—Pb/U data used to calculate zircon ages

1450 **Wetherill (1956) Concordia curve, along which $^{206}Pb/^{238}U$ and $^{207}Pb/^{235}U$ ages are equal**

Mean $^{207}Pb/^{206}Pb$ age

1-sigma uncertainty envelope

2-sigma uncertainty envelope

z7 **Error bar (2-sigma) of selected $^{207}Pb/^{206}Pb$ ages derived from CA-ID-TIMS data**—Used to calculate a weighted average age and uncertainty

Error bar (2-sigma) of selected $^{207}Pb/^{206}Pb$ ages derived from SHRIMP data—Used to calculate a weighted average age and uncertainty

Figure 3. CA-ID-TIMS and SHRIMP-RG zircon Pb/Pb weighted mean and U/Pb concordia plots for two samples of Mesoproterozoic igneous rock from the St. Francois Mountains terrane, southeast Missouri. Preferred dates shown in bold type. [CA-ID-TIMS, chemical abrasion-isotope dilution-thermal ionization mass spectrometry; SHRIMP-RG, sensitive high resolution ion microprobe-reverse geometry; Pb, lead; U, uranium]—Continued

Table 4. LA-ICPMS analyses of titanite from sample CLT-1-13.

[U ppm, uranium in parts per million; Th ppm, thorium in parts per million; Th/U, ratio of thorium and uranium abundances; $^{238}U/^{206}Pb$, ratio of the abundances of the mass 238 isotope of uranium to that of the mass 206 isotope of lead; +/- 2SE, two standard errors; $^{207}Pb/^{206}Pb$, ratio of the abundances of the mass 207 isotope of lead to that of the mass 206 isotope of lead; Rho, correlation coefficient between $^{238}U/^{206}Pb$ and $^{207}Pb/^{206}Pb$. Values in italics are outliers not used in age calculations]

Time resolved analysis session[1]	U ppm	Th ppm	Th/ U	$^{238}U/^{206}Pb$[2]	± 2SE	$^{207}Pb/^{206}Pb$[3]	± 2SE	Rho
				Cores				
T-8470	0.334	0.127	0.38	0.042	0.00	0.952	0.018	0.182
F = 0.8891±0.0035	0.744	0.391	0.53	0.061	0.00	0.938	0.014	0.175
	1.217	0.285	0.23	0.054	0.00	0.943	0.012	0.085
	0.864	0.491	0.57	0.097	0.01	0.927	0.012	0.127
	0.945	0.645	0.68	0.520	0.06	0.826	0.026	0.233
	6.75	1.318	0.20	0.798	0.03	0.774	0.017	−0.489
	0.421	0.358	0.85	0.108	0.01	0.918	0.017	−0.064
	0.731	0.387	0.53	0.644	0.03	0.816	0.019	−0.037
	3.23	0.365	0.11	0.320	0.04	0.876	0.015	−0.799
	0.611	0.356	0.58	0.054	0.00	0.918	0.013	0.357
	2.962	0.777	0.26	0.367	0.01	0.872	0.016	0.054
	0.363	0.441	1.21	0.057	0.00	0.925	0.012	0.262
	0.853	0.342	0.40	0.071	0.01	0.942	0.015	0.059
	1.127	0.503	0.45	*1.069*	*0.05*	*0.662*	*0.028*	*0.244*
	0.562	0.382	0.68	0.084	0.01	0.937	0.015	0.150
	7.69	1.908	0.25	*3.886*	*0.17*	*0.169*	*0.011*	*−0.235*
	8.07	2.19	0.27	0.729	0.02	0.798	0.012	0.353
	4.52	0.778	0.17	*1.740*	*0.10*	*0.596*	*0.021*	*−0.315*
	4.06	0.925	0.23	0.392	0.02	0.853	0.012	−0.088
	0.283	0.321	1.13	0.454	0.09	0.859	0.061	0.857
	0.345	0.183	0.53	0.021	0.00	0.950	0.014	0.521
	0.325	0.704	2.17	*0.175*	*0.01*	*0.837*	*0.023*	*0.183*
	1.19	0.142	0.12	*0.559*	*0.13*	*0.782*	*0.042*	*−0.801*
	0.494	0.551	1.12	0.078	0.00	0.910	0.020	0.221
	0.849	0.379	0.45	0.122	0.01	0.923	0.012	0.328
	0.278	0.1027	0.37	0.318	0.16	0.869	0.063	−0.104
	0.869	0.334	0.38	0.080	0.01	0.934	0.016	0.282
	8.95	1.011	0.11	0.896	0.02	0.773	0.012	0.230
	1.69	0.397	0.23	0.087	0.01	0.916	0.013	−0.163
	0.625	0.243	0.39	0.432	0.03	0.857	0.034	0.235
	2.14	0.384	0.18	0.143	0.00	0.925	0.016	0.129
	2.734	0.442	0.16	0.118	0.00	0.917	0.011	0.184
	2.79	0.657	0.24	0.320	0.02	0.885	0.011	0.329

Table 4. LA-ICPMS analyses of titanite from sample CLT-1-13.—Continued

[U ppm, uranium in parts per million; Th ppm, thorium in parts per million; Th/U, ratio of thorium and uranium abundances; $^{238}U/^{206}Pb$, ratio of the abundances of the mass 238 isotope of uranium to that of the mass 206 isotope of lead; +/- 2SE, two standard errors; $^{207}Pb/^{206}Pb$, ratio of the abundances of the mass 207 isotope of lead to that of the mass 206 isotope of lead; Rho, correlation coefficient between $^{238}U/^{206}Pb$ and $^{207}Pb/^{206}Pb$. Values in italics are outliers not used in age calculations]

Time resolved analysis session[1]	U ppm	Th ppm	Th/ U	$^{238}U/^{206}Pb$[2]	± 2SE	$^{207}Pb/^{206}Pb$[3]	± 2SE	Rho
				Cores				
T-8472	1.144	0.801	0.70	0.076	0.002	0.934	0.013	−0.023
F = 0.8924±0.0064	1.41	0.586	0.42	0.200	0.020	0.911	0.014	−0.064
	2.9	0.377	0.13	0.267	0.049	0.887	0.015	−0.710
	3.09	0.424	0.14	1.055	0.039	0.732	0.012	−0.445
	3.51	1.694	0.48	0.794	0.021	0.803	0.016	0.259
	5.39	2.28	0.42	0.607	0.046	0.815	0.013	−0.309
	4.68	1.176	0.25	0.733	0.026	0.785	0.010	−0.224
	4.43	0.471	0.11	0.558	0.059	0.825	0.015	−0.723
	3.57	2.03	0.57	1.075	0.049	0.718	0.014	0.378
	2.63	1.115	0.42	*0.939*	*0.067*	*0.674*	*0.014*	*−0.092*
	3.05	0.448	0.15	0.813	0.021	0.773	0.015	0.088
	3.65	0.274	0.08	0.261	0.016	0.898	0.010	0.016
	4.52	1.326	0.29	1.338	0.075	0.687	0.014	−0.415
	3.27	0.628	0.19	0.177	0.005	0.911	0.012	0.399
	3.51	1.143	0.33	1.250	0.081	0.682	0.017	−0.039
	1.855	0.438	0.24	0.078	0.004	0.935	0.010	0.443
	1.56	0.71	0.46	0.171	0.009	0.9006	0.0097	−0.146
	4.48	0.578	0.13	*1.821*	*0.157*	*0.588*	*0.033*	*−0.771*
	0.893	0.276	0.31	0.028	0.001	0.9426	0.0079	−0.079
	0.491	0.1287	0.26	0.031	0.002	0.942	0.011	−0.123
	8.06	1.618	0.20	0.432	0.017	0.8656	0.0098	0.016
	4.85	0.543	0.11	0.664	0.021	0.8101	0.0095	0.603
	3.37	0.833	0.25	0.576	0.060	0.816	0.016	−0.447
	3.258	0.683	0.21	0.370	0.017	0.869	0.013	0.329
	0.711	0.421	0.59	0.068	0.004	0.922	0.010	0.468
	0.207	0.167	0.81	0.112	0.014	0.904	0.040	−1.000
	0.488	0.416	0.85	0.065	0.004	0.934	0.010	−0.018
	0.768	0.391	0.51	0.102	0.003	0.93	0.015	0.236
	0.766	0.337	0.44	0.089	0.006	0.92	0.011	0.149
	0.952	0.343	0.36	0.191	0.012	0.887	0.018	−0.090
	7.23	0.598	0.08	*2.746*	*0.162*	*0.389*	*0.022*	*−0.740*
	4.29	0.58	0.14	*2.187*	*0.114*	*0.475*	*0.023*	*−0.732*
	2.433	0.316	0.13	0.259	0.035	0.894	0.014	−0.640
	2.14	0.848	0.40	*0.637*	*0.191*	*0.726*	*0.073*	*−0.891*
	1.76	0.191	0.11	*0.372*	*0.090*	0.828	0.019	−0.834
Median values	**1.8**	**0.45**	**0.32**					

Table 4. LA-ICPMS analyses of titanite from sample CLT-1-13.—Continued

[U ppm, uranium in parts per million; Th ppm, thorium in parts per million; Th/U, ratio of thorium and uranium abundances; $^{238}U/^{206}Pb$, ratio of the abundances of the mass 238 isotope of uranium to that of the mass 206 isotope of lead; +/- 2SE, two standard errors; $^{207}Pb/^{206}Pb$, ratio of the abundances of the mass 207 isotope of lead to that of the mass 206 isotope of lead; Rho, correlation coefficient between $^{238}U/^{206}Pb$ and $^{207}Pb/^{206}Pb$. Values in italics are outliers not used in age calculations]

Time resolved analysis session[1]	U ppm	Th ppm	Th/ U	$^{238}U/^{206}Pb$[2]	± 2SE	$^{207}Pb/^{206}Pb$[3]	± 2SE	Rho
				Rims				
T-8473	9.9	1.228	0.12	2.68	0.12	0.392	0.012	−0.583
F = 0.8876±0.0042	3.98	1.271	0.32	2.41	0.17	0.475	0.033	−0.614
	12.32	0.982	0.08	3.78	0.19	0.139	0.016	−0.670
	4.544	0.673	0.15	2.74	0.12	0.374	0.011	0.280
	3.619	1.55	0.43	3.10	0.20	0.319	0.031	−0.547
	7.25	1.587	0.22	3.41	0.13	0.271	0.021	−0.407
	5.46	1.756	0.32	3.90	0.16	0.201	0.010	0.360
	4.11	1.358	0.33	1.80	0.09	0.503	0.022	−0.438
	8.3	0.642	0.08	3.07	0.24	0.297	0.048	−0.851
	11.84	1.137	0.10	4.05	0.13	0.1355	0.0069	−0.439
	3.51	0.94	0.27	1.65	0.13	0.58	0.023	−0.729
	2.09	1.433	0.69	2.00	0.09	0.492	0.020	−0.010
	2.41	1.072	0.44	3.49	0.19	0.221	0.014	−0.093
	4.61	1.801	0.39	4.30	0.15	0.1628	0.0075	0.525
	2.86	1.784	0.62	3.18	0.17	0.264	0.022	−0.498
	7.09	1.84	0.26	3.16	0.14	0.317	0.017	−0.510
	3.8	1.309	0.34	2.90	0.14	0.361	0.021	−0.177
	2.057	1.394	0.68	2.15	0.15	0.452	0.027	−0.368
	5.87	0.958	0.16	3.53	0.14	0.235	0.015	−0.082
	11.02	1.417	0.13	4.12	0.12	0.1477	0.0043	0.412
	5.89	1.487	0.25	3.70	0.14	0.2172	0.0087	0.347
	9.96	1.623	0.16	2.84	0.31	0.352	0.034	−0.892
	6.11	2.129	0.35	3.02	0.30	0.338	0.037	−0.818
	4.34	0.669	0.15	3.19	0.12	0.288	0.012	−0.811
	7.64	1.442	0.19	4.07	0.12	0.18	0.014	−0.231
	16.2	1.491	0.09	3.47	0.11	0.187	0.006	−0.514
	8.18	1.633	0.20	3.22	0.20	0.299	0.028	−0.825
	19.1	2.05	0.11	1.06	0.06	0.638	0.013	−0.780
	15.28	1.602	0.10	4.20	0.12	0.1544	0.0050	0.389
	2.466	1.078	0.44	1.97	0.17	0.534	0.035	−0.711
	0.827	0.728	0.88	1.37	0.25	0.618	0.063	−0.830
	0.884	0.772	0.87	2.24	0.18	0.511	0.024	0.556
	9.4	0.783	0.08	4.19	0.14	0.1178	0.0036	0.436
	7.73	0.772	0.10	3.56	0.14	0.192	0.015	−0.413
	3.95	0.767	0.19	3.18	0.16	0.297	0.018	−0.473
	4.48	0.487	0.11	3.23	0.12	0.258	0.020	−0.347
Median values	***5.7***	***1.3***	***0.21***					

[1] Time-resolved analysis (TRA) session number. Correction factor (F) value is given with ±2SE uncertainty.

[2] U/Pb ratio corrected for instrumental mass-bias using BLR-1 titanite standard (see text for details).

[3] Ratio corrected for Pb-isotope fractionation using NIST 610 glass standard.

Table 5. LA-ICPMS instrumental and data acquisition parameters.

[LA-ICPMS, laser-ablation inductively coupled plasma mass spectrometry; ArF, argon fluoride; Hg, mercury; He, helium; Ar, argon; N_2, nitrogen; Ni, nickel]

Mass spectrometer:	AttoM ES™ sector field ICPMS
Laser:	Teledyne Photon-Machines Excite-Analyte™ 193 nanometer ArF excimer with HelEx cell
General parameters	
RF generator power	1,300 Watts
Acceleration voltage	Approximately 6,000 Volts
Coolant gas flow rate	13.0 liters per minute
Auxiliary gas flow rate	0.9-1.0 liters per minute
Instrument resolution	Approximately 300 (low)
Analysis mode	Deflector jump
Acquisition mode	Time resolved analysis
Peak center mass	^{206}Pb
Peak integration time durations (per sweep)	
^{238}U (250 microseconds)	
^{235}U (500 microseconds)	
^{232}Th (500 microseconds)	
^{208}Pb (500 microseconds)	
^{207}Pb (1.5 milliseconds)	
^{206}Pb (500 microseconds)	
^{204}Pb (500 microseconds)	
^{202}Hg (500 microseconds)	
Total peak integrations (per cycle)	150
Total signal acquisition time per spot	30 seconds
Total baseline acquisition time per spot	30 seconds
Laser-mode parameters	
Laser energy	3-5 millijoules
Energy density	4-5 joules per square centimeter
Spot size	50 microns
NIST 610, the titanite secondary reference material (BLR-1), and the titanite unknown (CLT-1-13) were analyzed with the same laser spot for a single analytical session	
Repetition rate	5 Hertz
Cell and carrier He gas flow rate	0.25-0.40 liters per minute
Make-up Ar gas flow rate	0.25-0.45 liters per minute
Accessory N_2 gas	5.5-6.0 milliliters per minute
Ni sampler cone	“Dry” plasma type, X (regular) or Y (ES) millimeter orifice
Ni skimmer cone	“Dry” plasma type, X (regular) or Y (ES) millimeter orifice
Total U sensitivity (SRM-610, 50 micron spot)	Approximately 3-4 $\times 10^3$ counts per second per part per million

Table 6. Uranium and lead isotopic concentrations and ages, determined by chemical abrasion-isotope dilution-thermal ionization mass spectrometry, for two samples of Mesoproterozoic igneous rock from the St. Francois Mountains terrane, southeast Missouri.

[$^{206}Pb/^{238}U$ <Th> age, Ma, age in millions of years indicated by the ratio of the abundances of the mass 206 isotope of lead to that of the mass 238 isotope of uranium corrected for initial Th/U disequilibrium; ±2σ, plus or minus 2-sigma age uncertainty, millions of years; $^{207}Pb/^{235}U$ age, Ma, age in millions of years indicated by the ratio of the abundances of the mass 207 isotope of lead to that of the mass 235 isotope of uranium; $^{207}Pb/^{206}U$ <ThPa> age, Ma, age indicated by the ratio of the abundances of the mass 207 isotope of lead to that of the mass 206 isotope of lead corrected for initial Pa/U disequilibrium; Th/U, ratio of the abundances of thorium and uranium; Pb*, radiogenic lead; Pb*/Pb, ratio of the abundance of radiogenic lead to that of common lead; $^{206}Pb/^{204}Pb$, ratio of the abundances of the mass 206 isotope of lead to that of the mass 204 isotope of lead; $^{206}Pb/^{238}U$, ratio of the abundances of the mass 206 isotope of lead to that of the mass 238 isotope of uranium; %, percent; $^{207}Pb/^{235}U$, ratio of the abundances of the mass 207 isotope of lead to that of the mass 235 isotope of uranium; $^{207}Pb/^{206}Pb$, ratio of the abundances of the mass 207 isotope of lead to that of the mass 206 isotope of lead]

Sample	Dates (Ma)							Composition					Isotopic Ratios					
	$^{206}Pb/^{238}U$ <Th>[1] age, Ma	±2 σ absolute Ma	$^{207}Pb/^{235}U$[2] age, Ma	±2 σ absolute Ma	Correlation coefficient	$^{207}Pb/^{206}Pb$ <ThPa>[1,3] age, Ma	±2 σ absolute Ma	Th/U[4]	Pb* picograms[5]	Pb common picograms[6]	Pb*/Pb common[7]	$^{206}Pb/^{204}Pb$[8]	$^{206}Pb/^{238}U$[9]	±2 σ %	$^{207}Pb/^{235}U$[9]	±2 σ %	$^{207}Pb/^{206}Pb$[9]	±2 σ %
MO16-001																		
z1	1,452.77	0.95	1,457.69	1.30	0.60	1,464.88	2.60	0.44	29.79	1.15	26.00	1,564.95	0.2528	0.0733	3.2022	0.1677	0.0919	0.1329
z2	1,465.71	1.03	1,465.43	1.02	0.79	1,465.02	1.60	0.44	41.21	0.85	48.48	2,901.06	0.2553	0.0784	3.2343	0.1311	0.0919	0.0780
z3	1,465.20	1.66	1,465.95	1.52	-0.05	1,467.04	4.51	0.44	18.14	1.35	13.39	815.37	0.2552	0.1263	3.2365	0.1953	0.0920	0.2354
z4	1,461.43	1.44	1,463.13	1.43	0.70	1,465.59	2.52	0.46	20.60	0.70	29.43	1,760.29	0.2544	0.1105	3.2248	0.1844	0.0920	0.1286
z6	1,460.91	0.94	1,463.32	0.99	0.78	1,466.81	1.61	0.44	46.47	0.83	56.16	3,360.23	0.2543	0.0722	3.2255	0.1274	0.0920	0.0781
z7	1,465.32	1.03	1,464.74	0.98	0.80	1,463.90	1.49	0.44	51.26	0.86	59.92	3,582.87	0.2552	0.0787	3.2315	0.1261	0.0919	0.0713
z8	1,466.40	2.01	1,466.15	2.08	0.57	1,465.77	4.19	0.45	12.21	0.76	16.07	971.50	0.2554	0.1534	3.2373	0.2687	0.0920	0.2180
z9	1,440.04	5.63	1,450.84	3.48	0.98	1,466.70	1.83	0.57	36.22	0.83	43.74	2,538.48	0.2503	0.4362	3.1739	0.4507	0.0920	0.0908
z10	1,465.75	1.46	1,466.20	1.96	0.46	1,466.84	4.28	0.47	19.98	1.37	14.55	878.94	0.2553	0.1111	3.2375	0.2532	0.0920	0.2230
MO16-015																		
z1	1,468.05	0.75	1,466.32	0.79	0.76	1,463.82	1.32	0.44	128.18	1.14	112.65	6,725.92	0.2557	0.0574	3.2381	0.1022	0.0919	0.0616
z2	1,468.44	0.79	1,466.61	0.83	0.76	1,463.96	1.38	0.48	126.33	0.97	130.01	7,691.03	0.2558	0.0604	3.2393	0.1064	0.0919	0.0650
z5	1,468.38	1.42	1,465.02	1.44	0.30	1,460.14	3.50	0.45	25.61	0.67	38.16	2,282.25	0.2558	0.1083	3.2326	0.1854	0.0917	0.1814
z7	1,468.49	0.71	1,466.35	0.87	0.75	1,463.26	1.53	0.47	41.78	0.47	88.37	5,236.66	0.2558	0.0542	3.2382	0.1127	0.0918	0.0735
z8	1,468.44	4.40	1,464.72	4.38	0.66	1,459.33	8.10	0.45	21.66	0.91	23.81	1,431.51	0.2558	0.3351	3.2314	0.5646	0.0917	0.4248
z9	1,466.63	3.57	1,463.97	3.25	0.99	1,460.10	2.91	0.47	12.68	0.43	29.73	1,776.16	0.2555	0.2724	3.2282	0.4190	0.0917	0.1494
z12	1,468.73	2.62	1,466.56	1.81	0.88	1,463.41	2.09	0.48	29.62	0.53	55.47	3,285.22	0.2559	0.1993	3.2390	0.2334	0.0919	0.1051

[1] Corrected for initial Th/U disequilibrium using radiogenic ^{208}Pb and Th/U[magma] = 4.0.

[2] Isotopic dates calculated using $\lambda^{238}U$ = 1.55125E-10 (Jaffey and others, 1971) and $\lambda^{235}U$ = 9.8485E-10 (Jaffey and others, 1971).

[3] Corrected for initial Pa/U disequilibrium using initial fraction activity ratio $[^{231}Pa]/[^{235}U]$ = 1.1.

[4] Th contents calculated from radiogenic ^{208}Pb and ^{230}Th-corrected $^{206}Pb/^{238}U$ date of the sample, assuming concordance between U-Pb Th-Pb systems.

[5] Total mass of radiogenic Pb.

[6] Total mass of common Pb.

[7] Ratio of radiogenic Pb (including ^{208}Pb) to common Pb.

[8] Measured ratio corrected for fractionation and spike contribution only.

[9] Measured ratios corrected for fractionation, tracer and blank.

Table 7. Summary of stratigraphic relations and new U-Pb ages for Mesoproterozoic igneous rocks in the St. Francois Mountains terrane, southeast Missouri.

Rock unit (sample number)	Sample source[1]	Age (Ma) [± 2 sig]	Age calc. method[2]	Figure	Map no. (fig. 1)
1.34-1.27 Ga Bimodal Plutonic Rocks					
Greenville pluton (63W20)	c	1,275 ± 13	76	2*A*1, 2*A*2	1
Van Buren pluton (CT-5)	c	1,278 ± 10	76	2*A*3, 2*A*4	2
Piedmont pluton (82MO-8)	c	1,290 ± 15	76	2*A*5, 2*A*6	3
Graniteville Granite (GVG-1-13)	o	1,311 ± 13	76	2*B*1, 2*B*2	4
Buick pluton (FED3)	c	1,317 ± 8	CA	2*B*3, 2*B*4	5
Alkali-feldspar granite, Missouri gravity low (124-14A)	c	[3]1,338 ± 10	76	2*B*5, 2*B*6	6
1.49-1.44 Ga Volcanic and Associated Plutonic Rocks					
Volcanic rocks of Marble Creek area					
Rhyolite of South Crane Mtn. (CLT-1-13)4	o	1,380 ± 27	Lower intercept age	2*C*1, 2*C*2, 2*C*3	7
Tuff at Crane Pond (MO14-053)	o	[3,5]1,460 ± 17	76	2*C*4, 2*C*5	8
Lower campground tuff at Marble Creek campground (MO14-043)	o	[3,6]1,473 ± 9	76	2*D*1, 2*D*2	9
Volcanic rocks of Taum Sauk caldera					
Royal Gorge Rhyolite (RGR-1-13)	o	1,459 ± 4	CA	2*D*3, 2*D*4	10
Shepherd Mountain Rhyolite (MO15-008)	o	[3]1,466 ± 8	76	2*D*5, 2*D*6	11
Volcanic and intrusive rocks of Butler Hill caldera					
Breadtray Granite (BTG-1-13)	o	1,453 ± 11	76	2*E*1, 2*E*2	12
Butler Hill Granite (BHG-1-13)	o	1,453 ± 8	76	2*E*3, 2*E*4	13
Grassy Mountain Ignimbrite (GMI-2-13)	o	1,460 ± 6	76	2*E*5, 2*E*6	14
Silvermine Granite (SMG-1-13)	o	1,461 ± 8	CA	2*F*1, 2*F*2	15
Slabtown Granite (STG-1-13)	o	1,462 ± 7	CA	2*F*3, 2*F*4	16
Knoblick Granite (KLG-1-13)	o	1,463 ± 7	CA	2*F*5, 2*F*6	17
Stono Granite (MO17-013)	o	[3]1,465 ± 9	CA	2*G*2, 2*G*3	18
Regional granitoids and rhyolite					
Massif-type granite (RE060)	c	1,456 ± 5	CA	2*H*1, 2*H*2	19
Granite near Redford pluton (RE037)	c	1,457 ± 7	CA	2*H*3, 2*H*4	20
Biotite granite (MO17-002)	o	[3]1,448 ± 12	76	2*H*5, 2*H*6	21
Rhyolite tuff (MR-3-1556)	c	[3]1,456 ± 9	76	2*I*1, 2*I*2	22
Massif-type granite (SV-5)	c	[3]1,458 ± 7	76	2*I*3, 2*I*4	23
Biotite granite (VB-23-2153)	c	[3]1,455 ± 11	76	2*I*5, 2*I*6	24
Quartz-alkali feldspar andesite dike (MO17-001)	o	[3]1,456 ± 8	CA	2*J*1, 2*J*2	25
Trachyandesite at Buford Mountain (PcF-076)	o	[3]1463 ± 9	76	2*K*3; 2*K*4	49
Massif-type biotite granite (M-DT-3-1)	c	[3]1,464 ± 8	76	2*J*3, 2*J*4	26
Rhyolite at Middlebrook Hill (PcF-077)	o	[3]1465 ± 6	76	2*K*5; 2*K*6	50
Trachyandesite at Iron Mountain (PcF-075)	o	[3]1465 ± 6	76	2*K*1; 2*K*2	48
Granite near Piedmont pluton (WY032)	c	1,468 ± 10	76	2*J*5, 2*J*6	27
Megacrystic granite, Missouri gravity low (W-6-2578)	c	[3]1,467 ± 8	76	2*K*1, 2*K*2	28
Massif-type granite (RE05)	c	1,469 ± 7	76	2*L*3, 2*L*4	29
Massif-type biotite granite (MH-1)	c	[3]1,471 ± 5	76	2*K*5, 2*K*6	30
Stouts Creek Rhyolite (GMI-1-13)	o	[3]1,471 ± 5	76	2*L*1, 2*L*2	31
Granite of Castor River Shut-Ins (MO17-006)	o	[3]1,472 ± 8	76	2*L*3, 2*L*4	32
Rhyolite near Silver Mines (OZ-5)	c	[3]1,479 ± 4	76	2*L*5, 2*L*6	33
Biotite granite (M-FK-1-1)	c	[3]1,484 ± 7	76	2*M*1, 2*M*2	34

Table 7. Summary of stratigraphic relations and new U-Pb ages for Mesoproterozoic igneous rocks in the St. Francois Mountains terrane, southeast Missouri.—Continued

Rock unit (sample number)	Sample source[1]	Age (Ma) [± 2 sig]	Age calc. method[2]	Figure	Map no. (fig. 1)
1.49-1.44 Ga Volcanic and Associated Plutonic Rocks					
Volcanic and intrusive rocks of Eminence area					
Upper unit of Coot Mountain (MO14-007)	o	1,464 ± 6	CA	2*N*1, 2*N*2	35
Lower unit of Coot Mountain (MO14-009)	o	1,463 ± 5	CA	2*N*3, 2*N*4	36
Rhyolite of Stegall Mountain (MO14-003)	o	1,462 ± 6	CA	2*N*5, 2*N*6	37
Biotite-hornblende granodiorite (SV-3)	c	[3]1,467 ± 7	CA	2*O*1, 2*O*2	38
Hypabyssal rocks related to Pea Ridge deposit					
Trachyandesite at Floyd Tower (MO13-006)	o	[3]1,463 ± 2	76	2*P*1, 2*P*2	39
Trachyandesite of Indian Creek mine (ICM-1-13)[4]	o	1,459 ± 13	76	2*P*3, 2*P*4	40
Intrusive rocks related to Boss deposit					
Rhyolite host (USA-50)	c	1,470 ± 10	76	2*Q*1, 2*Q*2	41
Trachyte host (J22-1541-1562)	c	[3]1,477 ± 17	76	2*Q*3, 2*Q*4	42
Post-mineralization diorite (S5)	c	1,471 ± 8	76	2*Q*5, 2*Q*6	43
Granite dike (S5-gr)	c	1,322 ± 10	76	2*R*1, 2*R*3	44
Biotite granite (J15)	c	1,327 ± 11	76	2*R*2, 2*R*4	45
Volcanic rocks related to Bourbon deposit					
Rhyolite (Bourb-435)	c	[3]1,472 ± 11	76	2*S*1, 2*S*2	46
Trachydacite (Bourb-204)	c	[3]1,463 ± 12	76	2*S*3, 2*S*4	47

[1] Sample source: c (sample collected from core), o (sample collected from outcrop).

[2] Age calculation method: CA (Concordia Age of Ludwig, 1980; 2003), 76 (weighted mean of selected $^{207}Pb/^{206}Pb$ ages).

[3] $^{207}Pb/^{206}Pb$ normalized to isotopic data obtained from concurrently analyzed secondary standard Z1242. $^{207}Pb/^{206}Pb$ for other samples validated by subjective comparison to data from secondary standards FC-1 (Paces and Miller, 1993) or OG1 (Stern and others, 2009).

[4] Titanite; all other ages from zircon.

[5] CA-ID-TIMS $^{207}Pb/^{206}Pb$ age (MO16-015) of 1468.28 ± 0.71 Ma (table 6) for Tile Red ash-flow tuff, which is interlayered with the tuff at Crane Pond (Brown, 1988).

[6] CA-ID-TIMS $^{207}Pb/^{206}Pb$ age (MO16-001) of 1465.52 ±0.71 Ma (table 6).

Table 8. Previously published ages for Mesoproterozoic igneous rocks in the St. Francois Mountains terrane, southeast Missouri.

[TIMS, thermal ionization mass spectrometry; CA-TIMS, chemical abrasion-thermal ionization mass spectrometry]

Rock unit	Age (Ma)	Method	Reference
Graniteville Granite	1,358 ± 25	TIMS U-Pb zircon	Van Schmus and others (1996)[1]
Graniteville Granite	1,317 ± 2	CA-TIMS U-Pb zircon	Thomas and others (2012)
Munger Granite Porphyry	1,378 ± 6	TIMS U-Pb zircon	Van Schmus and others (1996)
Munger Granite Porphyry	1,323 ± 2	CA-TIMS U-Pb zircon	Thomas and others (2012)
Devil's Tollgate Gabbro	1,323 ± 1	CA-TIMS U-Pb baddeleyite	Thomas and others (2012)
Skrainka Diabase	1,300 ± 10	TIMS Pb-Pb baddeleyite	Rämö and others (1994)
Muddy Knob gabbro, Skrainka Diabase	1,316 ± 6	TIMS Pb-Pb baddeleyite	Rämö and others (1994)
Shepherd Mountain Gabbro	1,333 ± 56	Sm-Nd isochron age	Lowell and Rämö (1999)
Cope Hollow Formation	1,462 ± 1	CA-TIMS U-Pb zircon	Thomas and others (2012)
Johnson Shut-ins rhyolite	1,464 ± 3	CA-TIMS U-Pb zircon	Thomas and others (2012)
Taum Sauk Rhyolite	1,466 ± 3	CA-TIMS U-Pb zircon	Thomas and others (2012)
Hawn Park Gneiss	1,478 ± 43	TIMS U-Pb zircon	Van Schmus and others (1996)
Hawn Park Gneiss	1,462 ± 1	CA-TIMS U-Pb zircon	Thomas and others (2012)
Rhyolite of Shut-In Mountain	1,470.4 ± 2.7	TIMS U-Pb zircon	Harrison and others (2000)
Royal Gorge Rhyolite	1,503 ± 20	TIMS U-Pb zircon	Van Schmus and others (1996)
Silvermine Granite	1,484 ± 7	TIMS U-Pb zircon	Van Schmus and others (1996)
Butler Hill Granite	1,465 ± 32	TIMS U-Pb zircon	Van Schmus and others (1996)
Breadtray Granite	1,480 ± 30	TIMS U-Pb zircon	Van Schmus and others (1996)
Knoblick Granite	1,491 ± 18	TIMS U-Pb zircon	Van Schmus and others (1996)

[1]Van Schmus and others (1996) list samples from cores according to the drill hole name. Although we used a similar naming convention, it is not known if the same units were sampled within the drill core. Thus, age comparisons are made only on samples collected at outcrops.

1.48–1.45 Ga Volcanic and Associated Plutonic Rocks

Volcanic Rocks of the Marble Creek Area

Near the summit of South Crane Mountain, a large outcrop area contains two compositionally distinct volcanic rock types (Brown, 1988). Rhyolite contains 68–71 weight percent SiO_2, whereas trachydacite contains 64–66 weight percent SiO_2 (du Bray and others, 2018b). Both rock types were sampled for geochronology, but neither sample yielded zircon. However, the rhyolite (sample CLT-1-13) does contain pale yellow, anhedral titanite. The color of this titanite is unusual (titanite commonly is honey-brown colored). BSE imaging identifies cores with concentric, wedge shaped, oscillatory zoning (consistent with an igneous origin), and unzoned or weakly patchy zoned overgrowths (fig. 2*C*1). Preliminary SHRIMP analysis indicated that this titanite has low uranium contents (mostly less than 10 ppm) and many grains have a high proportion of common lead contents (2–100 percent common ^{206}Pb). Additionally, a significant matrix mismatch between titanite standard BLR-1 and CLT-1-13 unknowns results in unusable SHRIMP data for this sample. To circumvent these issues, we used the USGS AttoM LA-ICPMS to analyze oscillatory-zoned cores and unzoned rims.

Three sessions of U-Pb analysis of CLT-1-13 titanite by LA-ICPMS (117 spot analyses total; table 4) indicate low concentrations of uranium in cores and rims, 0–9 and 0–20 ppm, respectively, and high proportions of common lead, confirming preliminary SHRIMP results. A regression through the data for cores (n = 74; 6 data points excluded) yields a Tera-Wasserburg lower intercept age of 1380 ± 27 Ma (fig. 2*C*2). However, because most of the data plot near the y-axis (indicative of high common lead content), the lower intercept age constitutes a large extrapolation, mostly controlled by only a few discordant data points. The geologic accuracy of the calculated age is suspect, especially because of a lack of similar-age rocks in the region. Although the BSE zoning of the cores suggests an igneous origin, we are unable to determine a crystallization age for the rhyolite at South Crane Mountain.

Isotopic data from titanite rims of sample CLT-1-13 indicate somewhat higher uranium content and lower proportions of common lead than was found for the cores, resulting in less discordant data (in other words, data that plot closer to the lower intercept). Regression through 37 rim analyses yields a lower intercept age of 1319 ± 28 Ma (fig. 2*C*3). This sample was collected just east of the interpreted occurrence of the buried Sabula pluton (fig. 1), which is considered a member of the 1.3 Ga igneous suite (Kisvarsanyi, 1981). Thus, the titanite rims may have formed by regional magmatic-hydrothermal activity related to emplacement of the Sabula pluton.

Three samples were collected from outcrops in the Marble Creek area (table 7). Zircon from the tuff at Crane Pond (sample MO14-053) have parallel (but not concentric) oscillatory zoning and yielded a weighted mean age of 1460 ± 17 Ma, MSWD = 1.5 (fig. 2*C*4, 2*C*5). The unit represented by this sample is interlayered with rhyolite of the Tile Red ash-flow tuff (Brown, 1988). CA-ID-TIMS data for seven grains from a sample (MO16-015) of Tile Red ash-flow tuff, collected about 35 m from our sample of tuff at Crane Pond, yielded a weighted mean age of 1468.28 ± 0.71 Ma, MSWD = 1.8 (table 6); data for an eighth analyzed grain were omitted from the age calculation because of poor analytical run characteristics.

Few zircons were extracted from a sample of the lower campground tuff at Marble Creek campground (sample MO14-043). These grains are relatively small (50–100 μm in length) and subhedral to euhedral; they yielded a weighted mean SHRIMP age of 1473 ± 9 Ma, MSWD = 1.6 (fig. 2*D*1, 2*D*2). Because of the paucity of zircon in this rock, a second sample (MO16-001) was collected from an adjacent layer (about 60 m from the first sample). This sample yielded better-preserved zircon grains; five of nine grains result in a weighted mean CA-ID-TIMS age of 1465.52 ± 0.71 Ma, MSWD = 1.3 (table 6); data for four grains were not included in the age calculation because data for these grains show evidence of lead loss.

Volcanic Rocks of the Taum Sauk Caldera

Two samples of rhyolite were collected from outcrops associated with the Taum Sauk caldera. Zircon extracted from the Royal Gorge Rhyolite (RGR-1-13) are subhedral to euhedral, blocky, and have faint, broad, irregular zoning (fig. 2*D*3). Most of the data points are concordant, enabling calculation of a Concordia Age of 1459 ± 4 Ma (fig. 2*D*4). Van Schmus and others (1996) obtained an age of 1503 ± 20 Ma for another sample of Royal Gorge Rhyolite. Slightly discordant data from zircon of the Shepherd Mountain Rhyolite (sample MO15-008) yielded a weighted mean age of 1466 ± 8 Ma, MSWD = 0.88 (fig. 2*D*5, 2*D*6).

Volcanic and Intrusive Rocks of the Butler Hill Caldera

Six samples of granite and one sample of felsic volcanic rock were collected from outcrops associated with the Butler Hill caldera in the east-central part of the study area. Based on our new SHRIMP data, intrusive and extrusive rocks in this group define a narrow age range (table 7). SHRIMP ages for the Breadtray Granite (sample BTG-1-13; weighted mean age 1453 ± 11 Ma, MSWD = 0.88) (fig. 2*E*1, 2*E*2), and Butler Hill Granite (sample BHG-1-13; weighted mean age 1453 ± 8 Ma, MSWD = 0.6) (fig. 2*E*3, 2*E*4) are younger and more precise than previous age data (1480 ± 30 Ma and 1465 ±32 Ma, respectively; Van Schmus and others, 1996) for these rocks. The Grassy Mountain Ignimbrite (sample GMI-2-13) yielded a weighted mean age of 1460 ± 6 Ma, MSWD = 1.32 (fig. 2*E*5, 2*E*6) and the Slabtown Granite (sample STG-1-13) yielded a Concordia Age of 1462 ±7 Ma (fig. 2*F*3, 2*F*4). SHRIMP

Concordia Ages for Silvermine Granite (sample SMG-1-13; 1461 ± 8 Ma; fig. 2*F*1, 2*F*2) and Knoblick Granite (sample KLG-1-13; 1463 ± 7 Ma; fig. 2*F*5, 2*F*6) are younger than previous age data (1484 ± 7 Ma and 1491 ±18 Ma, respectively; Van Schmus and others, 1996) for these rocks.

The Stono Granite is regionally unusual because it contains many mafic inclusions (up to 5 cm in diameter; fig. 2*G*1). In addition, $\delta^{18}O$ values for the Stono Granite are uncharacteristically low compared to all other Mesoproterozoic granitic rocks in the St. Francois Mountains terrane (King and others, 2008; Wenner and Taylor, 1996). The sampled granite (sample MO17-013) contains a minor but unavoidable amount of fine-grained mafic inclusions. Two types of CL zoning were observed in zircon from the Stono Granite: (1) typical light to dark grains with concentric, fine oscillatory zoning, and (2) dark, unzoned grains (fig. 2*G*2). Both types of zircon are partially resorbed and somewhat fractured. Type 1 grains have relatively low uranium concentrations (approximately 100–600 ppm) and Th/U (approximately 0.40–0.65), whereas type 2 grains have higher uranium (approximately 650–1,700 ppm) and higher Th/U (approximately 0.65–2.7). Analyses of five zircon grains with concentric oscillatory CL zoning and relatively high uranium concentrations yield concordant Pb/U data that result in a calculated Concordia Age of 1465 ± 9 Ma (fig. 2*G*3). Because the origin of the unzoned low-uranium zircon is uncertain, analytical data for those grains were excluded from the age calculation for the Stono Granite.

Regional Granitoids and Rhyolite

Ten samples of granite and two samples of rhyolite were collected from drill core and seven samples (two granites, two rhyolite, two trachyandesites, and one petrographically unusual andesite dike) were collected from outcrops for rocks of this group. These rocks have been divided into four subgroups, including (1) nine samples of massif-type granitoids (biotite granodiorite to granite on fig. 1), (2) two granitoids interpreted as ring-type intrusions surrounding 1.3 Ga plutons (hornblende-biotite granodiorite on fig. 1; Kisvarsanyi, 1981), (3) four rhyolites, two trachyandesites, and one hypabyssal andesite dike, and (4) one megacrystic granite that occurs at depth within the MGL, southwest of the study area.

Rocks within subgroup 1 range in age from about 1455 to 1485 Ma (table 7). All of these samples contain zircon with typical euhedral morphology, and concentric oscillatory CL zoning. Specific zircon U-Pb ages are a Concordia Age for sample RE060—1456 ± 5 Ma (fig. 2*H*1, 2*H*2) and weighted mean ages for sample MO17-002, 1448 ± 12 Ma, MSWD = 0.66 (fig. 2*H*5, 2*H*6); sample SV-5, 1458 ± 7 Ma, MSWD = 1.09 (fig. 2*I*3, 2*I*4); sample VB-23-2153, 1455 ± 11 Ma, MSWD = 1.9 (fig. 2*I*5, 2*I*6); sample M-DT-3-1, 1464 ± 8 Ma, MSWD = 0.83 (fig. 2*J*3, 2*J*4); sample RE05, 1469 ± 7 Ma, MSWD = 0.97 (fig. 2*L*3, 2*L*4); sample MH-1, 1471 ± 5 Ma, MSWD = 1.09 (fig. 2*L*5, 2*L*6); sample MO17-006, 1472 ±8, MSWD = 0.93 (fig. 2*M*3, 2*M*4); and sample M-FK-1-1, 1484 ±7 Ma, MSWD = 0.6 (fig. 2*N*1, 2*N*2).

Geophysical data (Kisvarsanyi, 1980, 1981) suggest that several granitoid units form annular intrusions surrounding Graniteville-type plutons representative of caldera-related resurgent magmatism. This model requires that the annular or ring-type intrusions are approximately coeval with hypothesized resurgent granitoid intrusions. To test this interpretation, ages were determined for two drill core samples of annular, ring-type intrusions. Sample RE037 is from an intrusion that surrounds the undated Redford pluton (fig. 1) and has a Concordia Age of 1457 ± 7 Ma (fig. 2*H*3, 2*H*4). Although the locations of some core holes are coincident with the projected areal extent of the Redford pluton, none of these holes penetrate to the granite. Thus, although the Redford pluton has not been dated, its age is presumed to be approximately 1.3 Ga based on its geophysical characteristics (Kisvarsanyi, 1981). Consequently, magmatism represented by the Redford pluton and its presumed ring intrusion do not seem to be coeval or cogenetic. Sample WY032 is from a granitoid intrusion that surrounds the Piedmont pluton and has a weighted mean age of 1468 ± 10 Ma, MSWD = 1.05 (fig. 2*J*5, 2*J*6). Similarly, because the Piedmont pluton crystallized at about 1290 ± 15 Ma (table 7), the annular intrusion cannot be petrologically associated with the Piedmont pluton, but rather represents basement into which the Piedmont pluton was subsequently intruded.

Six of the volcanic rock units in subgroup 3 were dated. Zircon grains from rhyolite tuff (sample MR-3-1556) are elongate to acicular (length-to-width ratios of 5–7), lack terminations, and have parallel CL zoning (fig. 2*I*1). These grains yielded a weighted mean age of 1456 ± 9 Ma, MSWD = 1.6 (fig. 2*I*2). This group of dated volcanic rocks also includes an unusual quartz-alkali feldspar-bearing andesite dike (sample MO17-001) that yielded a Concordia Age of 1456 ± 8 Ma (fig. 2J1, 2J2). Weighted mean ages of other dated felsic volcanic rocks within this subgroup include trachyandesite at Buford Mountain (sample PcF-076, 1463 ± 9 Ma, MSWD = 1.17; fig. 2K3, 2K4), rhyolite at Middlebrook Hill (sample PcF-077, 1465 ± 6 Ma, MSWD = 1.02; fig. 2K5, 2K6), trachyandesite at Iron Mountain (sample PcF-075, 1465 ± 6 Ma, MSWD = 1.12; fig. 2K1, 2K2), the Stouts Creek Rhyolite (sample GMI-1-13, 1471 ± 5 Ma, MSWD = 1.08; fig. 2*M*1, 2*M*2) and rhyolite that hosts Mesoproterozoic sphalerite mineralization near Silver Mines (sample OZ-5, 1479 ± 4 Ma, MSWD = 0.63; fig. 2*M*5, 2*M*6). The andesite dike intruded biotite granite (sample MO17-002—1448 ± 12 Ma, fig. 2*H*5, 2*H*6); the mapped intrusive relationship is plausible given analytical uncertainties associated with the relevant age determinations.

Subgroup 4 consists solely of a megacrystic granite from within the MGL. This sample of drill core (sample W-6-2578) was collected for comparison with age data for sample 124-14A (1338 ± 10 Ma, in text above in the 1.34–1.27 Ga bimodal plutonic rocks section), also coincident with the MGL. Zircon from the megacrystic granite yielded a weighted mean age of 1467 ± 8 Ma, MSWD = 1.33 (fig. 2*L*1, 2*L*2), demonstrating that both 1.3 and 1.4 Ga intrusions are spatially associated with the MGL.

Volcanic and Intrusive Rocks of the Eminence Area

Ages of volcanic rocks near Eminence, Mo. were determined by analysis of three samples collected from outcrops in the southwest part of the study area (fig. 1, table 7). In addition, we determined the age of a sample of granodiorite collected from core derived from a hole drilled in this area. The granodiorite forms an aeromagnetic high that encircles the rhyolite exposed near Eminence, Mo., and was interpreted as a ring-type intrusion associated with a caldera (Harrison and others, 2000, 2002; Kisvarsanyi, 1981). The volcanic rocks include samples of rhyolite tuff collected from the upper and lower units of Coot Mountain (Orndorff and others, 1999) and the rhyolite of Stegall Mountain located a few kilometers to the southeast (Harrison and others, 2002). Concordia Ages were determined for zircon from the upper unit of Coot Mountain (sample MO14-007; 1464 ± 6 Ma; fig. 2*O*1, 2*O*2) and from the lower unit (sample MO14-009; 1463 ± 5 Ma; fig. 2*O*3, 2*O*4). The rhyolite of Stegall Mountain (sample MO14-003) yielded a Concordia Age of 1462 ± 6 Ma (fig. 2*O*5, 2*O*6); it is considered correlative with the rhyolite of Shut-In Mountain (Harrison and others, 2002), whose stratigraphic relationship with the upper and lower units of Coot Mountain is indeterminate (Orndorff and others, 1999). The rhyolite of Shut-In Mountain was previously dated by multigrain and single grain TIMS analysis at 1470.4 ± 2.7 Ma (Harrison and others, 2000). Biotite-hornblende granodiorite sample SV-3 from the ring-type intrusion that surrounds the rhyolitic rocks of the Eminence caldera structure yielded a Concordia Age of 1467 ± 7 Ma (fig. 2*P*1, 2*P*2).

The maximum total age range (including analytical uncertainties) for volcanic rocks of the Eminence area is about 1456 to 1470 Ma, as determined from SHRIMP U-Pb zircon ages. (table 7). The individual uncertainty associated with each age determination (between 5 and 6 million years [m.y.]) is not sufficiently precise to constrain their relative stratigraphic positions. However, geologic relations suggest that rocks included in the upper and lower units of Coot Mountain may be slightly younger than the rhyolite of Stegall Mountain. The age of the biotite-hornblende granodiorite (sample SV-3) is consistent with it being part of a ring-type intrusion associated with the Eminence caldera of Harrison (2000) and Kisvarsanyi (1981).

Hypabyssal Rocks Related to the Pea Ridge Deposit

Geophysical data (Kisvarsanyi, 1981) suggest the presence of an arcuate mass of trachyandesite (previously termed trachyte) in the vicinity of the inferred Pea Ridge granitoid pluton, which presumably lies deeply buried beneath the Pea Ridge IOA deposit (Day and others, 2016). However, relative age relations and petrologic kinship of the trachyandesite and the hypothesized Pea Ridge granitoid pluton are unknown. Previous geochronologic investigations have shown that rare earth element (REE)-bearing dikes within approximately 1475-Ma rhyolitic rocks at Pea Ridge were emplaced at ~1465 Ma and that both of these rock types were subsequently intruded by felsic dikes at about 1440 Ma (Aleinikoff and others, 2016). These felsic intrusive rocks may represent apophyses of the concealed granitoid intrusion beneath the rhyolite host rocks at Pea Ridge deposit.

Two samples of trachyandesite were collected in order to constrain the age of these intermediate composition igneous rocks. Sample MO13-006 (from near Floyd Tower) was collected at a surface outcrop, whereas sample ICM-1-13 was collected from an extensive mine dump composed of rock excavated as part of mining activities associated with the Mississippi Valley-type deposit at the Indian Creek Mine. Both samples are fine grained and indurated. Zircon was not identified in the least magnetic fraction (its typical residence) from either sample, but it was recovered in the approximately 1.8 Amp magnetic fraction. These grains are dark gray, subhedral, elongate, and highly fractured. CL images show that these grains are composed of medium-gray (relatively low uranium) fragments bounded by cracks filled with unidentified black material with a high uranium content (fig. 2*Q*1, 2*Q*3). In sample MO13-006, the homogeneous gray areas are sufficiently large to accommodate SHRIMP analytical spots. In sample ICM-1-13, the grains are more highly fractured and do not preserve areas that have the requisite size and homogeneity required for SHRIMP analysis.

SHRIMP U-Pb data for gray (in CL) areas in zircon from sample MO13-006 indicate that these fragments contain between about 1,400 and 4,500 ppm uranium and have unusually high Th/U values of 0.7–2.0. Zircon with high uranium contents (greater than 2,500 ppm) tend to yield $^{206}Pb/^{238}U$ ages that are too old, probably because of matrix mismatch between standards and unknowns (White and Ireland, 2012; Williams and Hergt, 2000). However, in order to date the zircon in sample MO13-006, we used $^{207}Pb/^{206}Pb$ systematics (which are not affected by matrix effects) to calculate a weighted mean age of 1463 ± 2 Ma, MSWD = 1.4 (fig. 2*Q*2). Although no dateable zircon was obtained from ICM-1-13, we did extract titanite suitable for SHRIMP U-Pb geochronology. The titanite grains are medium brown, anhedral, and in BSE display oscillatory zoning, which suggests an igneous origin. These grains yielded a weighted mean age of 1459 ± 13 Ma, MSWD = 2.1 (fig. 2*Q*4). As described by Day and others (2017), this age is equivalent to the timing of mineralization at the Pea Ridge IOA deposit.

Intrusive Rocks Related to the Boss Deposit

The Boss deposit, in the west-central part of the study area, is unusual. Whereas other iron ore occurrences in southeast Missouri are IOA deposits, the mineralized rock at Boss constitutes an IOCG deposit (Day and others, 2016). Five rock samples associated with the Boss deposit were collected from drill core and dated by SHRIMP U-Pb geochronology in order to constrain the age of the deposit. These samples include rhyolite

(sample USA-50) and trachyandesite (sample J22-1541-1562), both of which host iron-copper ore. Both samples contain euhedral zircon with fine, concentric, and oscillatory zoning. Zircon grains from sample USA-50 are well-preserved, terminated prisms (fig. 2*R*1), whereas the grains from sample J22-1541-1562 are partially resorbed and have irregular outer edges (fig. 2*R*3). Zircon from the rhyolite yielded a weighted mean U-Pb age of 1470 ± 10 Ma, MSWD = 1.7 (fig. 2*R*1, 2*R*2), whereas zircon from the trachyandesite yielded a weighted mean age of 1477 ± 17 Ma, MSWD = 0.86, (fig. 2*R*3, 2*R*4). Sample S5 represents a diorite pluton that intruded magnetite mineralized rock, and therefore crystallized after ore deposition. Most of the few grains of zircon obtained from the diorite are unzoned and have CL features that are consistent with partial internal replacement (fig. 2*R*5). Zircon from this sample yielded a broad array of discordant data with a weighted mean $^{207}Pb/^{206}Pb$ age of 1471 ± 8 Ma, MSWD = 1.3 (fig. 2*R*6). Together, these three samples bracket the timing of IOCG ore mineralization at the Boss deposit to between about 1480 and 1465 Ma.

Two younger, crosscutting granitic dikes at Boss were also dated. Sample S5-gr is a relatively fresh granite dike that clearly intrudes diorite sample S5. Sample J15 is a biotite granite dike that intrudes the host rhyolite. Zircon from both granite dike samples contains oscillatory-zoned cores and black (in CL) overgrowths, some of which are broad enough to accommodate a SHRIMP spot (fig. 2*R*1, 2*R*2). U-Pb data for S5-gr and J15 zircon cores yield weighted mean ages of 1322 ± 10 Ma, MSWD = 1.6 and 1327 ± 11 Ma, MSWD = 1.17, respectively (fig. 2*S*3, 2*S*4). As suggested by CL imagery, dark zircon rims from both samples are significantly enriched in uranium (3,000–13,000 ppm). On a standard concordia plot, U-Pb data for rims form arrays with lower intercept ages of about 300 Ma and upper intercept ages of about 1.3 Ga. These data suggest that the rims formed in the late Paleozoic, possibly in association with regional Mississippi Valley type Pb-Zn ore formation, as epitomized by mineralized rock in the nearby Buick Mine. Determining a more precise and accurate lower intercept age was precluded by considerable data scatter. The measured isotopic systematics may have been affected by three independent processes including: (1) inheritance (for example, overlap of the SHRIMP analytical spots on core and narrow rim zones), (2) lead loss from very metamict zones (resulting in younger ages), and (3) matrix effects caused by compositional differences between standard and unknowns (likely resulting in older ages). These processes produce discrete trajectories in U-Pb space (fig. 2*R*5, 2*R*6).

Volcanic Rocks Related to the Bourbon Deposit

The Bourbon IOA deposit is approximately 20 km west of the Pea Ridge IOA deposit (fig. 1). It is associated with a bimodal sequence of early Mesoproterozoic basalt to basaltic andesite and trachydacite to high-silica rhyolite. Two samples were collected from drill core in order to constrain the ages of volcanic rocks associated with the Bourbon IOA deposit. These include a rhyolite (sample Bourb-435) associated with magnetite ore and a trachydacite unit, represented by sample Bourb-204, that is stratigraphically beneath the rhyolite (C. Meighan, written communication, 2018). Both samples yielded euhedral, slightly resorbed, oscillatory-zoned zircon (fig. 2*S*1, 2*S*3); because of the possibility of inheritance in cores (Watts and Mercer, 2020), only zoned mantles were analyzed. The SHRIMP U-Pb weighted mean age for the trachydacite is 1463 ± 12 Ma, MSWD = 0.65 (fig. 2*T*4), whereas the weighted mean age of the rhyolite is 1472 ± 11 Ma, MSWD = 1.5 (fig. 2*T*2). Within error, these new data suggest that the Bourbon rhyolite and Bourbon trachydacite are coeval.

Synthesis of Geochronologic Data

Our new geochronologic data better constrain the role of magmatism in the Mesoproterozoic geologic evolution of southeast Missouri. As shown by Van Schmus and others (1996) and Thomas and others (2012), this area was the locus of magmatism during two Mesoproterozoic episodes (fig. 4*A*). The first of these, the principal subject of findings reported herein, was volumetrically dominant and spanned 1.48 to 1.45 billion years ago. A second, volumetrically less significant episode, consists of intrusions emplaced between 1.33 and 1.28 billion years ago and may exhibit a systematic north-to-south younging progression. Importantly, magmatism between 1.48 and 1.45 billion years ago was essentially continuous; no significant temporal gaps were detected using presently available technology. The new data also suggest that no particular period within this 30 m.y. episode was characterized by a disproportionate magmatic volume (fig. 4*B*). The older magmatic episode was succeeded by a volumetrically minor magmatic component depicted by late, crosscutting dikes emplaced at about 1440 Ma (Aleinikoff and others, 2016; Neymark and others, 2016). Significantly, on a regional basis, intrusive and extrusive magmatic products of the older magmatic episode are coeval (fig. 4), as are the ring- and massif-type intrusions of Kisvarsanyi (1981). The observation that granitic rocks intrude rhyolite (Kisvarsanyi, 1981; Sides and others, 1981) establishes their relative age relations but our data do not indicate a significant time gap between the emplacement of volcanic and granitic rocks in the St. Francois Mountains terrane. Our geochronologic data also confirm that rocks previously interpreted (on the basis of geophysical studies by Kisvarsanyi, 1980, 1981) as ring-type intrusions associated with 1.3 Ga plutons are in fact part of the 1.4 Ga magmatic episode. Importantly, our geochronologic data demonstrate that the Pea Ridge iron ore deposit formed between about 1475 and 1460 Ma (Aleinikoff and others, 2016; Neymark and others, 2016) and therefore is entirely coeval with the older period of Mesoproterozoic magmatism in southeast Missouri (fig. 4).

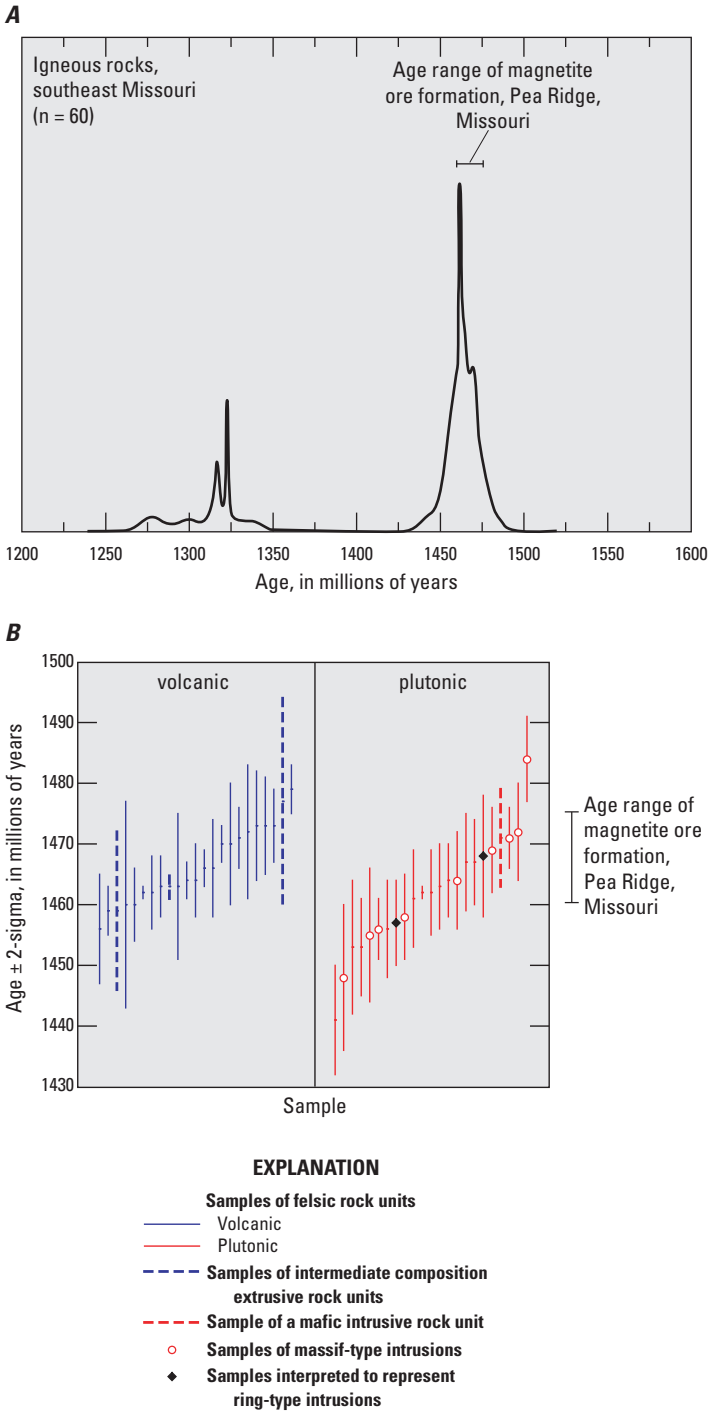

Figure 4. Compilation of age data for Mesoproterozoic igneous rocks in the St. Francois Mountains terrane, southeast Missouri. *A*, Relative probability plot of all high precision ages displaying two major episodes of magmatism (Harrison and others, 2000; Lowell and Rämö, 1999; Rämö and others, 1994; Thomas and others, 2012; this study). *B*, Comparison of ages (± 2-sigma errors) for samples of approximately 1400 Ma extrusive and intrusive rocks, each shown in chronologic order.

Petrographic Characteristics

Approximately 1.4 Ga Mesoproterozoic igneous rocks in the St. Francois Mountains terrane are principally rhyolite (Le Maitre, 1989) and granite (Streckeisen, 1976) but also include lesser amounts of mafic- to intermediate-composition rocks. The data compilation of du Bray and others (2015) shows that the phenocryst assemblage in rhyolite tuffs and lavas is dominated by variable amounts of plagioclase, alkali feldspar, and quartz, of which plagioclase is dominant (table 9). Primary mafic silicate phenocryst phases are relatively minor in the rhyolites and are usually replaced by secondary iron-titanium (Fe-Ti) oxide minerals, which reflect pervasive postdepositional alteration that affects all crystalline phases and commonly obscures primary mafic phases. Most of the 1.48 to 1.45 Ga mafic to intermediate composition volcanic rocks in the St. Francois Mountains terrane, principally lavas or hypabyssal intrusions, contain fewer phenocrysts than their felsic volcanic counterparts and some are aphyric. Most phenocrysts in these rocks consist of plagioclase but include clinopyroxene, hornblende, and minor biotite.

Modal data compiled by du Bray and others (2015) indicate that phaneritic intrusive rocks in the St. Francois Mountains terrane are composed of alkali-feldspar granite, syenogranite, monzogranite, and minor granodiorite (fig. 5). Most of these rocks are medium to coarse grained, hypidiomorphic, and inequigranular. These rocks contain both albite-twinned plagioclase and variably exsolved microcline-twinned alkali feldspar, which is consistent with their cooling and solidification from relatively hydrous crustal reservoirs favorable for subsolvus feldspar crystallization. Biotite, 1 to 3 modal percent, is the principal mafic silicate mineral in the 1.48 to 1.45 Ga intrusive rocks in the St. Francois Mountains terrane, although 1 to 2 percent hornblende is sometimes present. Although biotite is the principal mafic silicate mineral in the massif-type intrusions, hornblende is dominant among the ring-type intrusions (Day and others, 2016; Kisvarsanyi, 1981). Fine-grained primary Fe-Ti oxide crystals account for about 0.5 to 1.5 percent of both the extrusive and intrusive rocks. Accessory mineral assemblages in these rocks commonly include apatite, zircon, allanite, and titanite; monazite is a less common accessory constituent. Secondary epidote, chlorite, actinolite, and sericite reflect weak postmagmatic alteration of most of these rocks.

Whole-Rock Geochemistry

Whole-rock geochemical data were compiled from available literature sources and additional, new analyses were obtained for samples collected in support of this investigation (du Bray and others, 2018b; Granitto and others, 2018). Obviously altered samples were eliminated from the interpreted database. Other altered samples were identified as samples with any of the following characteristics: SiO_2 abundances greater 78 weight percent, Na_2O abundances greater than 6.5 weight percent or less than 0.5 weight percent, K_2O abundances greater than 8 weight percent, Na_2O/K_2O greater than 5, K_2O/Na_2O greater than 1.5, CO_2 concentrations greater than 0.35 weight percent, or total volatile concentrations greater than 3 weight percent. Analyses with any of these characteristics were eliminated from the interpreted data compilation because samples with any of these characteristics probably do not preserve primary igneous rock compositions. In addition, samples with analytical totals greater than 103 or less than 97 probably reflect inaccurate analyses; data for these samples were also eliminated. Although many of the 1.48 to 1.45 Ga igneous rocks in the St. Francois Mountains terrane have been affected by alkali metasomatism (Slack and others, 2016), resulting dominantly in sodium losses and potassium gains, the alkali data interpreted herein constitute the best available and quite plausible values for the abundances of these constituents. The identities of samples that convey representative compositions of individual 1.48 to 1.45 Ga igneous rock units exposed in the St. Francois Mountains terrane are listed in table 10.

Formal and informal stratigraphic nomenclature for rock unit names used in this report (table 10) are consistent with those defined in previous investigations (Anderson, 1962; Berry, 1970; Brown, 1988; Pippin, 1996; Sides, 1981; Sylvester, 1984). However, the data compiled by du Bray and others (2018b) indicate that the compositional designations included in some extrusive or hypabyssal intrusion rock unit names, for example, trachyte in the trachyte of Kratz Spring, are either inconsistent with available geochemical data and (or) are not in agreement with the standard major oxide abundance classification schema of Le Maitre (1989). In these instances, we assigned correct compositional designations for previously defined but inaccurate rock unit names, as appropriate (table 11).

Major Oxide Data

The compositions of 1.48 to 1.45 Ga igneous rocks in the St. Francois Mountains terrane are essentially bimodally distributed with respect to silica content. The great majority of both the extrusive and intrusive igneous rocks constitute a felsic end member; this population is dominated by rhyolite with 72 to 78 weight percent SiO_2 but includes rhyolite with SiO_2 contents as low as about 69 weight percent. In the St. Francois Mountains terrane, a small but important mafic end member is composed of samples that contain about 49 to 57 weight percent SiO_2 and includes basalt, basaltic andesite, and basaltic trachyandesite. An even smaller group of samples, with compositions intermediate between those of the felsic and mafic populations, represents just four geologic units; these trachyandesites and trachydacites contain about 60 to 68 weight percent SiO_2. Compositions of intrusive rocks across the St Francois Mountains terrane are almost exclusively felsic and essentially indistinguishable from those of cospatial rhyolitic rocks. With the exception of the fine-grained phase of the Silvermine Granite, all of the ring-type intrusive rocks in

Table 9. Average phenocryst abundances, in percent, in extrusive and shallow hypasbyssal geologic units of the St. Francois Mountains terrane, southeast Missouri; averages calculated from the data of du Bray and others (2015).

[N, number of samples; Pl, plagioclase; AFS, alkali feldspar; Qtz, quartz; Hbl, hornblende; Cpx, clinopyroxene; Bt, biotite; Opq, opaque Fe-Ti oxides; —, species not present]

Geologic unit	N	Pl	AFS	Qtz	Hbl	Cpx	Bt	Opq
Mafic								
Silver Mines basaltic andesite	5	9	—	—	—	—	—	3
Intermediate								
Trachyandesite of Floyd Tower/Indian Creek	2	15	5	3	4	—	—	4
Stouts Creek rhyolite	1	10	5	—	—	—	—	—
Trachyte at South Crane Mountain	3	14	—	—	—	3	—	4
Felsic								
Fenceline rhyolite ash-flow tuff	1	15	—	—	—	—	—	1
Tilk Hollow rhyolite ash-flow tuff	1	12	—	—	—	—	—	—
Marble Creek rhyolite ash-flow tuff	4	7	—	—	—	—	—	1
Saddle rhyolite ash-flow tuff	1	6	—	—	—	—	—	1
Ironton Hollow-Cedar Bluff Rhyolite breccia	2	2	—	5	—	—	—	1
Creekbed rhyolite ash-flow tuff	1	19	2	—	—	—	—	2
Rhyolite at South Crane Mountain	2	14	1	—	—	—	—	3
Upper Orchard rhyolite ash-flow tuff	1	10	7	—	—	—	—	2
Logroad rhyolite ash-flow tuff	1	7	5	—	—	—	—	1
Shepherd Mountain Rhyolite	4	6	4	—	—	—	1	3
Forked Creek rhyolite ash-flow tuff	1	4	4	—	—	—	—	2
Lower Ridge rhyolite ash-flow tuff	6	3	4	—	—	—	—	1
Upper Ridge rhyolite ash-flow tuff	8	2	5	—	—	—	—	2
Lower campground tuff at Marble Creek campground	2	1	8	—	—	—	—	1
Little Rock Creek rhyolite ash-flow tuff	2	15	5	1	—	—	—	2
Tuff at Crane Pond	7	9	4	1	—	—	—	1
Iron Mountain Lake rhyolite ash-flow tuff	1	3	1	2	—	—	—	1
Tile Red ash-flow tuff	3	2	2	3	—	—	—	1
Brown's rhyolite ash-flow tuff	1	1	3	1	—	—	—	1
Clearcut rhyolite ash-flow tuff	1	—	3	—	—	—	—	—
Green rhyolite	1	—	25	4	—	—	—	1
Grassy Mountain Ignimbrite	15	—	13	8	1	—	—	1
Stouts Creek rhyolite	3	—	13	10	4	—	—	—
Lake Killarney Formation	6	—	12	5	—	—	—	1
Brushy rhyolite ash-flow tuff	1	—	11	7	—	—	—	1
Ketcherside Mountain rhyolite ash-flow tuff	1	—	10	5	—	—	—	1
Transition rhyolite ash-flow tuff	6	—	9	7	—	—	—	1
Hogan Mountain	1	—	6	1	—	—	—	—
Royal Gorge Rhyolite	4	—	5	5	—	—	—	2
Reader Hollow rhyolite ash-flow tuff	2	—	5	3	—	—	—	2
Sawmill rhyolite ash-flow tuff	1	—	4	8	—	—	—	1
Mountain View rhyolite	6	—	4	1	—	—	—	1
Oak Mountain rhyolite	1	—	1	1	—	—	—	1
Black rhyolite ash-flow tuff	1	—	—	1	—	—	—	1

the St. Francois Mountains terrane have SiO_2 contents that are less than those characteristic of the massif-type intrusive rocks as defined by Kisvarsanyi (1981) (fig. 6; table 10). However, major oxide compositions of the ring-type intrusions are distinct from those of the massif-type intrusive rocks only because they extend geochemical arrays or fields to less evolved, lower silica compositions that are continuous or collinear with trends defined by the massif-type intrusive rocks (Cullers and others, 1981). Most igneous rocks in the St. Francois Mountains terrane, including the intrusive rocks, are subalkaline (Irvine and Baragar, 1971) although compositions of the trachyte that hosts the Kratz Spring IOA deposit and the trachyandesite host of the Boss IOCG deposit appear to be alkaline (fig. 6). Similarly, melt inclusions in zircon from some samples of the Pea Ridge 1825 rhyolite porphyry, the upper and lower units of Coot Mountain, and the rhyolite of Stegall Mountain are alkaline, whereas the majority of inclusions in these units and those in zircon from the Bourbon trachydacite are subalkaline (Watts and Mercer, 2020). Na_2O/K_2O values for extrusive igneous rocks are also bimodally distributed. The median Na_2O/K_2O value among the mafic rocks is 2.26, whereas that for the intermediate and felsic rocks is 0.76. Na_2O/K_2O values within each of these populations vary inconsistently with respect to SiO_2 content, possibly as a consequence of undetected alkali metasomatic alteration of these rocks. Alumina saturation indices (Shand, 1951; ASI, molar $Al_2O_3/[Na_2O+K_2O+CaO]$) of these rocks straddle the metaluminous-peraluminous boundary (fig. 7). However, among the felsic extrusive rocks, a significant majority are weakly peraluminous (ASI between 1.0 and 1.1) and about 10 percent of the population is strongly peraluminous (ASI greater than 1.1). The intermediate and mafic extrusive rocks have lower ASI indices (0.6 to 1.0) and higher alumina to total alkali ratios (1.3 to 2.9) with decreasing SiO_2 content. Among the intrusive rocks, most samples are weakly peraluminous, although relatively minor groups of samples are either metaluminous (ASI between 0.9 and 1.0) or strongly peraluminous. Rare weakly peralkaline compositions (fig. 7) probably represent cryptic, undetected alkali metasomatism. Relative to the modified alkali-lime index (Frost and others, 2001), compositions of most of the felsic and intermediate extrusive rocks in the St. Francois Mountains terrane have alkali-calcic compositions, although compositions for some samples range into the adjacent alkalic and calc-alkalic fields (fig. 8). Compositions of melt inclusions in zircon from some samples of the Pea Ridge 1825 rhyolite porphyry, the upper and lower units of Coot Mountain, and the rhyolite of Stegall Mountain are alkalic, whereas the majority of inclusions in these units and those in zircon from the Bourbon trachydacite are alkali calcic or calc alkalic (Watts and Mercer, 2020). Compositions for the trachyte of Kratz Spring are distinctly alkalic, whereas compositions for most of the mafic extrusive rocks elsewhere are calc alkalic. In contrast, compositions of the intrusive rocks in the St. Francois Mountains terrane are about equally divided between the alkali-calcic and calc-alkalic fields; the preponderance of samples with the highest SiO_2 contents are calc alkalic.

As summarized by Bickford and others (2015), the preponderance of the Mesoproterozoic igneous rocks in the St. Francois Mountains terrane have A (anorogenic)-type (Loiselle and Wones, 1979) compositions. However, Frost and Frost (2008) suggest that the A-type nomenclature has become confused to the point of nonusefulness by inclusion of diverse igneous rocks that have varied compositional characteristics and petrogenetic histories. They proposed that many igneous rocks previously described as A type, including most of the 1.48 to 1.45 Ga igneous rocks in the St. Francois Mountains terrane, are more suitably termed ferroan granites. Using their classification scheme, all intermediate and felsic 1.48 to 1.45 Ga igneous rocks in the study area are ferroan and, therefore, tholeiitic (fig. 9). Compositions of some, mostly mafic, 1.48 to 1.45 Ga rocks, including the diorite that hosts the Boss IOCG deposit, basalt in the Cope Hollow Formation, Silver Mines basaltic andesite (Sylvester, 1984), lower and upper andesites of Marble Creek campground (Brown, 1988) and the fine-grained facies of the Silvermine Granite, have compositions that are transitional between ferroan and magnesian types. In contrast, those for other, principally mafic rocks, including the Bourbon basalt, Knoblick Granite, basaltic andesite host of the Kratz Spring IOA deposit, medium-grained facies of the Silvermine Granite, and the basalt of Kratz Spring, are magnesian and calc alkaline. Importantly, the transition from ferroan to magnesian compositions among 1.48 to 1.45 Ga igneous rocks in the St. Francois Mountains terrane is continuous (fig. 9). Although samples can be classified as either ferroan or magnesian, the data define a single population with no compositionally distinct outliers. As confirmation of the intrinsically ferroan character of most 1.48 to 1.45 Ga igneous rocks in the St. Francois Mountains terrane, most of these rocks, especially those with the least evolved compositions, follow the iron-enrichment differentiation trend (fig. 10) defined by Irvine and Baragar (1971) for tholeiitic magmatic systems.

Diagnostic major oxide geochemical features of igneous rocks, especially the relative proportions of iron and magnesium, alkalis and alumina, and alkalis and calcium (Frost and Frost, 2008), allow these rocks to be classified in accordance with their petrogenesis. Among 1.48 to 1.45 Ga igneous rocks, the vast majority of the defined geologic map units are ferroan and peraluminous (figs. 7, 9, and 10; table 11). Within that subset, the alkali-calcic subtype is dominant, although the compositions of six units are alkalic, six are calc alkalic, and one unit has a calcic composition (table 11). A significantly smaller number of the 1.48 to 1.45 Ga igneous rock units are composed of ferroan and metaluminous rock (figs. 7, 9, and 10; table 11). Five units consist of rock that is transitional between ferroan and magnesian compositions. One of these is peraluminous and alkali calcic, whereas the remaining four units are mafic, metaluminous, and calc alkalic (table 11). Finally, five of the approximately 1.4 Ga igneous rock units in the St. Francois Mountains terrane are magnesian; each of these is also

Table 10. Identification and characteristics of igneous rock samples from the St. Francois Mountains terrane, southeast Missouri for which representative geochemical analyses are presented by du Bray and others (2018b) and Granitto and others (2018).

Sample number	Geologic unit	Unit type	Form	North latitude	West longitude
WA11-1291	Lake Four Winds basalt	Mafic extrusive	lava	38.0478	−90.8652
JCB5	Basalt in the Cope Hollow Fm	Mafic extrusive	lava	37.5393	−90.8376
56W167-1555	Basalt of Kratz Spring	Mafic extrusive	lava	38.2600	−91.1900
JSIQ-20-7	Silver Mines basaltic andesite	Mafic extrusive	lava	37.5418	−90.8411
MO16-013	Lower andesite of Marble Creek campground	Mafic extrusive	lava	37.4310	−90.5140
JS-13-5	Upper andesite of Marble Creek campground	Mafic extrusive	lava	37.4490	−90.5420
CW28-1300	Trachyte host of Camels Hump IOA deposit	Mafic extrusive	lava	37.7980	−91.2320
J2-0030	Boss trachyandesite	Mafic extrusive	lava	37.6460	−91.1728
56W167-1613	Basaltic andesite host of Kratz Spring IOA deposit	Mafic extrusive	lava	38.2600	−91.1900
S5-1530-1559	Diorite host of Boss IOCG deposit	Mafic intrusive	pluton	37.6500	−91.2800
J2-0015	Boss basaltic trachyandesite	Mafic intrusive	dike	37.6460	−91.1728
Bourb-039	Bourbon basalt	Mafic intrusive	dike	38.1218	−91.2574
MO13-06	Floyd Tower/Indian Creek trachyandesite	Intermediate extrusive	lava	37.9750	−90.9913
MO16-012	Trachyte at South Crane Mountain	Intermediate extrusive	lava	37.4280	−90.5177
Bourb-096	Bourbon trachydacite	Intermediate extrusive	lava	38.1218	−91.2574
PR009A	Pea Ridge trachyte-1975	Intermediate extrusive	tuff	38.1300	−91.0500
24	French Mills felsite	Intermediate extrusive	lava	37.4387	−90.3706
RA-MO-13-10	Tiemann quartz diorite	Intermediate intrusive	pluton	37.5704	−90.4643
54W159-1558	Trachyte of Kratz Spring	Intermediate intrusive	plug	38.2600	−91.1900
MO16-059	Iron Mountain Lake rhyolite	Felsic extrusive	tuff	37.6905	−90.6054
ARC5/96−9	Ironton Rhyolite	Felsic extrusive	tuff	37.5992	−90.6928
CB216-5	Creekbed rhyolite ash-flow tuff	Felsic extrusive	tuff	37.4647	−90.5609
FL814-5	Fenceline rhyolite ash-flow tuff	Felsic extrusive	tuff	37.4439	−90.5005
3	Oak Mountain rhyolite	Felsic extrusive	lava	37.6729	−90.6080
BR627-8	Brown's rhyolite ash-flow tuff	Felsic extrusive	tuff	37.4303	−90.5210
BT216-4	Black rhyolite ash-flow tuff	Felsic extrusive	tuff	37.4656	−90.5596
MO13-001	Trachyte at South Crane Mountain	Felsic extrusive	lava	37.4770	−90.6219
ST218-8	Saddle rhyolite ash-flow tuff	Felsic extrusive	tuff	37.4632	−90.5661
T339	Johnson Shut-ins Rhyolite	Felsic extrusive	tuff	37.6290	−90.8660
MO15-002	Rhyolite tuff of Little Rock Creek	Felsic extrusive	tuff	37.4573	−90.5010
GR216-2	Green rhyolite	Felsic extrusive	lava	37.4671	−90.5600
ARC5/96-4	Russell Mountain Rhyolite	Felsic extrusive	tuff	37.5718	−90.7065
16	Stouts Creek Rhyolite	Felsic extrusive	lava	37.5883	−90.5276
TK827-7	Tilk Hollow rhyolite ash-flow tuff	Felsic extrusive	tuff	37.4037	−90.5228
JCR24	Rhyolite in the Cope Hollow Fm	Felsic extrusive	tuff	37.5393	−90.8376
MO14-020	Cedar Bluff Rhyolite	Felsic extrusive	tuff	37.5916	−90.6586
MO93-136	Cuthbertson Mountain rhyolite	Felsic extrusive	tuff	37.5405	−90.6514
MO16-057	Shepherd Mountain Rhyolite	Felsic extrusive	tuff	37.6059	−90.6466
FC222-7	Forked Creek rhyolite ash-flow tuff	Felsic extrusive	tuff	37.4856	−90.6245
MC813-2	Marble Creek rhyolite ash-flow tuff	Felsic extrusive	tuff	37.4391	−90.5077
CP82-5	Tuff at Crane Pond	Felsic extrusive	tuff	37.4169	−90.6152
MO16-007	Upper Ridge rhyolite tuff	Felsic extrusive	tuff	37.4243	−90.5730
UO218-3	Upper Orchard rhyolite ash-flow tuff	Felsic extrusive	tuff	37.4592	−90.5777
LG80-15	Logroad rhyolite ash-flow tuff	Felsic extrusive	tuff	37.4870	−90.6012
ARC5/96-7	Pond Ridge Rhyolite	Felsic extrusive	tuff	37.5922	−90.6601

Table 10. Identification and characteristics of igneous rock samples from the St. Francois Mountains terrane, southeast Missouri for which representative geochemical analyses are presented by du Bray and others (2018b) and Granitto and others (2018).—Continued

Sample number	Geologic unit	Unit type	Form	North latitude	West longitude
MO16-004	Lower Ridge rhyolite tuff	Felsic extrusive	tuff	37.4352	−90.6007
MO16-015	Tile Red ash-flow tuff	Felsic extrusive	tuff	37.4133	−90.5829
PEA10/95-16	Pea Ridge 1825 rhyolite porphyry	Felsic extrusive	tuff	38.1269	−91.0458
TN908	Transition rhyolite ash-flow tuff	Felsic extrusive	tuff	37.4777	−90.5252
RH917-6	Reader Hollow rhyolite ash-flow tuff	Felsic extrusive	tuff	37.4042	−90.5959
SM914-1	Sawmill rhyolite ash-flow tuff	Felsic extrusive	tuff	37.3788	−90.6214
CC80-12A	Clearcut rhyolite ash-flow tuff	Felsic extrusive	tuff	37.4872	−90.6059
BH22-8	Brushy rhyolite ash-flow tuff	Felsic extrusive	tuff	37.4601	−90.5041
MV82-3	Mountain View rhyolite	Felsic extrusive	lava	37.4210	−90.6107
T345	Goggins Mountain rhyolite ash-flow tuff	Felsic extrusive	tuff	37.5580	−90.8980
MGS28-1	Ketcherside Mountain rhyolite ignimbrite	Felsic extrusive	tuff	37.5288	−90.6772
ARC5/96-3	Bell Mountain Rhyolite ash-flow tuff	Felsic extrusive	tuff	37.5790	−90.9090
22	Hogan Mountain rhyolite	Felsic extrusive	lava	37.5108	−90.8543
MO16-024	Grassy Mountain Ignimbrite	Felsic extrusive	tuff	37.5853	−90.5826
MGS37-4	Royal Gorge Rhyolite	Felsic extrusive	lava	37.5140	−90.6767
MO15-004	Lake Killarney Formation	Felsic extrusive	tuff	37.5482	−90.5223
MO16-023B	Ironton Hollow-Cedar Bluff Rhyolite	Felsic extrusive	breccia	37.6329	−90.6407
MO14-043	Lower campground tuff at Marble Creek campground	Felsic extrusive	tuff	37.4500	−90.5418
ARC5/96-2	Taum Sauk Rhyolite	Felsic extrusive	tuff	37.5684	−90.7175
N6976	Stono Granite	Felsic intrusive	pluton	37.7160	−90.5480
RA-MO-13-5	Knoblick Granite	Felsic intrusive	pluton	37.6689	−90.3885
RA-MO-13−9	Silvermine Granite	Felsic intrusive	pluton	37.5571	−90.4481
MO16-003	Brown Mountain granite porphyry	Felsic intrusive	pluton	37.5953	−90.5589
IGCP1-3a	Slabtown Granite	Felsic intrusive	pluton	37.6067	−90.3391
39	Buford Granite Porphyry	Felsic intrusive	pluton	37.7431	−90.6736
RA-MO-13-4	Butler Hill Granite	Felsic intrusive	pluton	37.7045	−90.3993
BS 111	Big Spring granite	Felsic intrusive	pluton	36.9712	−90.9770
233	Silvermine Granite	Felsic intrusive	pluton	37.5920	−90.4740
60W-183-1071	Bunker granite	Felsic intrusive	pluton	37.3463	−91.1189
RA-MO-13-3	Breadtray Granite	Felsic intrusive	pluton	37.6937	−90.5458
USA2-1196	Boss rhyolite	Felsic intrusive	dike	37.6561	−91.1576
29	Mudlick rhyolite	Felsic intrusive	sill	37.1797	−90.6861
J4-1533	Boss granite	Felsic intrusive	dike	37.6427	−91.1772
B-USBM 2-1421	Bourbon rhyolite	Felsic intrusive	plug	38.1500	−91.2500

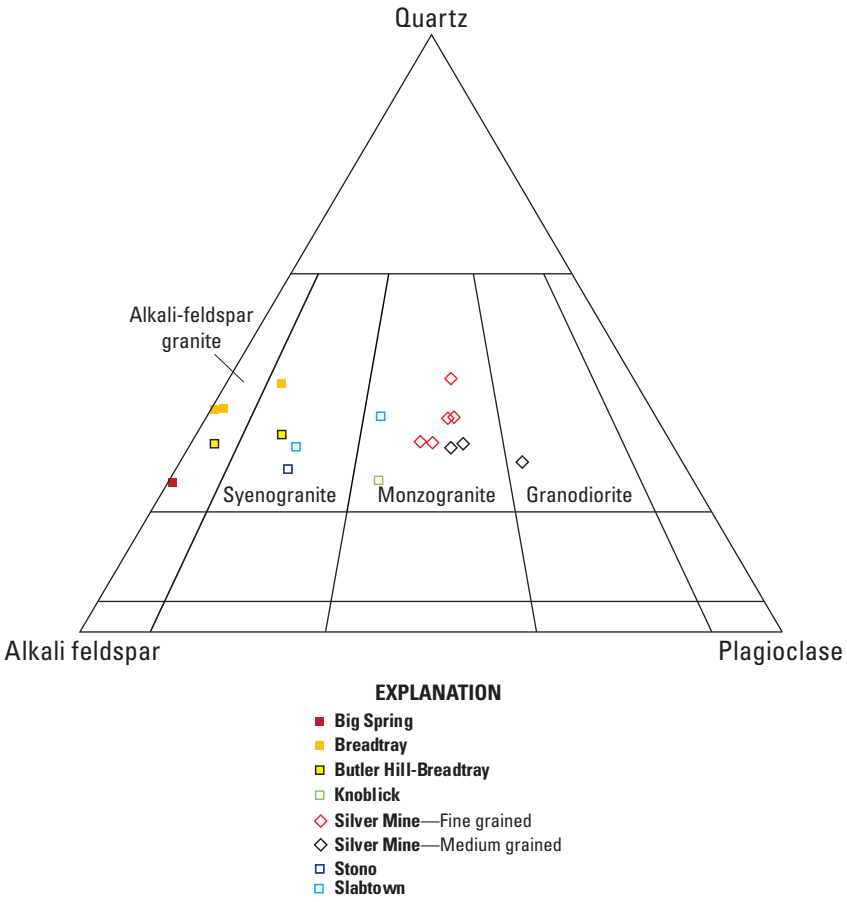

Figure 5. Quartz-alkali feldspar-plagioclase ternary diagram showing modal compositions of 1.48 to 1.45 billion year old granitoid intrusions in the St. Francois Mountains terrane, southeast Missouri. Data from Bickford and others (1981) and Kisvarsanyi (1972). Classification grid and rock names are from Streckeisen (1976).

metaluminous and all but one are mafic and compositionally primitive (figs. 7, 9, and 10; table 11). Four of these units have compositions that are calc alkalic and one is calcic (table 11). Within this composition-based classification schema, extrusive and intrusive rocks are indistinguishable.

Major oxide compositions of individual 1.48 to 1.45 Ga igneous rocks in the St. Francois Mountains terrane form diffuse clusters or irregular arrays, each somewhat diagnostic of particular geologic units (fig. 11). These overlapping clusters and arrays define two discrete major oxide composition populations, one mafic and the other felsic; the previously identified third population consists of samples from just four intermediate-composition geologic units that also form distinct major oxide compositional clusters and arrays. Among 1.48 to 1.45 Ga igneous rocks, TiO_2, MgO (magnesium oxide), CaO (calcium oxide), and P_2O_5 (phosphorous pentoxide) abundances vary considerably at SiO_2 abundances less than about 60 weight percent but scatter less and decrease with increasing SiO_2 contents. Similarly, Al_2O_3 abundances vary considerably at lower SiO_2 abundances; Al_2O_3 abundances vary irregularly in samples with less than about 60 weight percent SiO_2, but decrease significantly and consistently, forming a concave downward data array, in samples with more than 70 weight percent SiO_2. Concentrations of FeO* (total iron expressed as ferrous oxide) and MnO decrease systematically with increasing SiO_2. Abundances of Na_2O and K_2O vary considerably at all SiO_2 contents, but particularly at high SiO_2 contents (fig. 11). At any given SiO_2 content, Na_2O abundances vary by as much as about 3 weight percent. Similarly, at any given SiO_2 content among the mafic rocks, K_2O abundances vary by about 2 weight percent and by as much as 4.5 weight percent among the felsic rocks. These highly variable Na_2O and K_2O abundances do not systematically correlate with SiO_2 content and may reflect cryptic alkali metasomatism of some of these rocks. K_2O abundances of the 1.48 to 1.45 Ga igneous rocks in the St. Francois Mountains terrane are broadly coincident with the high potassium (Le Maitre, 1989) and shoshonitic (Ewart, 1982) fields. Major

oxide compositions of the 1.48 to 1.45 Ga igneous rocks in the St. Francois Mountains terrane are indistinguishable (fig. 11) from those of all other Mesoproterozoic granitoid rocks exposed throughout the United States (du Bray and others, 2018a). However, mafic to intermediate composition rocks in the St. Francois Mountains terrane have no analog in the compilation of du Bray and others (2015), which was restricted to rocks with >56 weight percent SiO_2.

With the exception of loss on ignition data, relatively limited information is available concerning volatile component abundances in 1.48 to 1.45 Ga igneous rocks of the St. Francois Mountains terrane. Median loss on ignition values and chlorine and fluorine abundances in these rocks are 0.88, 0.03, and 0.08 weight percent, respectively. Low halogen contents imply that H_2O is the principal volatile constituent in these rocks. Inferred H_2O abundances, ranging from 0.1 to about 3 weight percent and symmetrically and unimodally distributed about a maximum frequency value of about 0.7 weight percent, are similar to abundances in subalkalic silicic obsidians (Macdonald and others, 1992), which are compositionally similar to 1.48 to 1.45 Ga felsic igneous rocks of the St. Francois Mountains terrane. One attribute of A-type igneous rocks, which are grossly similar to the ferroan 1.48 to 1.45 Ga igneous rocks in the St. Francois Mountains terrane, is their low volatile content (Loiselle and Wones, 1979). Although H_2O contents of 1.48 to 1.45 Ga felsic igneous rocks of the St. Francois Mountains terrane are not especially low relative to values characteristic of A-type igneous rocks nor to the obsidians, they are significantly lower than the >4 weight percent H_2O characteristic of hornblende-bearing andesitic arc magmas (Rutherford and Hill, 1993). Fluorine abundances determined for about 60 samples of 1.48 to 1.45 Ga felsic igneous rocks from the St. Francois Mountains terrane range from about 0.01 to 0.3 weight percent and define a maximum frequency value of 0.05 weight percent (500 ppm). The median fluorine content of these rocks, 800 ppm, is comparable to the average (850 ppm) for low-calcium granites (Turekian and Wedepohl, 1961), somewhat elevated relative to abundances (average, 500 ppm) in silicic obsidians associated with magmatic arcs, and low relative to average abundances (1,500 ppm) in intracontinental silicic obsidians (Macdonald and others, 1992). Chlorine abundances determined for about 40 samples of these rocks range from 0.01 to about 0.13 weight percent and are strongly skewed to values between 0.01 and 0.02 weight percent. The maximum frequency value is 0.01 weight percent (100 ppm) and the median chlorine abundance of these rocks, 300 ppm, is similar to the average chlorine content (200 ppm) of low-calcium granite (Turekian and Wedepohl, 1961) and low relative to abundances in most silicic obsidians (Macdonald and others, 1992).

Trace Element Data

Trace element abundances of the 1.48 to 1.45 Ga igneous rocks in the St. Francois Mountains terrane vary widely but certain of these characteristics are consistent among particular rock types and inform our understanding of the petrogenesis and tectonic setting pertinent to the associated magmatism. Relative to the average low-calcium granite (Turekian and Wedepohl, 1961), most of the felsic 1.48 to 1.45 Ga igneous rocks from the St. Francois Mountains terrane contain elevated Hf and Zr and low Cu, Nb, Sr, Ta, Th, and V. In contrast, relative to average basaltic rocks (Turekian and Wedepohl, 1961), mafic rocks in the St. Francois Mountains terrane contain low Cr, Cu, Nb, Ni, Sr, and Th. Abundances of Ba, Hf, La, Nb, Rb, Th, U, Y, and Zr in igneous rocks of the St. Francois Mountains terrane increase slightly with increasing silica content; those for Co, Cr, Cu, Ni, Sc, Sr, V, and Zn decrease with increasing silica content; and abundances of Be, Cs, Ga, Pb, Sn, and Ta display no consistent covariation with SiO_2 content.

Among 1.48 to 1.45 Ga igneous rocks in the St. Francois Mountains terrane, representative REE abundances vary by nearly a full order of magnitude; however, their chondrite-normalized REE patterns are grossly similar (fig. 12). These representative patterns are moderately negatively sloping; most have La_N/Yb_N (ratio of the chondrite-normalized abundances of lanthanum and ytterbium) that varies from about 2.5 to 8.7 (median, 4.7) (table 12). In contrast, negative europium (Eu) anomaly magnitudes vary systematically with respect to whole-rock composition. The median Eu/Eu* (ratio of determined europium abundance to europium abundance interpolated from the abundances of samarium and gadolinium) for mafic igneous rocks of the St. Francois Mountains terrane is 0.89; those for the intermediate and felsic rocks are 0.66 and 0.43, respectively (table 12). The extent of REE abundance variation within each geologic unit, expressed as chondrite-normalized pattern dispersion, is conveyed by standard deviation values calculated from the REE data for each unit. For any given unit, standard deviations calculated for each of the REE vary within relatively narrow ranges, which suggests that the standard deviation for any particular REE (such as La, which is abundant and easily determined with high precision) depicts REE abundance dispersion for each unit. The standard deviation of La abundance calculated for each unit, divided by its associated average La abundance, yields a consistent, normalized REE dispersion metric (table 12, Dispersion). Among 1.48 to 1.45 Ga igneous rocks in the St. Francois Mountains terrane, calculated REE dispersion, La_N/Yb_N and total REE do not vary systematically with respect to SiO_2 content, although the mafic rocks, as group, have systematically lower total REE contents than the intermediate and felsic igneous rocks.

Representative chondrite-normalized REE patterns for 1.48 to 1.45 Ga igneous rocks in the St. Francois Mountains terrane exhibit some similarities, regardless of whole-rock

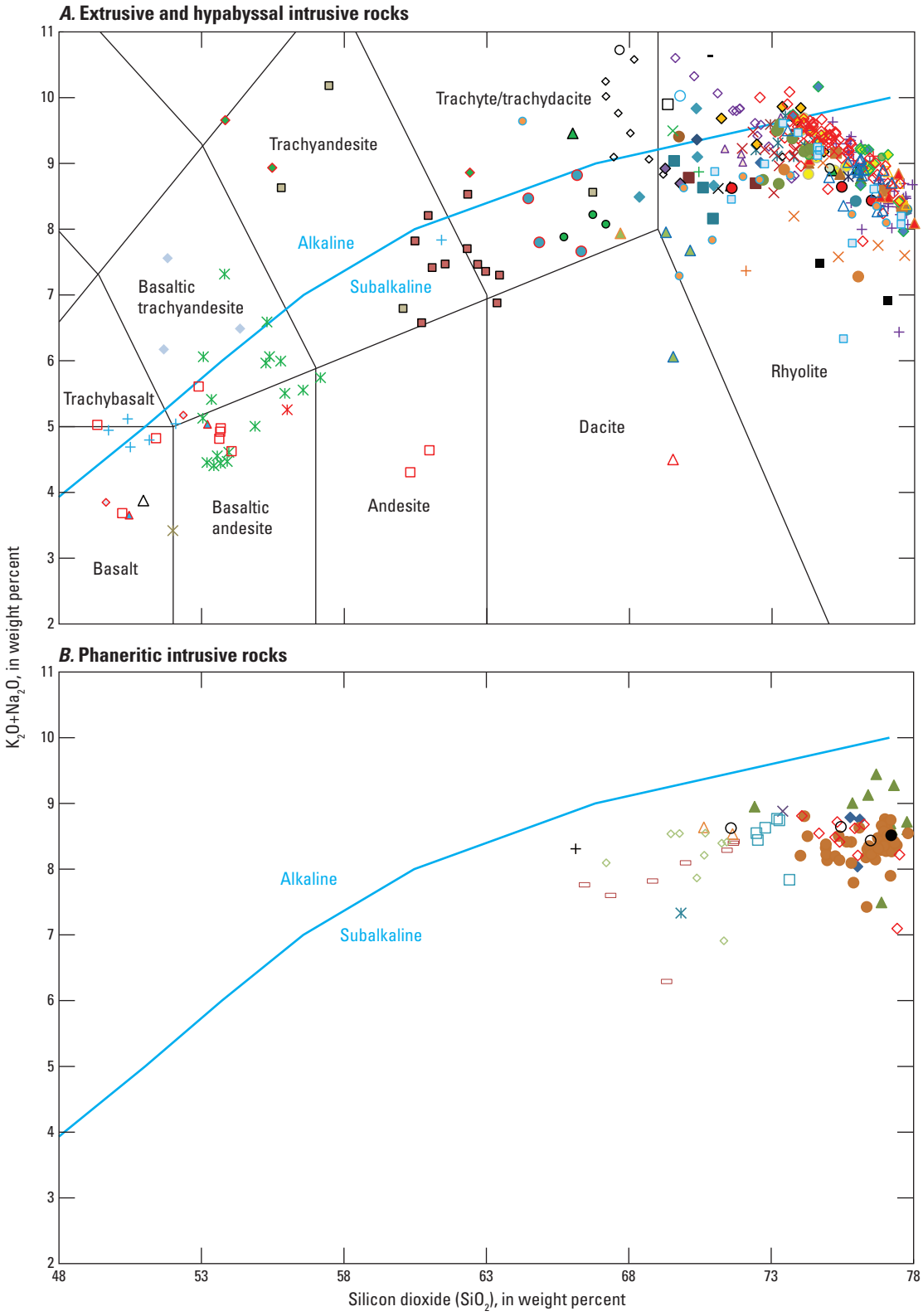

Figure 6. Total alkali-silica variation diagrams showing compositions of 1.48 to 1.45 billion year old igneous rocks in the St. Francois Mountains terrane, southeast Missouri. Alkaline-subalkaline dividing line from Irvine and Baragar (1971). Extrusive rock classification grid from Le Maitre (1989).

A. Extrusive and hypabyssal intrusive rocks

EXPLANATION

- Bell Mountain Rhyolite
- Black rhyolite
- Boss diorite
- Boss andesite
- Boss rhyolite
- Boss trachyte
- Bourbon basalt
- Bourbon rhyolite
- Bourbon trachydacite
- Brown Mountain
- Brown's rhyolite
- Brushy rhyolite
- Trachyte host of Camels Hump IOA deposit
- Cedar Bluff Rhyolite
- Clearcut rhyolite
- Lower unit of Coot Mountain
- Basalt in Cope Hollow Formation
- Rhyolite in Cope Hollow Formation
- Tuff at Crane Pond
- Creekbed rhyolite
- Cuthbertson Mountain rhyolite
- Fenceline rhyolite
- Forked Creek rhyolite
- French Mills felsite
- Goggins Mountain rhyolite
- Grassy Mountain Ignimbrite
- Green rhyolite
- Hogan Mountain rhyolite
- Trachyandesite of Floyd Tower/Indian Creek
- Iron Mountain Lake rhyolite
- Ironton Rhyolite
- Ironton Hollow Rhyolite
- Johnson shut-ins rhyolite
- Ketcherside Mountain rhyolite
- Kratz Spring basalt
- Kratz Spring rhyolite
- Kratz Spring trachyte
- Lake Four Winds basalt
- Lake Killarney Formation
- Little Rock Creek rhyolite
- Logroad rhyolite
- Lower campground tuff at Marble Creek campground
- Lower Ridge rhyolite
- Marble Creek rhyolite
- Mountain View rhyolite
- Mudlick rhyolite
- Oak Mountain rhyolite
- Pea Ridge rhyolite
- Pea Ridge trachyte
- Pond Ridge Rhyolite
- Reader Hollow rhyolite
- Royal Gorge Rhyolite
- Russell Mountain Rhyolite
- Saddle rhyolite
- Sawmill rhyolite
- Shepherd Mountain Rhyolite
- Silver Mines basaltic andesite
- Rhyolite at South Crane Mountain
- Trachydacite at South Crane Mountain
- Stouts Creek rhyolite
- Taum Sauk Rhyolite
- Tile Red ash-flow tuff
- Tilk Hollow rhyolite
- Transition rhyolite
- Upper and Lower andesites of Marble Creek campground
- Upper Orchard rhyolite
- Upper Ridge rhyolite

B. Intrusive rocks

EXPLANATION

Massif intrusions

- Big Spring granite
- Buford Granite Porphyry
- Butler Hill Granite
- Breadtray Granite
- Bunker granite
- Granite of Castor River Shut-Ins

Minor intrusion

- Brown Mountain granite porphyry

Ring intrusions

- Knoblick Granite
- Slabtown Granite
- Silvermine Granite—Medium grained
- Silvermine Granite—Fine grained
- Stono Granite
- Tiemann quartz diorite

Figure 6. Total alkali-silica variation diagrams showing compositions of 1.48 to 1.45 billion year old igneous rocks in the St. Francois Mountains terrane, southeast Missouri. Alkaline-subalkaline dividing line from Irvine and Baragar (1971). Extrusive rock classification grid from Le Maitre (1989). —Continued

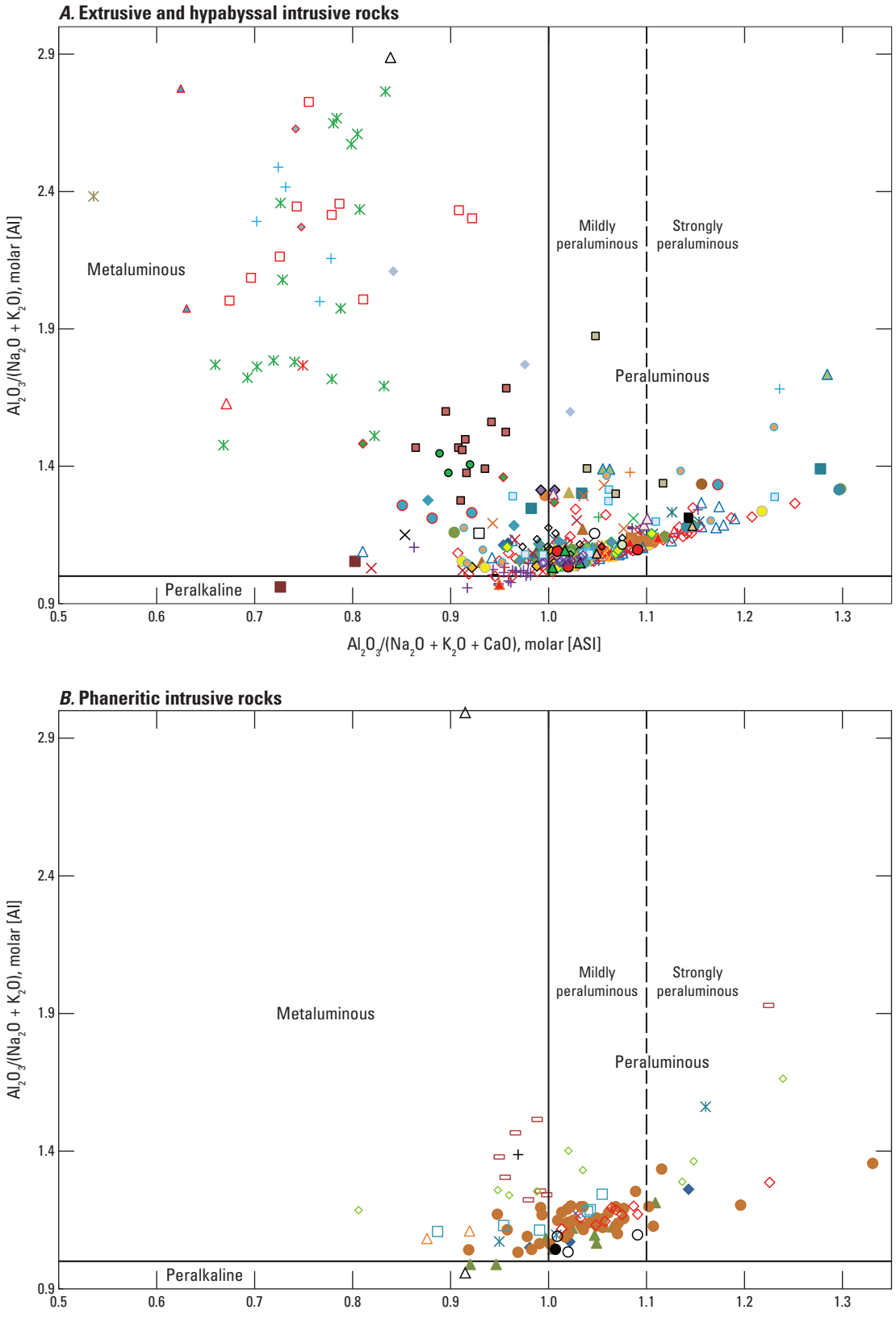

Figure 7. Variation diagrams showing molar major-oxide compositions of 1.48 to 1.45 billion year old igneous rocks in the St. Francois Mountains terrane, southeast Missouri as a function of relative alumina and alkali saturation.

A. Extrusive and hypabyssal intrusive rocks

EXPLANATION

- Bell Mountain Rhyolite
- Black rhyolite
- Boss diorite
- Boss andesite
- Boss rhyolite
- Boss trachyte
- Bourbon basalt
- Bourbon rhyolite
- Bourbon trachydacite
- Brown Mountain
- Brown's rhyolite
- Brushy rhyolite
- Trachyte host of Camels Hump IOA deposit
- Cedar Bluff Rhyolite
- Clearcut rhyolite
- Lower unit of Coot Mountain
- Basalt in Cope Hollow Formation
- Rhyolite in Cope Hollow Formation
- Tuff at Crane Pond
- Creekbed rhyolite
- Cuthbertson Mountain rhyolite
- Fenceline rhyolite
- Forked Creek rhyolite
- French Mills felsite
- Goggins Mountain rhyolite
- Grassy Mountain Ignimbrite
- Green rhyolite
- Hogan Mountain rhyolite
- Trachyandesite of Floyd Tower/Indian Creek
- Iron Mountain Lake rhyolite
- Ironton Rhyolite
- Ironton Hollow Rhyolite
- Johnson shut-ins rhyolite
- Ketcherside Mountain rhyolite
- Kratz Spring basalt
- Kratz Spring rhyolite
- Kratz Spring trachyte
- Lake Four Winds basalt
- Lake Killarney Formation
- Little Rock Creek rhyolite
- Logroad rhyolite
- Lower campground tuff at Marble Creek campground
- Lower Ridge rhyolite
- Marble Creek rhyolite
- Mountain View rhyolite
- Mudlick rhyolite
- Oak Mountain rhyolite
- Pea Ridge rhyolite
- Pea Ridge trachyte
- Pond Ridge Rhyolite
- Reader Hollow rhyolite
- Royal Gorge Rhyolite
- Russell Mountain Rhyolite
- Saddle rhyolite
- Sawmill rhyolite
- Shepherd Mountain Rhyolite
- Silver Mines basaltic andesite
- Rhyolite at South Crane Mountain
- Trachydacite at South Crane Mountain
- Stouts Creek rhyolite
- Taum Sauk Rhyolite
- Tile Red ash-flow tuff
- Tilk Hollow rhyolite
- Transition rhyolite
- Upper and Lower andesites of Marble Creek campground
- Upper Orchard rhyolite
- Upper Ridge rhyolite

B. Intrusive rocks

EXPLANATION

Massif intrusions

- Big Spring granite
- Buford Granite Porphyry
- Butler Hill Granite
- Breadtray Granite
- Bunker granite
- Granite of Castor River Shut-Ins

Minor intrusion

- Brown Mountain granite porphyry

Ring intrusions

- Knoblick Granite
- Slabtown Granite
- Silvermine Granite—Medium grained
- Silvermine Granite—Fine grained
- Stono Granite
- Tiemann quartz diorite

Figure 7. Variation diagrams showing molar major-oxide compositions of 1.48 to 1.45 billion year old igneous rocks in the St. Francois Mountains terrane, southeast Missouri as a function of relative alumina and alkali saturation. —Continued

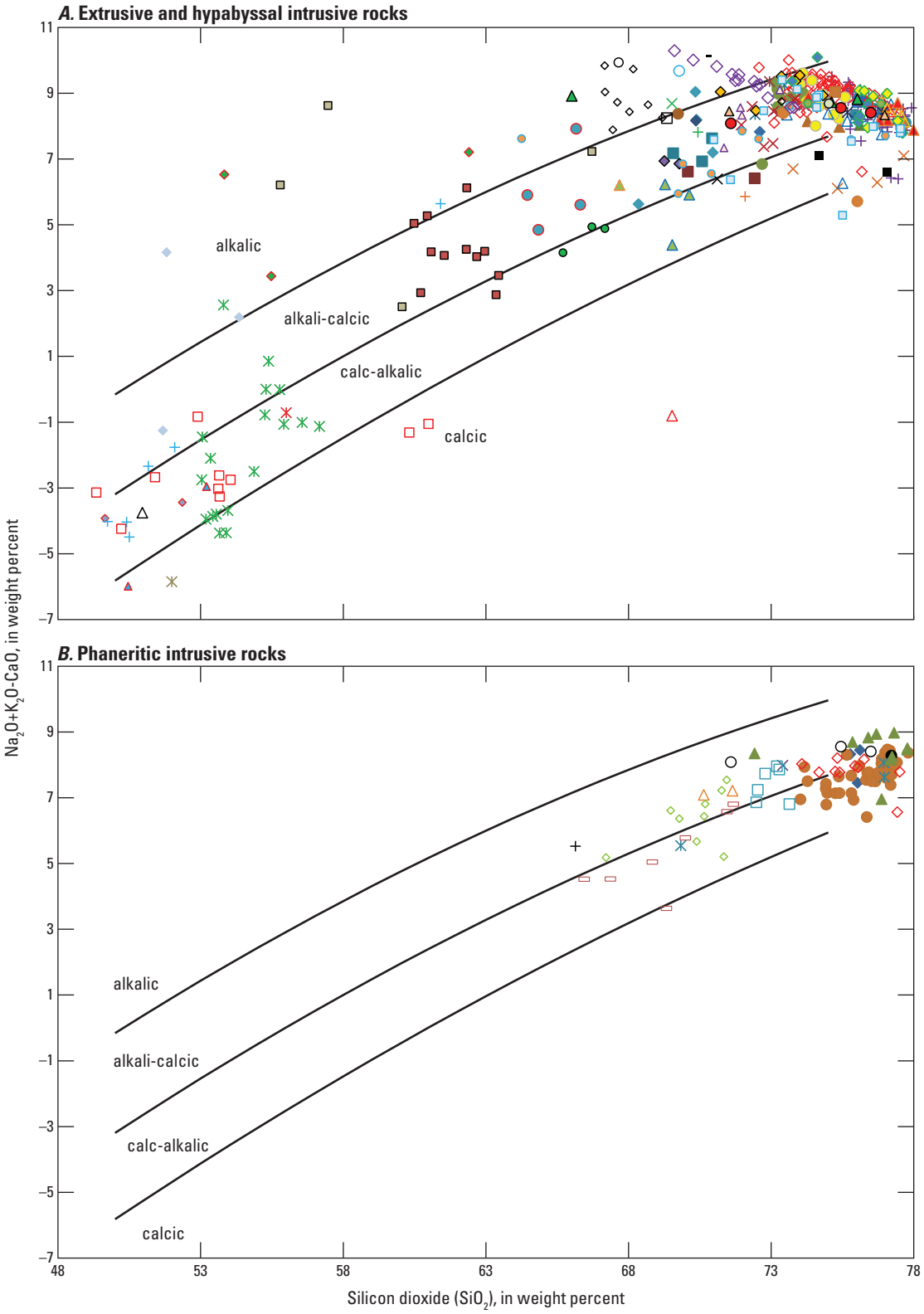

Figure 8. $Na_2O + K_2O - CaO$ relative to SiO_2 variation diagram showing the compositions of 1.48 to 1.45 billion year old igneous rocks in the St. Francois Mountains terrane, southeast Missouri relative to boundaries between alkalic, alkali-calcic, calc-alkalic, and calcic rock series. Boundaries between various rock series from Frost and others (2001).

A. Extrusive and hypabyssal intrusive rocks

EXPLANATION

- Bell Mountain Rhyolite
- Black rhyolite
- Boss diorite
- Boss andesite
- Boss rhyolite
- Boss trachyte
- Bourbon basalt
- Bourbon rhyolite
- Bourbon trachydacite
- Brown Mountain
- Brown's rhyolite
- Brushy rhyolite
- Trachyte host of Camels Hump IOA deposit
- Cedar Bluff Rhyolite
- Clearcut rhyolite
- Lower unit of Coot Mountain
- Basalt in Cope Hollow Formation
- Rhyolite in Cope Hollow Formation
- Tuff at Crane Pond
- Creekbed rhyolite
- Cuthbertson Mountain rhyolite
- Fenceline rhyolite
- Forked Creek rhyolite
- French Mills felsite
- Goggins Mountain rhyolite
- Grassy Mountain Ignimbrite
- Green rhyolite
- Hogan Mountain rhyolite
- Trachyandesite of Floyd Tower/Indian Creek
- Iron Mountain Lake rhyolite
- Ironton Rhyolite
- Ironton Hollow Rhyolite
- Johnson shut-ins rhyolite
- Ketcherside Mountain rhyolite
- Kratz Spring basalt
- Kratz Spring rhyolite
- Kratz Spring trachyte
- Lake Four Winds basalt
- Lake Killarney Formation
- Little Rock Creek rhyolite
- Logroad rhyolite
- Lower campground tuff at Marble Creek campground
- Lower Ridge rhyolite
- Marble Creek rhyolite
- Mountain View rhyolite
- Mudlick rhyolite
- Oak Mountain rhyolite
- Pea Ridge rhyolite
- Pea Ridge trachyte
- Pond Ridge Rhyolite
- Reader Hollow rhyolite
- Royal Gorge Rhyolite
- Russell Mountain Rhyolite
- Saddle rhyolite
- Sawmill rhyolite
- Shepherd Mountain Rhyolite
- Silver Mines basaltic andesite
- Rhyolite at South Crane Mountain
- Trachydacite at South Crane Mountain
- Stouts Creek rhyolite
- Taum Sauk Rhyolite
- Tile Red ash-flow tuff
- Tilk Hollow rhyolite
- Transition rhyolite
- Upper and Lower andesites of Marble Creek campground
- Upper Orchard rhyolite
- Upper Ridge rhyolite

B. Intrusive rocks

EXPLANATION

Massif intrusions

- Big Spring granite
- Buford Granite Porphyry
- Butler Hill Granite
- Breadtray Granite
- Bunker granite
- Granite of Castor River Shut-Ins

Minor intrusion

- Brown Mountain granite porphyry

Ring intrusions

- Knoblick Granite
- Slabtown Granite
- Silvermine Granite—Medium grained
- Silvermine Granite—Fine grained
- Stono Granite
- Tiemann quartz diorite

Figure 8. $Na_2O + K_2O - CaO$ relative to SiO_2 variation diagram showing the compositions of 1.48 to 1.45 billion year old igneous rocks in the St. Francois Mountains terrane, southeast Missouri relative to boundaries between alkalic, alkali-calcic, calc-alkalic, and calcic rock series. Boundaries between various rock series from Frost and others (2001). —Continued

Table 11. Chemical classification of 1.48 to 1.45 Ga igneous rock geologic map units in the St. Francois Mountains terrane, southeast Missouri.

[Units with compositions transitional between more than one category are listed in each appropriate category. Entries in parentheses represent reclassification of unit compositions based on the data of du Bray and others (2018b) and the classification schema of Le Maitre (1989)]

Peraluminous				Metaluminous			
Alkalic	**Alkali-calcic**	**Calc-alkalic**	**Calcic**	**Alkalic**	**Alkali-calcic**	**Calc-alkalic**	**Calcic**
Ferroan							
Boss trachyte (trachyandesite)	Bell Mountain Rhyolite	Butler Hill Granite	Cuthbertson Mountain rhyolite	Trachyte host of Camels Hump IOA deposit (trachyandesite)	Boss andesite (basaltic trachyandesite)	Bourbon trachydacite	
Rhyolite in the Cope Hollow Fm	Big Spring granite	Lower unit of Coot Mountain		Johnson Shut-ins Rhyolite	Brown's rhyolite	Brushy rhyolite	
Fenceline rhyolite	Boss rhyolite	Lower campground tuff at Marble Creek campground (rhyolite)			Black rhyolite	Bunker granite	
Ironton Rhyolite	Boss trachyte (trachyandesite)	Mudlick (rhyolite)			Brushy rhyolite	Green rhyolite	
Rhyolite of Kratz Spring (trachyte)	Bourbon rhyolite	Pea Ridge 1825 rhyolite porphyry			Goggins Mountain rhyolite	Lake Four Winds basalt	
Pea Ridge 1975 trachyte porphyry	Breadtray Granite	Russell Mountain Rhyolite			Grassy Mountain Ignimbrite	Trachyte of Kratz Spring (basaltic andesite)	
	Brown Mountain granite porphyry				Trachyandesite of Floyd Tower/Indian Creek/		
	Buford Granite Porphyry				Iron Mountain Lake rhyolite		
	Cedar Bluff Rhyolite				Logroad rhyolite		
	Clearcut rhyolite				Oak Mountain rhyolite		
	Rhyolite in the Cope Hollow Fm				Rhyolite at South Crane Mountain		
	Tuff at Crane Pond (rhyolite)				Trachyte at South Crane Mountain		
	Creekbed rhyolite				Stono Granite		
	Cuthbertson Mountain rhyolite				Stouts Creek rhyolite		
	Forked Creek rhyolite				Tiemann quartz diorite		
	French Mills felsite (trachydacite)				Tilk Hollow (rhyolite)		
	Grassy Mountain Ignimbrite (rhyolite)				Upper Ridge (rhyolite)		
	Hogan Mountain rhyolite						
	Ironton Hollow-Cedar Bluff Rhyolite						
	Ketcherside Mountain rhyolite						
	Lake Killarney Formation (rhyolite)						
	Little Rock Creek rhyolite						

Table 11. Chemical classification of 1.48 to 1.45 Ga igneous rock geologic map units in the St. Francois Mountains terrane, southeast Missouri.—Continued

[Units with compositions transitional between more than one category are listed in each appropriate category. Entries in parentheses represent reclassification of unit compositions based on the data of du Bray and others (2018b) and the classification schema of Le Maitre (1989)]

Peraluminous				Metaluminous			
Alkalic	Alkali-calcic	Calc-alkalic	Calcic	Alkalic	Alkali-calcic	Calc-alkalic	Calcic
	Lower Ridge rhyolite						
	Marble Creek rhyolite ash-flow tuff						
	Mountain View rhyolite						
	Oak Mountain rhyolite						
	Pea Ridge rhyolite porphyry-1675						
	Pea Ridge rhyolite porphyry-2275						
	Pond Ridge Rhyolite						
	Reader Hollow rhyolite						
	Royal Gorge Rhyolite						
	Saddle rhyolite						
	Sawmill rhyolite						
	Shepherd Mountain Rhyolite						
	Slabtown Granite						
	Stouts Creek rhyolite						
	Taum Sauk Rhyolite						
	Tile Red ash-flow tuff						
	Transition rhyolite						
	Upper Orchard rhyolite						
Transitionally Ferroan-Magnesian							
	Silvermine Granite-fine grained					Diorite host Boss IOCG deposit	
						Basalt in the Cope Hollow Fm	
						Silver Mines basaltic andesite	
						Lower and upper andesites of Marble Creek campground (basaltic andesite)	
Magnesian							
						Basalt host of the Bourbon IOA deposit	Basalt of Kratz Spring
						Knoblick Granite	
						Basaltic andesite host of the Kratz Spring IOA deposit	
						Silvermine Granite-medium grained	

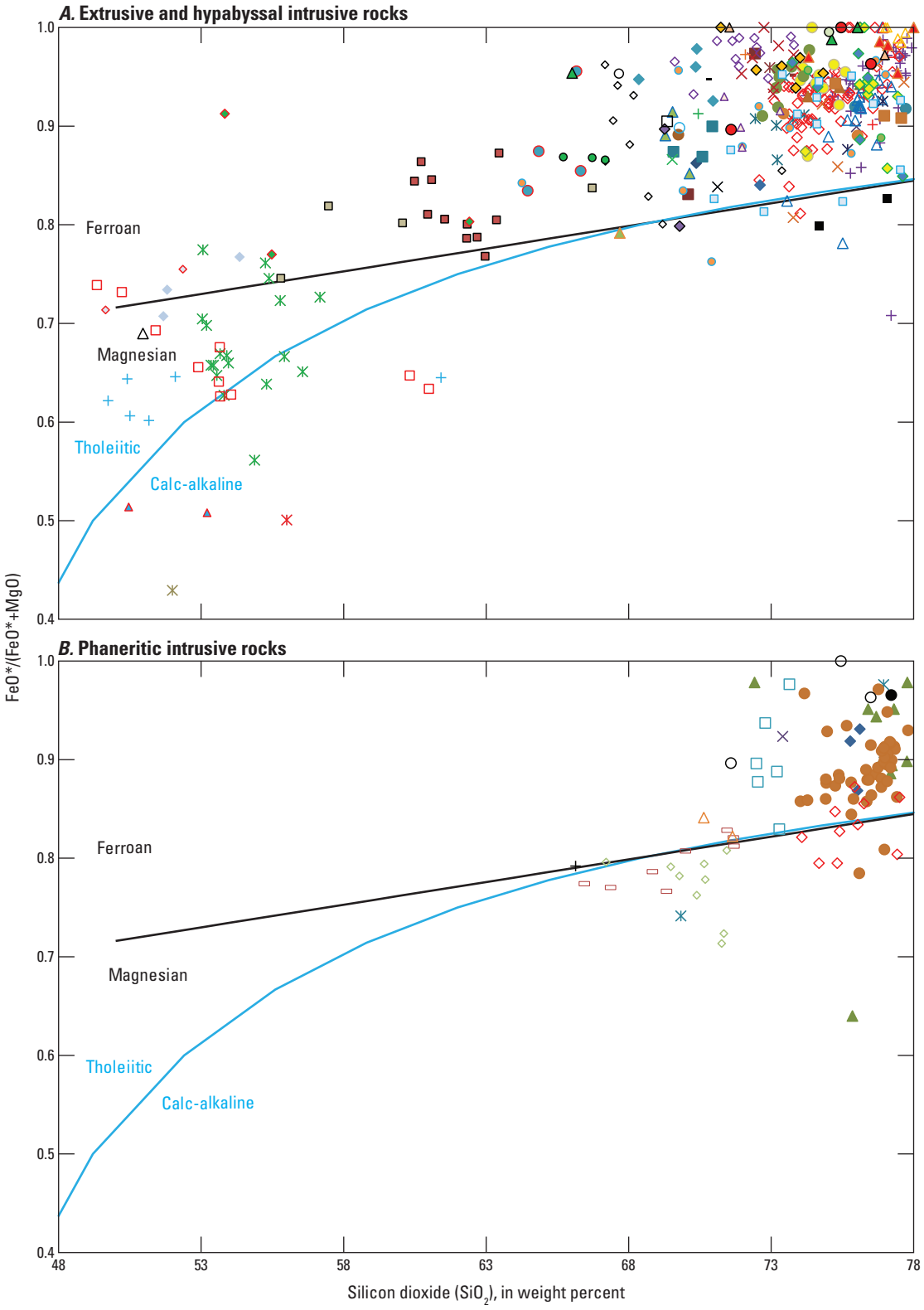

Figure 9. FeO*/(FeO* + MgO) variation diagram showing the composition of 1.48 to 1.45 billion year old igneous rocks in the St. Francois Mountains terrane, southeast Missouri relative to boundaries between ferroan and magnesian rocks as well as between tholeiitic and calc-alkaline rocks. Ferroan-magnesian boundary from Frost and others (2001); tholeiitic-calc-alkaline boundary from Miyashiro (1974).

A. Extrusive and hypabyssal intrusive rocks

EXPLANATION

- Bell Mountain Rhyolite
- Black rhyolite
- Boss diorite
- Boss andesite
- Boss rhyolite
- Boss trachyte
- Bourbon basalt
- Bourbon rhyolite
- Bourbon trachydacite
- Brown Mountain
- Brown's rhyolite
- Brushy rhyolite
- Trachyte host of Camels Hump IOA deposit
- Cedar Bluff Rhyolite
- Clearcut rhyolite
- Lower unit of Coot Mountain
- Basalt in Cope Hollow Formation
- Rhyolite in Cope Hollow Formation
- Tuff at Crane Pond
- Creekbed rhyolite
- Cuthbertson Mountain rhyolite
- Fenceline rhyolite
- Forked Creek rhyolite
- French Mills felsite
- Goggins Mountain rhyolite
- Grassy Mountain Ignimbrite
- Green rhyolite
- Hogan Mountain rhyolite
- Trachyandesite of Floyd Tower/Indian Creek
- Iron Mountain Lake rhyolite
- Ironton Rhyolite
- Ironton Hollow Rhyolite
- Johnson shut-ins rhyolite
- Ketcherside Mountain rhyolite
- Kratz Spring basalt
- Kratz Spring rhyolite
- Kratz Spring trachyte
- Lake Four Winds basalt
- Lake Killarney Formation
- Little Rock Creek rhyolite
- Logroad rhyolite
- Lower campground tuff at Marble Creek campground
- Lower Ridge rhyolite
- Marble Creek rhyolite
- Mountain View rhyolite
- Mudlick rhyolite
- Oak Mountain rhyolite
- Pea Ridge rhyolite
- Pea Ridge trachyte
- Pond Ridge Rhyolite
- Reader Hollow rhyolite
- Royal Gorge Rhyolite
- Russell Mountain Rhyolite
- Saddle rhyolite
- Sawmill rhyolite
- Shepherd Mountain Rhyolite
- Silver Mines basaltic andesite
- Rhyolite at South Crane Mountain
- Trachydacite at South Crane Mountain
- Stouts Creek rhyolite
- Taum Sauk Rhyolite
- Tile Red ash-flow tuff
- Tilk Hollow rhyolite
- Transition rhyolite
- Upper and Lower andesites of Marble Creek campground
- Upper Orchard rhyolite
- Upper Ridge rhyolite

B. Intrusive rocks

EXPLANATION

Massif intrusions

- Big Spring granite
- Buford Granite Porphyry
- Butler Hill Granite
- Breadtray Granite
- Bunker granite
- Granite of Castor River Shut-Ins

Minor intrusion

- Brown Mountain granite porphyry

Ring intrusions

- Knoblick Granite
- Slabtown Granite
- Silvermine Granite—Medium grained
- Silvermine Granite—Fine grained
- Stono Granite
- Tiemann quartz diorite

Figure 9. FeO*/(FeO* + MgO) variation diagram showing the composition of 1.48 to 1.45 billion year old igneous rocks in the St. Francois Mountains terrane, southeast Missouri relative to boundaries between ferroan and magnesian rocks as well as between tholeiitic and calc-alkaline rocks. Ferroan-magnesian boundary from Frost and others (2001); tholeiitic-calc-alkaline boundary from Miyashiro (1974).—Continued

A. **Extrusive and hypabyssal intrusive rocks**

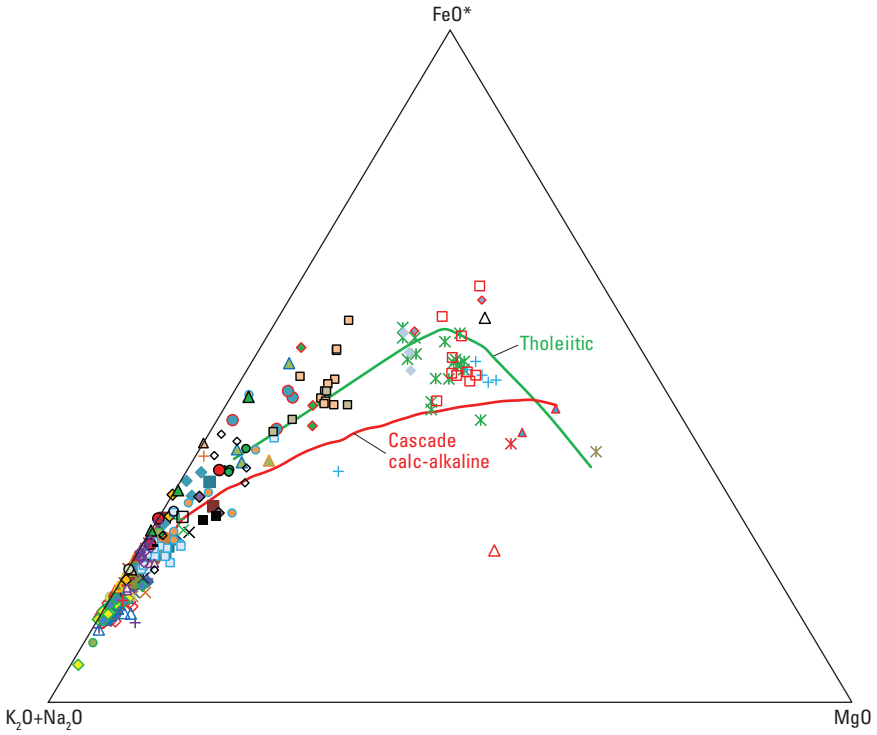

B. **Phaneritic intrusive rocks**

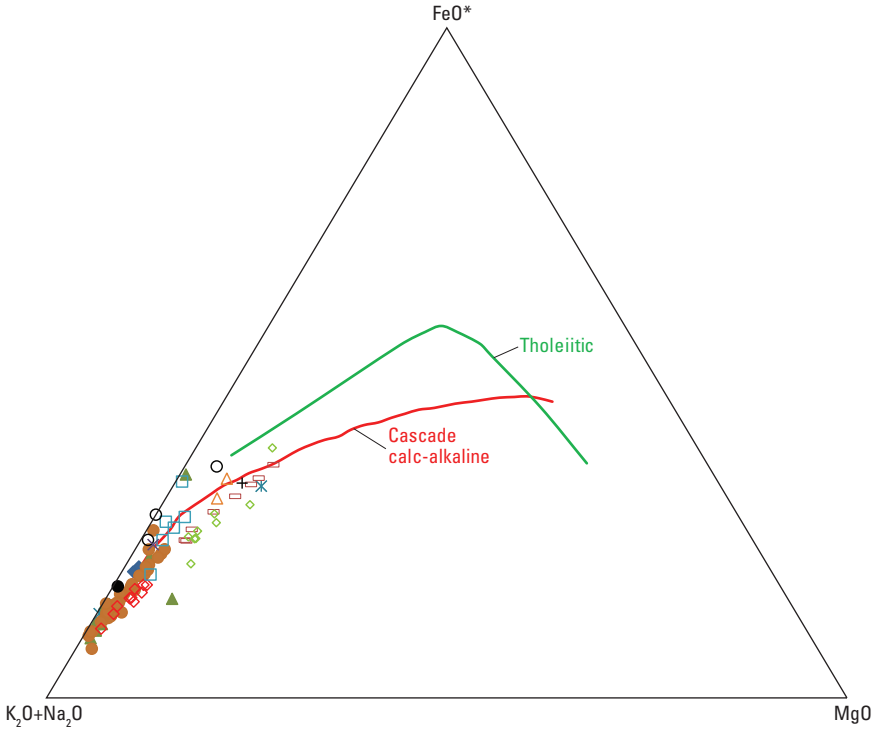

Figure 10. Ternary AFM (Na_2O+K_2O–FeO*–MgO) diagram showing compositions of 1.48 to 1.45 billion year old igneous rocks in the St. Francois Mountains terrane, southeast Missouri. Calc-alkaline and tholeiitic trend lines from Irvine and Baragar (1971).

A. Extrusive and hypabyssal intrusive rocks

EXPLANATION

- Bell Mountain Rhyolite
- Black rhyolite
- Boss diorite
- Boss andesite
- Boss rhyolite
- Boss trachyte
- Bourbon basalt
- Bourbon rhyolite
- Bourbon trachydacite
- Brown Mountain
- Brown's rhyolite
- Brushy rhyolite
- Trachyte host of Camels Hump IOA deposit
- Cedar Bluff Rhyolite
- Clearcut rhyolite
- Lower unit of Coot Mountain
- Basalt in Cope Hollow Formation
- Rhyolite in Cope Hollow Formation
- Tuff at Crane Pond
- Creekbed rhyolite
- Cuthbertson Mountain rhyolite
- Fenceline rhyolite
- Forked Creek rhyolite
- French Mills felsite
- Goggins Mountain rhyolite
- Grassy Mountain Ignimbrite
- Green rhyolite
- Hogan Mountain rhyolite
- Trachyandesite of Floyd Tower/Indian Creek
- Iron Mountain Lake rhyolite
- Ironton Rhyolite
- Ironton Hollow Rhyolite
- Johnson shut-ins rhyolite
- Ketcherside Mountain rhyolite
- Kratz Spring basalt
- Kratz Spring rhyolite
- Kratz Spring trachyte
- Lake Four Winds basalt
- Lake Killarney Formation
- Little Rock Creek rhyolite
- Logroad rhyolite
- Lower campground tuff at Marble Creek campground
- Lower Ridge rhyolite
- Marble Creek rhyolite
- Mountain View rhyolite
- Mudlick rhyolite
- Oak Mountain rhyolite
- Pea Ridge rhyolite
- Pea Ridge trachyte
- Pond Ridge Rhyolite
- Reader Hollow rhyolite
- Royal Gorge Rhyolite
- Russell Mountain Rhyolite
- Saddle rhyolite
- Sawmill rhyolite
- Shepherd Mountain Rhyolite
- Silver Mines basaltic andesite
- Rhyolite at South Crane Mountain
- Trachydacite at South Crane Mountain
- Stouts Creek rhyolite
- Taum Sauk Rhyolite
- Tile Red ash-flow tuff
- Tilk Hollow rhyolite
- Transition rhyolite
- Upper and Lower andesites of Marble Creek campground
- Upper Orchard rhyolite
- Upper Ridge rhyolite

B. Intrusive rocks

EXPLANATION

Massif intrusions

- Big Spring granite
- Buford Granite Porphyry
- Butler Hill Granite
- Breadtray Granite
- Bunker granite
- Granite of Castor River Shut-Ins

Minor intrusion

- Brown Mountain granite porphyry

Ring intrusions

- Knoblick Granite
- Slabtown Granite
- Silvermine Granite—Medium grained
- Silvermine Granite—Fine grained
- Stono Granite
- Tiemann quartz diorite

Figure 10. Ternary AFM (Na_2O+K_2O–FeO*–MgO) diagram showing compositions of 1.48 to 1.45 billion year old igneous rocks in the St. Francois Mountains terrane, southeast Missouri. Calc-alkaline and tholeiitic trend lines from Irvine and Baragar (1971).—Continued

compositions (fig. 13). REE patterns for the felsic and intermediate igneous rocks are almost indistinguishable. In particular, patterns for these two groups of rocks overlap and are parallel, consistent with the interpretation of insignificant relative REE fractionation among magmas represented by these two groups of rocks. Only the magnitude of negative europium anomalies, moderate among intermediate composition rocks and more well developed among the felsic rocks, distinguish REE characteristics of these two groups of rocks. REE patterns for the mafic rocks, although parallel to, and in part overlapping with, those of the other two groups, depict abundances that are, on average, somewhat lower than those characteristic of the other two groups. In addition, the mafic rocks have small to nonexistent negative europium anomalies. Although chondrite-normalized REE patterns for the massif- and ring-type intrusions overlap considerably, the massif-type intrusions are characterized by subtly smaller negative europium anomalies and greater overall REE contents than the ring-type intrusions (fig. 12; table 12).

Essential characteristics of representative primitive-mantle normalized patterns for the 1.48 to 1.45 Ga igneous rocks of the St. Francois Mountains terrane are also generally similar (fig. 14). These patterns are gently negatively sloping, depict relative large-ion lithophile element (LILE) enrichment, and include several superimposed abundance anomalies, including variably developed negative Ba, Sr, P, and Ti anomalies, which are most- or least-well developed in the felsic and mafic rocks, respectively. The primitive-mantle-normalized patterns also include moderately well developed negative niobium and tantalum anomalies similar to those characteristic of subduction-related magmas (Gill, 1981; Pearce and others, 1984; Wood and others, 1979). Representative primitive-mantle-normalized patterns for the igneous rocks of the St. Francois Mountains terrane also include variably developed positive thorium and lead anomalies. Similar to their variable chondrite-normalized REE patterns, primitive-mantle-normalized patterns for individual igneous rock geologic units in the St. Francois Mountains terrane exhibit considerable dispersion, regardless of whole-rock bulk composition (fig. 15). In particular, the felsic and intermediate rocks are again essentially indistinguishable, except that negative trace element anomalies are somewhat less well developed among the intermediate composition rocks. This trend continues among trace element abundances for the mafic rocks, which although grossly similar to, and in part overlapping with, those of the felsic and intermediate composition rocks, are characterized by even smaller negative anomalies. Primitive-mantle-normalized patterns for massif- and ring-type intrusions are also almost indistinguishable (fig. 14). In addition to previously identified REE differences, the massif-type intrusions have somewhat lower Ba, Sr, P, and Ti contents and higher Rb, Th, and Pb contents than the ring-type intrusions. These characteristics are in agreement with the massif intrusions being somewhat more chemically evolved than the ring-type intrusions.

Tectonic Setting During 1.48 to 1.45 Ga Magmatism in the St. Francois Mountains Terrane

Comparing volcanologic features, physical characteristics of igneous intrusions, and compositional attributes of igneous rocks helps constrain the tectonic setting that prevailed during 1.48 to 1.45 Ga magmatism in the St. Francois Mountains terrane. Previously, two principal settings have been suggested for 1.48 to 1.45 Ga magmatism (Ayuso and others, 2016; Day and others, 2016): (1) subduction-related, plate boundary convergent arc magmatism, and (2) within-plate, anorogenic magmatism. As described by Rogers and Santosh (2002), 1.4 Ga ferroan granitoid magmatism across the United States, including the St. Francois Mountains terrane, was coeval with the final fragmentation of supercontinent Columbia (Nuna) but was completed before amalgamation of the Rodinian supercontinent.

As epitomized by the Andean arc (Hildreth and Moorbath, 1988) and magmatism associated with the modern and ancestral Cascades arc (du Bray and John, 2011; Hildreth, 2007), subduction-related arc magmatism is dominated by formation of mafic- to intermediate-composition stratovolcanoes and associated lava dome complexes. The principal eruptive products associated with this arc magmatism include, lava flows, central-volcano associated pyroclastic deposits, massive debris flow deposits, and endogenous and exogenous lava dome complexes. In contrast, intraplate, anorogenic volcanism, such as that characteristic of the modern-day Yellowstone region, is dominated by bimodal, mafic-felsic volcanism. The associated products are principally those formed as a consequence of felsic, caldera-forming eruptions but also include coeval and cospatial mafic volcanism (Christiansen and McCurry, 2008). The eruptive products associated with bimodal intraplate magmatism are dominated by large volume ash-flow tuffs, related but much less voluminous rhyolite lavas deposited proximal to intracaldera environments, and somewhat less voluminous effusive magmatism manifested as numerous relatively thin mafic lava flows and associated pyroclastic fall deposits. As previously described, the style of volcanism and types of eruptive products characteristic of 1.48 to 1.45 Ga igneous rocks in the St. Francois Mountains terrane are unlike those typical of subduction-related arc magmatism but are consistent with those commonly encountered among the products of intraplate, anorogenic magmatism.

The physical characteristics, especially the shape of plutons in subduction-related arc and intraplate, anorogenic settings, are also distinct. For instance, plutons of the Sierra Nevada batholith, the roots of a typical Mesozoic subduction-related magmatic arc, are typified by elongate shapes that parallel the ancestral subduction zone (Bateman, 1992). In contrast, plutons emplaced in an intraplate, anorogenic setting have circular outlines, as epitomized by ovoid postorogenic plutons emplaced into the Arabian Shield during the

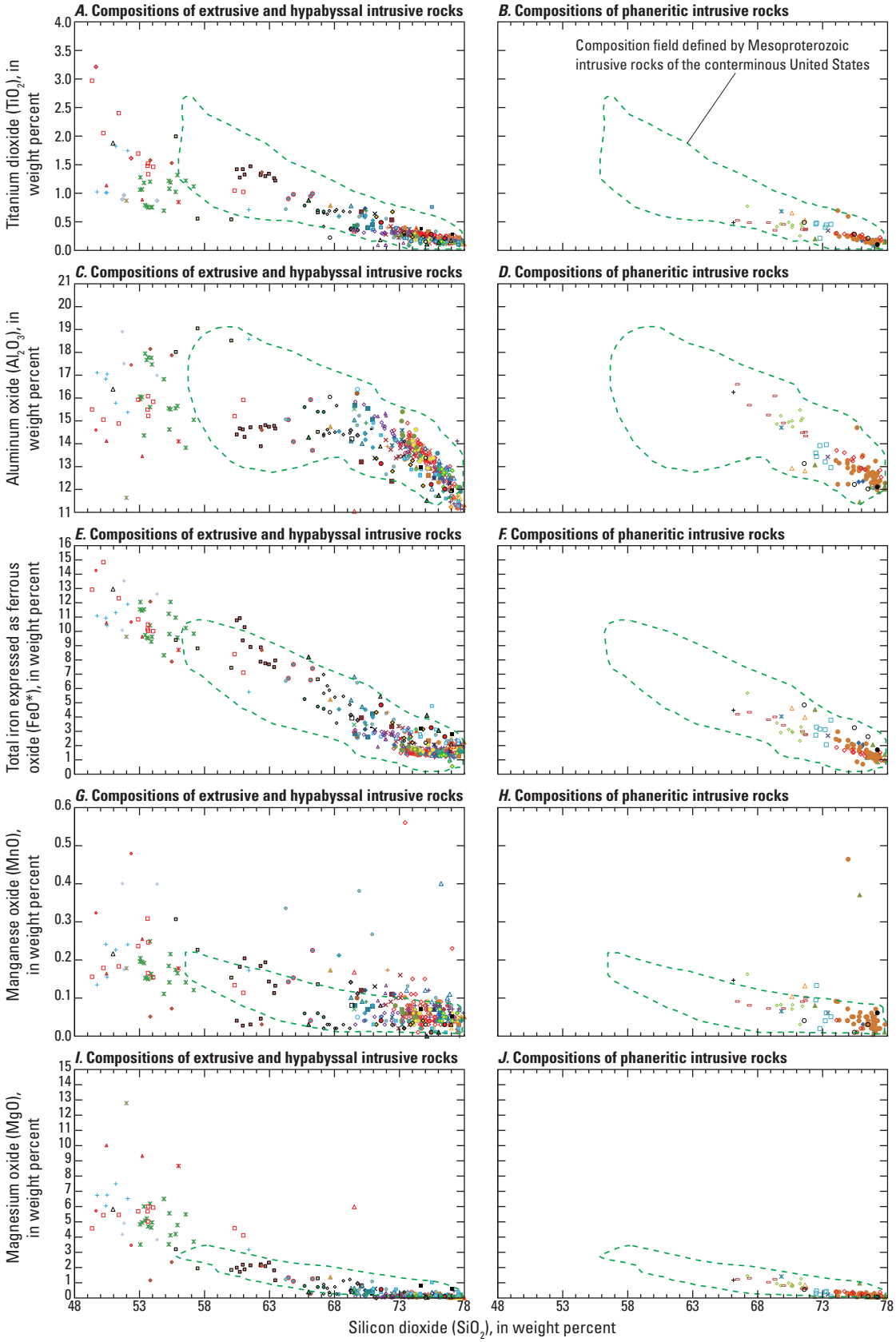

Figure 11. Variation diagrams showing abundances of major oxides (weight percent) in 1.48 to 1.45 billion year old igneous rocks in the St. Francois Mountains terrane, southeast Missouri. Field boundaries on K_2O relative to SiO_2 diagram from Le Maitre (1989); high-potassium shoshonitic dividing line from Ewart (1982). For comparison, dashed green lines delineate the compositional fields defined by Mesoproterozoic intrusive rocks of the conterminous United States (du Bray and others, 2018a).

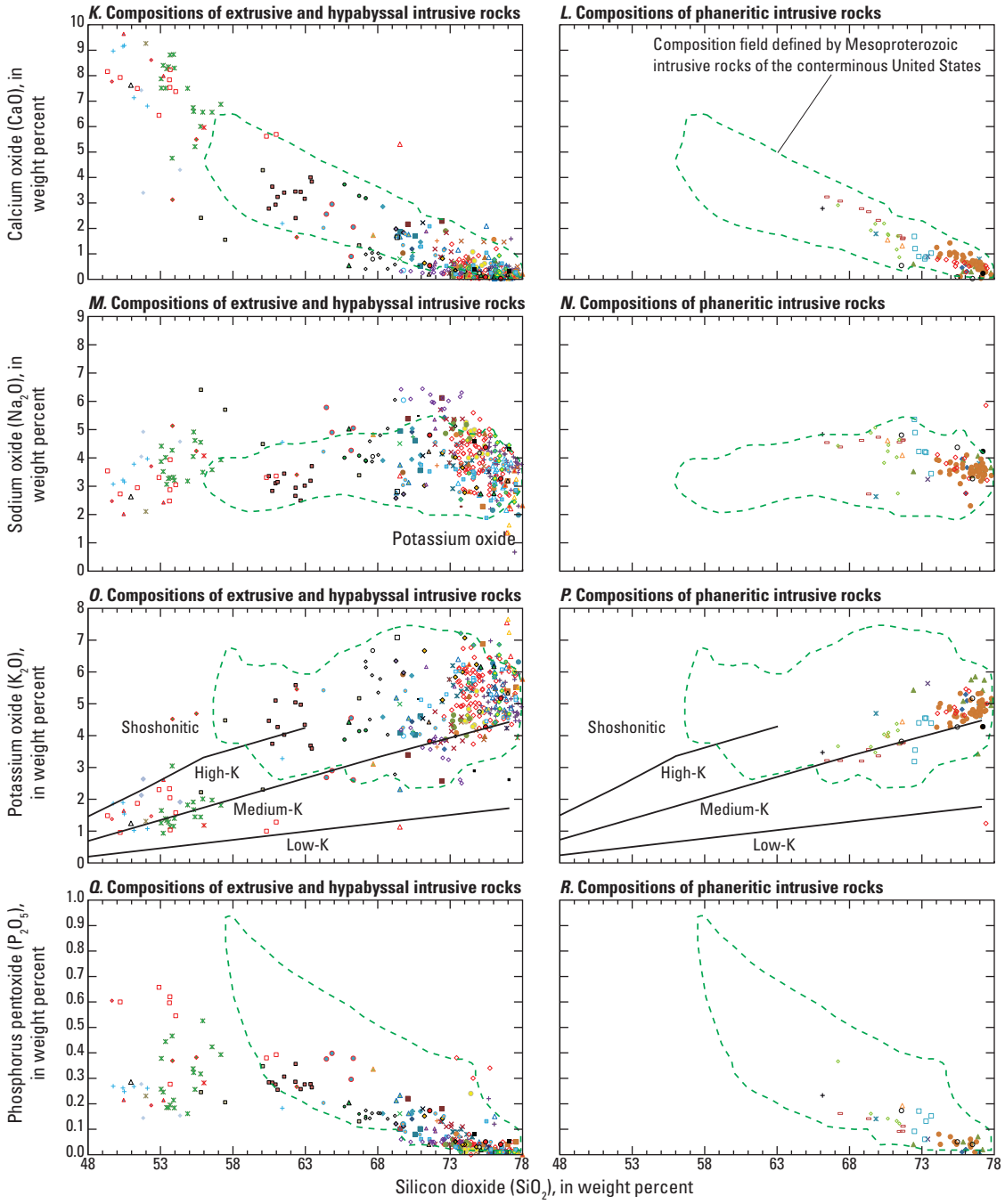

Figure 11. Variation diagrams showing abundances of major oxides (weight percent) in 1.48 to 1.45 billion year old igneous rocks in the St. Francois Mountains terrane, southeast Missouri. Field boundaries on K_2O relative to SiO_2 diagram from Le Maitre (1989); high-potassium shoshonitic dividing line from Ewart (1982). For comparison, dashed green lines delineate the compositional fields defined by Mesoproterozoic intrusive rocks of the conterminous United States (du Bray and others, 2018a).—Continued

A. Extrusive and hypabyssal intrusive rocks

EXPLANATION

- Bell Mountain Rhyolite
- Black rhyolite
- Boss diorite
- Boss andesite
- Boss rhyolite
- Boss trachyte
- Bourbon basalt
- Bourbon rhyolite
- Bourbon trachydacite
- Brown Mountain
- Brown's rhyolite
- Brushy rhyolite
- Trachyte host of Camels Hump IOA deposit
- Cedar Bluff Rhyolite
- Clearcut rhyolite
- Lower unit of Coot Mountain
- Basalt in Cope Hollow Formation
- Rhyolite in Cope Hollow Formation
- Tuff at Crane Pond
- Creekbed rhyolite
- Cuthbertson Mountain rhyolite
- Fenceline rhyolite
- Forked Creek rhyolite
- French Mills felsite
- Goggins Mountain rhyolite
- Grassy Mountain Ignimbrite
- Green rhyolite
- Hogan Mountain rhyolite
- Trachyandesite of Floyd Tower/Indian Creek
- Iron Mountain Lake rhyolite
- Ironton Rhyolite
- Ironton Hollow Rhyolite
- Johnson shut-ins rhyolite
- Ketcherside Mountain rhyolite
- Kratz Spring basalt
- Kratz Spring rhyolite
- Kratz Spring trachyte
- Lake Four Winds basalt
- Lake Killarney Formation
- Little Rock Creek rhyolite
- Logroad rhyolite
- Lower campground tuff at Marble Creek campground
- Lower Ridge rhyolite
- Marble Creek rhyolite
- Mountain View rhyolite
- Mudlick rhyolite
- Oak Mountain rhyolite
- Pea Ridge rhyolite
- Pea Ridge trachyte
- Pond Ridge Rhyolite
- Reader Hollow rhyolite
- Royal Gorge Rhyolite
- Russell Mountain Rhyolite
- Saddle rhyolite
- Sawmill rhyolite
- Shepherd Mountain Rhyolite
- Silver Mines basaltic andesite
- Rhyolite at South Crane Mountain
- Trachydacite at South Crane Mountain
- Stouts Creek rhyolite
- Taum Sauk Rhyolite
- Tile Red ash-flow tuff
- Tilk Hollow rhyolite
- Transition rhyolite
- Upper and Lower andesites of Marble Creek campground
- Upper Orchard rhyolite
- Upper Ridge rhyolite

B. Intrusive rocks

EXPLANATION

Massif intrusions

- Big Spring granite
- Buford Granite Porphyry
- Butler Hill Granite
- Breadtray Granite
- Bunker granite
- Granite of Castor River Shut-Ins

Minor intrusion

- Brown Mountain granite porphyry

Ring intrusions

- Knoblick Granite
- Slabtown Granite
- Silvermine Granite—Medium grained
- Silvermine Granite—Fine grained
- Stono Granite
- Tiemann quartz diorite

Figure 11. Variation diagrams showing abundances of major oxides (weight percent) in 1.48 to 1.45 billion year old igneous rocks in the St. Francois Mountains terrane, southeast Missouri. Field boundaries on K_2O relative to SiO_2 diagram from Le Maitre (1989); high-potassium shoshonitic dividing line from Ewart (1982). For comparison, dashed green lines delineate the compositional fields defined by Mesoproterozoic intrusive rocks of the conterminous United States (du Bray and others, 2018a).—Continued

Table 12. REE characteristics of the 1.48 to 1.45 Ga igneous rocks in the St. Francois Mountains terrane, southeast Missouri.

[SiO_2, in weight percent. Total REE, in parts per million. La_N/Yb_N, ratio of the chondrite-normalized abundance of lanthanum to that of ytterbium; Eu/Eu*, ratio of determined europium abundance to europium abundance interpolated from the abundances of samarium and gadolinium; Dispersion, standard deviation of La abundance divided by average La abundance; —, no data]

Sample number	Geologic unit	SiO_2	Total REE	La_N/Yb_N	Eu/Eu*	Dispersion
	Mafic volcanic rocks					
WA11-1291	Lake Four Winds basalt	49.65	168	4.92	1.00	0.36
JCB5	Basalt in the Cope Hollow Fm	50.41	70	4.66	1.03	0.29
J2-0015	Boss trachyandesite	51.67	93	4.49	0.95	0.33
56W167-1555	Basalt of Kratz Spring	51.99	107	4.24	0.79	0.37
JSIQ-20-7	Silver Mines basaltic andesite	52.51	112	7.53	0.94	0.28
MO16-013	Lower andesite of Marble Creek campground	53.06	113	3.59	0.97	0.17
Bourb-039	Bourbon basalt	53.21	96	4.46	0.82	0.20
JS-13-5	Upper andesite of Marble Creek campground	53.43	83	3.59	0.89	0.03
CW28-1317	Trachyte host of Camels Hump IOA deposit	53.83	184	4.98	0.98	0.12
J2-0030	Boss trachyandesite	55.79	131	4.55	0.66	0.24
56W167-1613	Basaltic andesite host of Kratz Spring IOA deposit	56.00	170	6.95	0.70	0.74
	Mafic intrusion					
S5-1530-1559	Diorite host Boss IOCG deposit	50.96	93	2.48	0.98	—
	Intermediate volcanic rocks					
MO13-006	Floyd Tower/Indian Creek trachydacite	61.08	244	5.44	0.68	0.08
MO16-012	South Crane Mountain trachydacite	64.84	234	4.33	0.66	0.14
Bourb-096	Trachydacite associated with the Bourbon IOA deposit	66.72	313	5.49	0.59	0.01
54W159-1558	Trachyte of Kratz Spring	67.45	303	8.74	0.62	0.74
	Intermediate intrusion					
RA-MO-13-10	Tiemann quartz diorite	66.14	144	5.70	0.79	—
	Felsic volcanic rocks					
MO16-059	Iron Mountain Lake rhyolite	69.34	211	2.94	0.57	—
ARC5/96–9	Ironton Rhyolite	69.52	149	8.69	0.68	—
MO13-001	Rhyolite at South Crane Mountain	70.38	204	3.76	0.61	0.20
MO15-002	Little Rock Creek rhyolite	70.93	240	5.41	0.63	—
USA2-1196	Boss rhyolite	71.97	126	32.08	0.61	0.46
ARC5/96-4	Russell Mountain Rhyolite	72.09	204	6.01	0.60	—
MO14-020	Cedar Bluff Rhyolite	72.95	86	2.16	0.44	—
MO16-057	Shepherd Mountain Rhyolite	73.36	150	5.04	0.64	0.37
MO16-007	Upper Ridge rhyolite	73.78	245	7.07	0.48	0.23
MO93-136	Cuthbertson Mountain rhyolite	74.72	181	4.18	0.85	0.31
ARC5/96-7	Pond Ridge Rhyolite	75.02	159	2.70	0.41	—
MO16-004	Lower Ridge rhyolite	75.20	235	5.95	0.35	—
MO16-015	Tile Red ash-flow tuff	75.24	310	4.43	0.20	—
PEA10/95-16	Pea Ridge 1825 rhyolite porphyry	75.50	220	4.53	0.48	0.33
B-USBM2-1421	Bourbon rhyolite	76.02	112	4.62	0.31	1.06
MGS28-1	Ketcherside Mountain rhyolite	76.84	213	4.42	0.23	0.24
MO16-024	Grassy Mountain Ignimbrite	77.08	284	4.87	0.31	0.37
MGS37-4	Royal Gorge Rhyolite	77.16	125	2.61	0.20	0.68
MO15-004	Lake Killarney Formation	77.48	237	3.71	0.17	0.18
MO16-023B	Ironton Hollow-Cedar Bluff Rhyolite	77.60	157	2.53	0.37	0.56
MO14-043	Lower campground tuff at Marble Creek campground	77.65	307	6.93	0.27	0.14
ARC5/96-2	Taum Sauk Rhyolite	77.99	297	4.13	0.13	—

Table 12. REE characteristics of the 1.48 to 1.45 Ga igneous rocks in the St. Francois Mountains terrane, southeast Missouri.—Continued

[SiO_2, in weight percent. Total REE, in parts per million. La_N/Yb_N, ratio of the chondrite-normalized abundance of lanthanum to that of ytterbium; Eu/Eu*, ratio of determined europium abundance to europium abundance interpolated from the abundances of samarium and gadolinium; Dispersion, standard deviation of La abundance divided by average La abundance; —, no data]

Sample number	Geologic unit	SiO_2	Total REE	La_N/Yb_N	Eu/Eu*	Dispersion
	Felsic intrusions					
	Massif-type					
RA-MO-13-4	Butler Hill Granite	74.28	303	5.62	0.25	0.38
RA-MO-13-3	Breadtray Granite	77.76	290	4.29	0.10	—
60W-183-1071	Bunker granite	76.97	265	5.65	0.27	0.16
BS 111	Big Spring granite	75.78	182	4.05	0.44	0.05
	Ring-type					
N6976	Stono Granite	70.64	153	3.88	0.47	—
RA-MO-13-5	Knoblick Granite	71.36	163	6.25	0.63	0.07
RA-MO-13−9	Silvermine Granite—medium grained	71.44	129	4.10	0.64	0.23
233	Silvermine Granite—fine grained	75.93	114	5.71	0.43	—
IGCP1-3a	Slabtown Granite	72.48	241	4.75	0.67	0.02
	Minor intrusions					
J4-1533	Boss granite	73.23	214	7.21	0.32	0.46
MO16-003	Brown Mountain granite porphyry	71.59	238	4.99	0.64	0.02

Neoproterozoic (Stoeser and Elliott, 1980). Many of the 1.48 to 1.45 Ga igneous intrusions in the St. Francois Mountains terrane have been depicted as roughly circular masses (Kisvarsanyi, 1981) that accordingly are consistent with intraplate, anorogenic magmatism.

The spatial extent and distribution of 1.48 to 1.45 Ga igneous rocks in the St. Francois Mountains terrane provide additional constraints on the tectonic setting that prevailed during the associated magmatism. Approximately 1.4 Ga Mesoproterozoic igneous rocks in the St. Francois Mountains terrane extend over length scales of at least 150 km (Day and others, 2016; Kisvarsanyi, 1981). Similarly, approximately 1.4 Ga igneous complexes arrayed across the continental United States have minimum extents that range from similar to significantly greater proportions (du Bray and others, 2015). In contrast, magmatic arcs associated with subduction processes are narrow; their widths range from more than 10 to, in rare case cases, as much as 100 km (du Bray and John, 2011; England and Katz, 2010; Hildreth, 2007; Hildreth and Moorbath, 1988). Accordingly, the minimum spatial extent of 1.48 to 1.45 Ga igneous rocks in the St. Francois Mountains terrane is much greater than the width characteristic of subduction-related arcs. In addition, 1.48 to 1.45 Ga igneous rocks in the St. Francois Mountains terrane are part of a group of coeval igneous rocks that are widely distributed across the conterminous United States (fig. 1, du Bray and others, 2018a). They extend from the northern to southern midcontinent, are abundant beneath Paleozoic sedimentary rocks throughout the Great Plains region, are voluminous across southern Arizona, extend north along the Rocky Mountains throughout New Mexico, Colorado, and southern Wyoming, and form isolated outcrops in north-central Idaho (du Bray and others, 2015). This distribution is inconsistent with these rocks being related to subduction-related magmatism, because it requires that all of these areas, dispersed across the Laurentian craton, were sites of coeval arc magmatism. A geometry that requires coeval subduction-related magmatism at each of these disparate and irregularly oriented locales is implausible. Therefore, the spatial characteristics and distribution of 1.4 Ga igneous rocks throughout the conterminous United States, including those in the St. Francois Mountains terrane, are inconsistent with an arc magmatism genesis.

The geochemical characteristics of 1.48 to 1.45 Ga igneous rocks in the St. Francois Mountains terrane provide compelling evidence pertinent to the tectonic environment prevailing during their genesis. As previously described, the great majority of these igneous rocks are ferroan (fig. 9). Subduction-related arc magmas are characteristically magnesian or calc alkaline (du Bray and John, 2011; Hildreth, 2007; Hildreth and Moorbath, 1988; Irvine and Baragar, 1971), whereas intraplate, anorogenic magmas are ferroan and tholeiitic (Christiansen and McCurry, 2008; Frost and Frost, 2008, 2011). Similarly, compositions of subduction-related magmatic arc rocks follow a calc-alkaline trend, whereas those of intraplate, anorogenic rocks follow a tholeiitic trend (fig. 10). Most 1.48 to 1.45 Ga intermediate- to felsic-composition igneous rocks in the St. Francois Mountains terrane have relative abundances of Rb and Y + Nb that are consistent with a

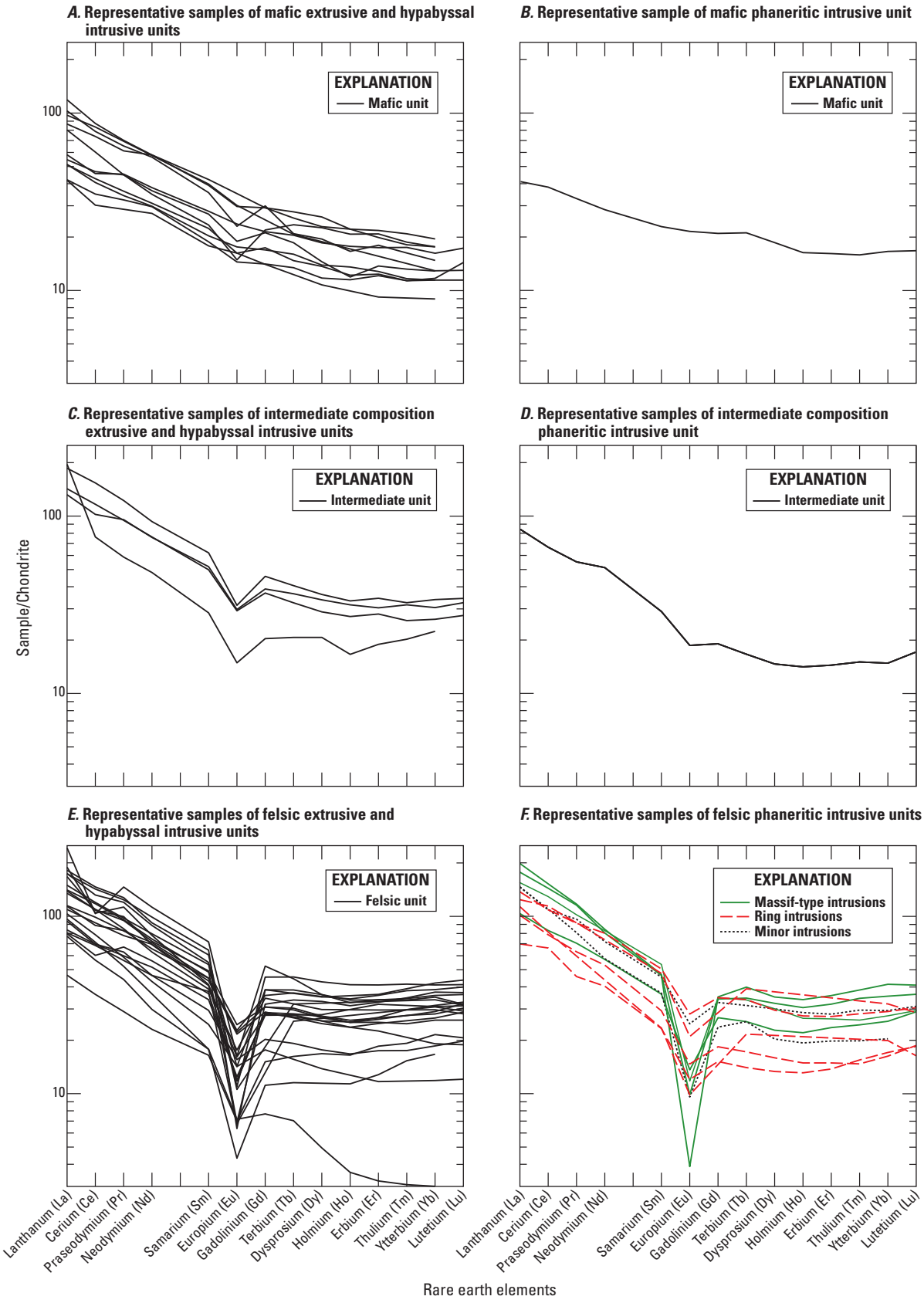

Figure 12. Representative chondrite-normalized rare earth element patterns for 1.48 to 1.45 billion year old igneous rocks in the St. Francois Mountains terrane, southeast Missouri. Chondrite abundances from Anders and Ebihara (1982). Truncated pattern segments indicate missing data.—Continued

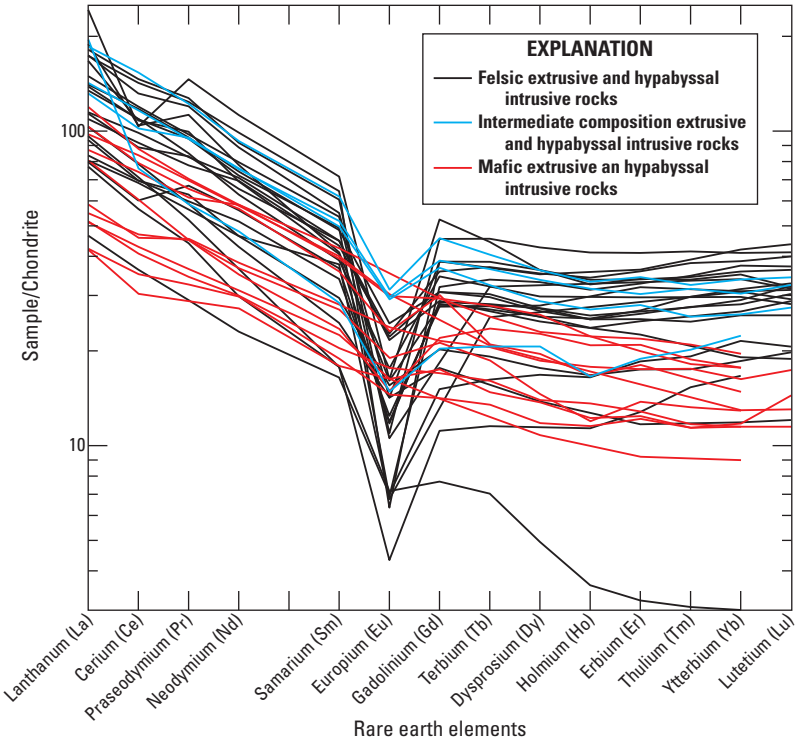

Figure 13. Comparison of representative chondrite-normalized rare earth element patterns for 1.48 to 1.45 billion year old extrusive and hypabyssal intrusive rocks in the St. Francois Mountains terrane, southeast Missouri, compiled from all data for these rocks (fig. 12). Chondrite abundances from Anders and Ebihara (1982). Discontinuous patterns indicate missing data.

within-plate setting although the compositions of several geologic units extend to those characteristic of volcanic arc magmas (fig. 16). Whalen and others (1987) used the relative abundances of Zr, Ga, and Al to distinguish I (igneous source)- and S (sedimentary source)-type compositions of subduction-related arc environments from A-type compositions, which have traditionally been associated with an anorogenic, intraplate setting. Relative abundances of these components in the preponderance of 1.48 to 1.45 Ga igneous rocks from the St. Francois Mountains terrane that have been analyzed are also consistent with an intraplate, anorogenic setting though a notable few analyses plot in the I- and S-type fields (fig. 16). Finally, Grebennikov (2014) used relative abundances of several major oxide components to distinguish the compositions of magmas generated in a variety of tectonic settings. As with other geochemical criteria, compositions of the vast majority of 1.48 to 1.45 Ga rocks from the St. Francois Mountains terrane are consistent with petrogenesis in an intracratonic setting that was affected by rifting and associated mantle upwelling. Each of these geochemical criteria is in agreement with all physical, volcanologic, and distribution characteristics of 1.48 to 1.45 Ga igneous rocks in the St. Francois Mountains terrane that are consistent with these rocks being products of intracratonic, anorogenic magmatism.

Major oxide compositions of ferroan igneous rocks define eight subtypes (Frost and Frost, 2008). These include the alkali-calcic and calc-alkalic variants of both ferroan peraluminous and ferroan peralkaline granitoids, as well as the alkalic, alkali-calcic, calc-alkalic, and calcic variants of ferroan metaluminous granitoids. Although these discrete subtypes allow unique compositional classification (Frost and Frost, 2008), each ostensibly associated with a particular petrogenetic history, compositional data (du Bray and others, 2018b; Granitto and others, 2018) suggest that many 1.48 to 1.45 Ga igneous rocks in the St. Francois Mountains terrane have compositions that extend across subtype boundaries (figs. 7 and 8) and, therefore, reflect continuous variation of corresponding petrologic processes. Experimental petrologic investigations, for which pressure, temperature, and compositional characteristics are known, define the magma compositions that result from various combinations of these parameters (Frost and Frost, 2008) and constrain the relevant petrogenetic conditions prevailing during genesis of the magmas represented by 1.48 to 1.45 Ga igneous rocks in the St. Francois Mountains terrane (table 11).

Low-degree dehydration partial melting of granodiorite or magnesian tonalite gneiss yields ferroan, strongly peraluminous, calc-alkalic melts (Patiño Douce, 1997; Skjerlie and Johnston, 1993). With relatively higher-degree partial melting, the resulting magmas become increasingly magnesian, metaluminous, and alkali calcic. With relatively lower

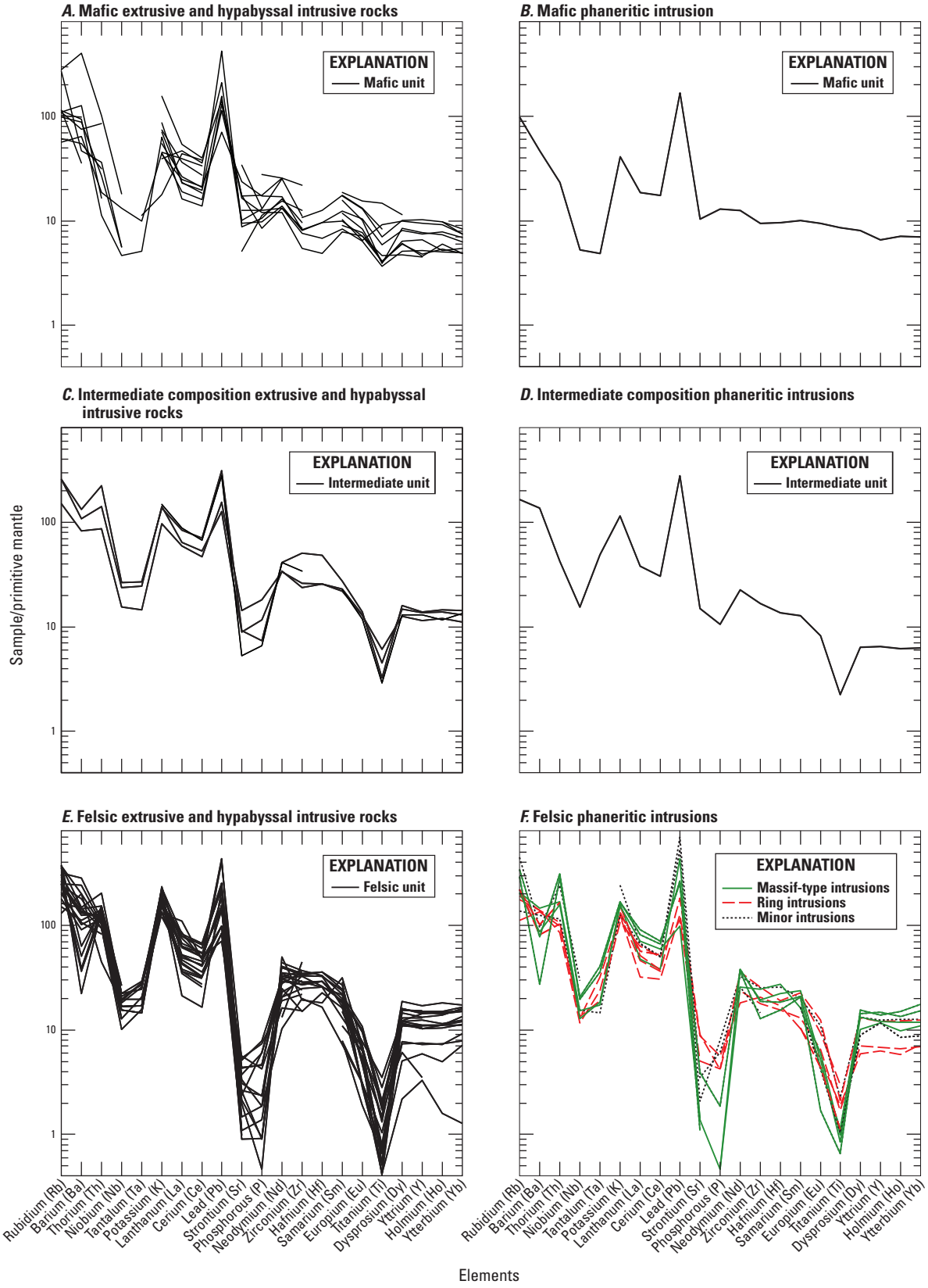

Figure 14. Representative primitive-mantle-normalized (Sun and McDonough, 1989) trace element diagrams for igneous rocks in the St. Francois Mountains terrane, southeast Missouri. Discontinuous patterns indicate missing data.

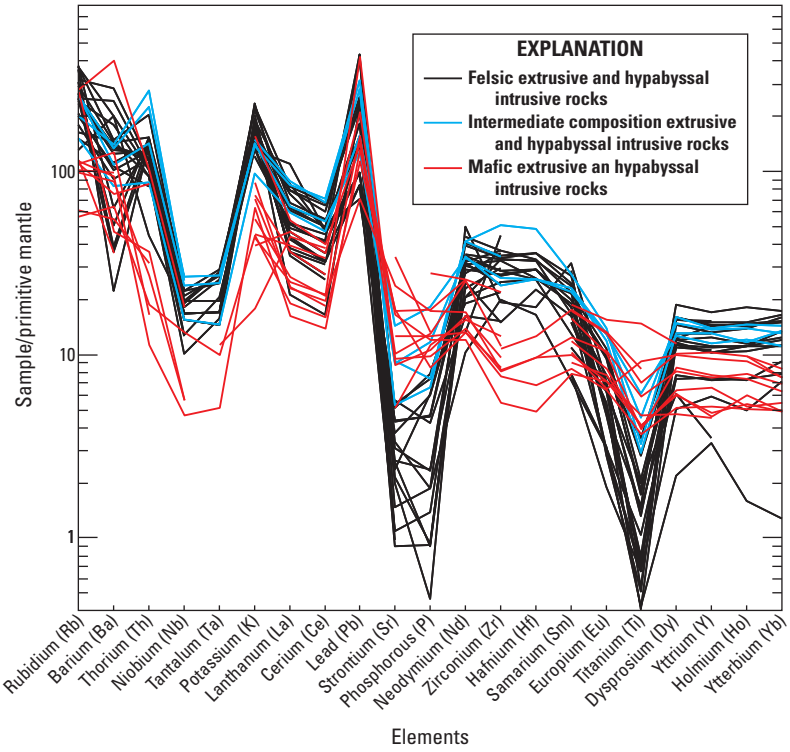

Figure 15. Comparison of representative primitive-mantle-normalized (Sun and McDonough, 1989) trace element patterns for 1.48 to 1.45 billion year old extrusive and hypabyssal intrusive rocks in the St. Francois Mountains terrane, southeast Missouri. Discontinuous patterns indicate missing data.

pressure melting, the resulting partial melts are magnesian, metaluminous, and calc alkalic. These relations suggest that the large group of 1.48 to 1.45 Ga igneous rocks in the St. Francois Mountains terrane (table 11) which have ferroan, peraluminous, and calc-alkalic to alkali-calcic compositions are consistent with high pressure (8–10 kilobar), low-degree partial melting of crustal material of granodioritic to tonalitic compositions; members of the alkali-calcic subtype probably represent partial melting at higher pressure conditions than those prevailing during genesis of the calc-alkalic subtype (Patiño Douce, 1997).

Differentiation of tholeiitic basalt can produce metaluminous ferroan granites (Frost and Frost, 2011). The balance of plagioclase relative to clinopyroxene crystallization and fractionation determines whether these partial melts are alkali calcic or calc alkalic, or even alkalic. Tholeiitic compositions are increasingly alkalic with clinopyroxene crystallization as plagioclase crystallization limits residual liquid alkalinity (Frost and Frost, 2011). Consequently, (1) the alkalic and metaluminous compositions of the trachyte host of Camels Hump IOA deposit and the Johnson Shut-ins rhyolite (table 11) may represent extensive clinopyroxene fractionation, (2) the alkali-calcic metaluminous compositions of a significant group (table 11) of 1.48 to 1.45 Ga igneous rocks in the St. Francois Mountains terrane reflect less significant clinopyroxene fractionation, and (3) the calc-alkalic metaluminous compositions of six geologic units (table 11) in the St. Francois Mountains terrane manifests the dominance of plagioclase fractionation. Clinopyroxene crystallizes at higher pressures than those associated with plagioclase crystallization (Frost and Frost, 2011). Consequently, the most alkalic of the metaluminous 1.48 to 1.45 Ga igneous rocks in the St. Francois Mountains terrane probably represent magma genesis in systematically higher-pressure environments than those characteristic of the calc-alkalic subtype.

A small group of 1.48 to 1.45 Ga igneous rocks in the St. Francois Mountains terrane (table 11) have alkali-calcic and calc-alkalic metaluminous compositions that are transitionally magnesian to magnesian, not ferroan, and are therefore superficially similar to characteristically magnesian and calc-alkaline, subduction-related magmatic arc rocks (Menuge and others, 2002; Walker and others, 2002). However, many lines of evidence indicate that 1.48 to 1.45 Ga igneous rocks in the St. Francois Mountains terrane rocks represent magmatism in an intracratonic setting (Bickford and others, 2015) rather than in a magmatic arc setting. The petrogenesis of the magnesian variants reflects variations of processes not entirely different from those responsible for ferroan granitoid petrogenesis, as indicated by a smooth and continuous transition from ferroan to magnesian compositions. Weakly magnesian compositions

may reflect relatively lower pressure partial melting conditions (Skjerlie and Johnston, 1993). Relatively high-degree partial melting (Skjerlie and Johnston, 1993) of granodioritic to tonalitic protolith compositions in relatively high-pressure, lower-crust regimes (Patiño Douce, 1997) is probably responsible for the small group of transitionally magnesian to magnesian and metaluminous 1.48 to 1.45 Ga igneous rocks. Those geologic units that have alkali-calcic compositions reflect genesis under high pressure conditions, whereas those with calc-alkalic compositions manifest magma genesis at somewhat lower pressures (Patiño Douce, 1997).

Relatively primitive Sm-Nd and Pb isotopic values (Ayuso and others, 2016; du Bray and others, 2015; Gleason and others, 2000) for 1.48 to 1.45 Ga igneous rocks in the St. Francois Mountains terrane suggest that the petrogenesis of the associated magmas includes a significant mantle-derived component. Similarly, oxygen isotope data for zircon from the Pea Ridge 1825 rhyolite porphyry and volcanic rocks near the Bourbon deposit are commensurate with mantle inputs (Watts and Mercer, 2020). Derivation of 1.48 to 1.45 Ga igneous rocks in the St. Francois Mountains terrane exclusively by differentiation from tholeiitic basalt magmas or by partial melting of tonalite to granodiorite in the crust is inconsistent with available geochemical data. The petrogenesis of these magmas probably requires a combination of processes. Similarly, Frost and Frost (2011) have suggested that most ferroan granites represent variable mixing of crust-derived partial melts with differentiates of mantle-derived tholeiitic magma. The heat required to initiate variable degrees of crustal melting was probably supplied by primary, mantle-derived mafic magma, which likely also contributed mass to the evolving magma reservoirs. The conclusion that most 1.48 to 1.45 Ga igneous rocks in the St. Francois Mountains terrane represent petrogenesis in an intracratonic or continental setting (Kisvarsanyi and Kisvarsanyi, 1990) and the inference that this magmatism involved mantle-derived inputs, require extensional tectonism, mantle upwelling, and crustal underplating to initiate and sustain the observed magmatism (Day and others, 2016). Processes accompanying intracratonic extension and crustal underplating by upwelling, mantle-derived tholeiitic magma have likely also contributed directly to the worldwide spatial and temporal association of felsic ferroan granitoids and relatively mafic igneous rocks described by Anderson (1983) and Hoffman (1989).

The 1.48 to 1.45 Ga igneous rocks in the St. Francois Mountains terrane have major oxide compositions similar to those of ferroan granites throughout the world, which are subalkaline, weakly to moderately peraluminous, alkali calcic to calc alkalic, iron enriched, have moderately evolved compositions, and major oxide abundance variations within many of these ferroan granitoid intrusions are consistent with crystallization and fractionation of their contained mineral assemblages (Dall'Agnol and others, 2012). Correspondingly, the onset of plagioclase crystallization and fractionation among the 1.48 to 1.45 Ga igneous rocks in the St. Francois Mountains terrane is denoted by decreasing Al_2O_3, among those rocks with ≥68 weight percent SiO_2 (fig. 11). The importance of plagioclase fractionation in the petrogenesis of these more evolved rocks is consistent with moderate to large negative europium anomalies characteristic of these rocks. In contrast, the mafic rocks of the St. Francois Mountains terrane have the smallest negative europium anomalies (fig. 13). Among these rocks, systematic decreases in TiO_2, FeO*, MnO, MgO, and CaO abundances with increasing SiO_2 are consistent with hornblende, biotite, and lesser Fe-Ti oxide crystallization and fractionation from the associated magmas (fig. 11). Decreasing P_2O_5 and TiO_2 abundances with increasing SiO_2 content suggest apatite and Fe-Ti oxide crystallization and fractionation, respectively.

Abundances of zirconium in 1.48 to 1.45 Ga igneous rocks in the St. Francois Mountains terrane increase somewhat with increasing SiO_2 content, indicating that zircon did not nucleate and fractionate from the associated magmas (Bickford and others, 2015). Zirconium abundances, as high as about 500 ppm in these rocks, are noteworthy given the 140 to 175 ppm range characteristic of granitoid rocks (Turekian and Wedepohl, 1961). Most of the 1.48 to 1.45 Ga igneous rocks in the St. Francois Mountains terrane are subalkaline, which is inconsistent with their somewhat elevated zirconium content because the abundance of zirconium in ordinary subalkaline silicate melts is limited to about 100 ppm (Watson, 1979). Elevated zirconium abundances among 1.48 to 1.45 Ga igneous rocks in the St. Francois Mountains terrane is unexpected. Bickford and others (2015) noted this feature and the relative lack of inherited zircon in the felsic rocks of the St. Francois Mountains terrane and concluded that the source magmas were too hot to promote zircon crystallization. Elevated zirconium abundances characteristic of these rocks contrast with their apparently low zircon content. Consequently, much of the zirconium in the 1.48 to 1.45 Ga igneous rocks in the St. Francois Mountains terrane may reside in pyroxene, small, inseparable zircon crystals, or in some other mineral, including perhaps Fe-Ti oxides.

Continental magmatic arc rocks (du Bray and others, 2015; Hildreth and Moorbath, 1988) have considerably greater strontium abundances than those of the 1.48 to 1.45 Ga igneous rocks in the St. Francois Mountains terrane. Because plagioclase is the principal residence of strontium in the common rock-forming minerals, its retention in the source residuum during partial melting and (or) crystallization and removal from evolving, residual silicate liquids may be responsible for relatively low strontium abundances in these rocks. Magma genesis in relatively low pressure (<20 kilobar) lower- to mid-crustal environments (Green, 1982) favors plagioclase stability, which suggests petrogenesis of the magmas represented by 1.48 to 1.45 Ga igneous rocks in the St. Francois Mountains terrane in the lower- to mid-crust regions, at depths significantly less than those that prevail in continental magmatic arc environments. Source-region plagioclase retention and subsequent plagioclase fractionation from magmas having basaltic andesite compositions, with characteristically small negative europium anomalies, are likely responsible for moderately- to well-developed negative europium anomalies characteristic of

1.48 to 1.45 Ga intermediate to felsic igneous rocks in the St. Francois Mountains terrane.

Relative Rb and Y + Nb concentrations for most 1.48 to 1.45 Ga igneous rocks in the St. Francois Mountains terrane are consistent with a within-plate setting (fig. 16). Y + Nb concentrations for the rhyolite in the Cope Hollow Formation and Shepherd Mountain Rhyolite, however, are low and consistent with a volcanic arc setting. Similarly, melt inclusions in zircon from the upper and lower units of Coot Mountain have Y + Nb abundances similar to those of volcanic arc setting rocks; these rocks also have elevated H_2O contents and zircon with high $\delta^{18}O$ values that are consistent with arc magmatism (Watts and Mercer, 2020). Although the Y + Nb abundances for these rhyolites are low relative to within-plate igneous rocks, they are part of a continuous compositional array for 1.48 to 1.45 Ga igneous rocks of the St. Francois Mountains terrane that is centered in the within-plate field but ranges to compositions consistent with petrogenesis in a volcanic arc setting. As such, these low Y + Nb abundances represent compositional variants that may have hybrid geochemical signatures characteristic of inputs derived from other petrologic processes. In addition, primitive-mantle-normalized trace element plots for most 1.48 to 1.45 Ga igneous rocks include negative Nb-Ta anomalies that, paradoxically, resemble those characteristic of subduction-related arc magmas. By analogy, du Bray and others (2015) identified similar negative Nb-Ta anomalies among intermediate-composition rocks of the Aurora volcanic field (California and Nevada) that were erupted almost 10 m.y. after arc magmatism had ceased in this area. Negative Nb-Ta anomalies for the Aurora volcanic field rocks have been interpreted as inherited from the crustal rocks that contributed to their petrogenesis. Similarly, because all other geologic characteristics of 1.48 to 1.45 Ga igneous rocks in the St. Francois Mountains terrane are inconsistent with arc magmatism, their negative Nb-Ta anomalies may reflect the geochemistry of older, lower crustal rocks, with an arc-related prehistory, that contributed to petrogenesis of magmas represented by the 1.48 to 1.45 Ga igneous rocks in the St. Francois Mountains terrane, as suggested by Ayuso and others (2016). Importantly however, as shown by Bickford and others (2015), the oldest Nd model ages for igneous rocks in the St. Francois Mountains terrane are about 1.55 Ga. Correspondingly, very rare, approximately 1.55 Ga zircon xenocrysts have been identified in samples collected near the Pea Ridge and Bourbon deposits (Watts and Mercer, 2020). Given the oldest igneous rocks in this area are about 1.48 Ga, partially melted, older lower crustal sources that contributed to Mesoproterozoic magmatism in the St. Francois Mountains terrane are juvenile and can be no more than about 0.07 Ga older than exposed Mesoproterozoic igneous rocks in this area.

Compositional diversity among 1.48 to 1.45 Ga igneous rocks in the St. Francois Mountains terrane, as reflected by several additional geochemical parameters, are also consistent with mantle-derived magmas having been variably contaminated by crustal assimilants (fig. 17). P_2O_5/K_2O decreases with increasing SiO_2 content, consistent with progressive mafic magma contamination by assimilation of crustally derived inputs because crustal materials generally have $P_2O_5/K_2O < 0.1$ (Farmer and others, 2002). In addition, CaO/Al_2O_3 systematically decreases with increasing SiO_2, consistent with magma compositions that have been modified by crustal contamination (Cousens and others, 2008).

The petrogenetic evolution of 1.48 to 1.45 Ga igneous rocks in the St. Francois Mountains terrane is further constrained by their relative REE abundances. These rocks have moderately steep, negatively sloping chondrite-normalized REE patterns (table 12); values of (La_N/Yb_N) in most of these rocks range from about 2 to 9, median value is 4.7. The corresponding heavy rare earth element (HREE) depletion characteristic of these rocks signifies garnet stability and HREE retention in the source region because garnet is the principal petrologically relevant residence of HREE (Hanson, 1980). Although zircon is another significant HREE residence (Hanson, 1980), the somewhat elevated zirconium abundances characteristic of these rocks precludes significant zircon crystallization and removal from the associated magmas as a cause for relative HREE depletion. The 1.48 to 1.45 Ga igneous rocks in the St. Francois Mountains terrane, as a group, have chondrite-normalized patterns that are essentially parallel and overlapping (fig. 15), which suggests that the representative magma reservoirs evolved by similar petrogenetic processes. In particular, the mineral assemblages that crystalized and fractionated from the representative magmas must have had similar bulk mineral-melt distribution coefficients. Specifically, the relatively broad range of chondrite-normalized REE patterns suggests fractionation of variable mineral assemblages, and (or) dilution by assimilants, with relatively unfractionated REE abundances. Negative europium anomalies that are progressively better developed among increasingly felsic igneous rocks of the St. Francois Mountains terrane (fig. 13) suggest a significant role for progressively greater plagioclase (the principal residence of Eu, Hanson, 1980) fractionation among the most felsic of these rocks. Among most of the 1.48 to 1.45 Ga igneous rocks in the St. Francois Mountains terrane, a relatively well developed negative correlation exists between europium anomaly magnitude and SiO_2 content (table 12); consequently, the most evolved magmas reflect the greatest amount of plagioclase fractionation. In contrast, among these rocks, both (La_N/Yb_N) and total REE contents are poorly correlated with SiO_2 content (table 12).

Among 1.48 to 1.45 Ga igneous rocks in the St. Francois Mountains terrane, within-unit REE dispersion (table 12) is uncorrelated with SiO_2 content. Consequently, REE dispersion is apparently unrelated to the degree of petrogenetic evolution and likely reflects the extent of compositional homogenization achieved within the representative magma reservoirs. Many of the igneous rock units have REE dispersion values less than or equal to 0.3 (table 12) consistent with reasonably homogenous magma reservoirs; in fact, a significant subset of these have REE dispersion values ≤ 0.2 and are indicative of very homogenous intrusions. In contrast, a small group of these geologic units (basaltic andesite host of Kratz Spring IOA deposit,

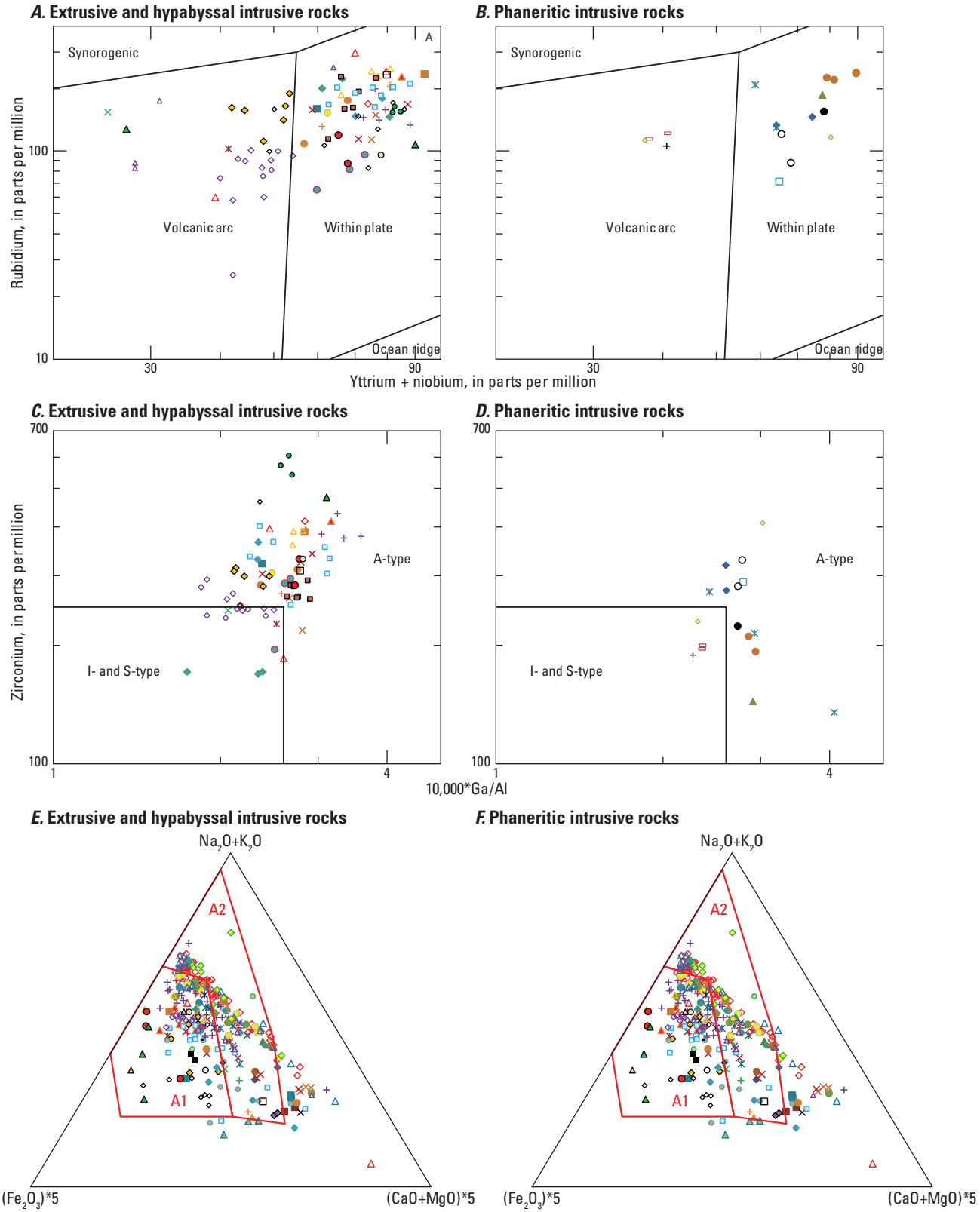

Figure 16. Variation diagrams showing that compositions of 1.48 to 1.45 billion year old igneous rocks in the St. Francois Mountains terrane, southeast Missouri are consistent with their petrogenesis in an intraplate, anorogenic setting. *A*, *B*, From Pearce and others (1984); applicable to rocks with >56 weight percent SiO_2; *C*, *D*, After Whalen and others (1987) showing the range of compositions for typical I (igneous source)-, S (sedimentary source)-, and A (anorogenic)-type igneous rocks with >60 weight percent SiO_2. *E*, *F*, Discriminant diagram after Grebennikov (2014) showing the range of compositions for magmas, with >67 weight percent SiO_2, associated with oceanic islands and continental rifts (field A1) and those associated with intracratonic settings (field A2).

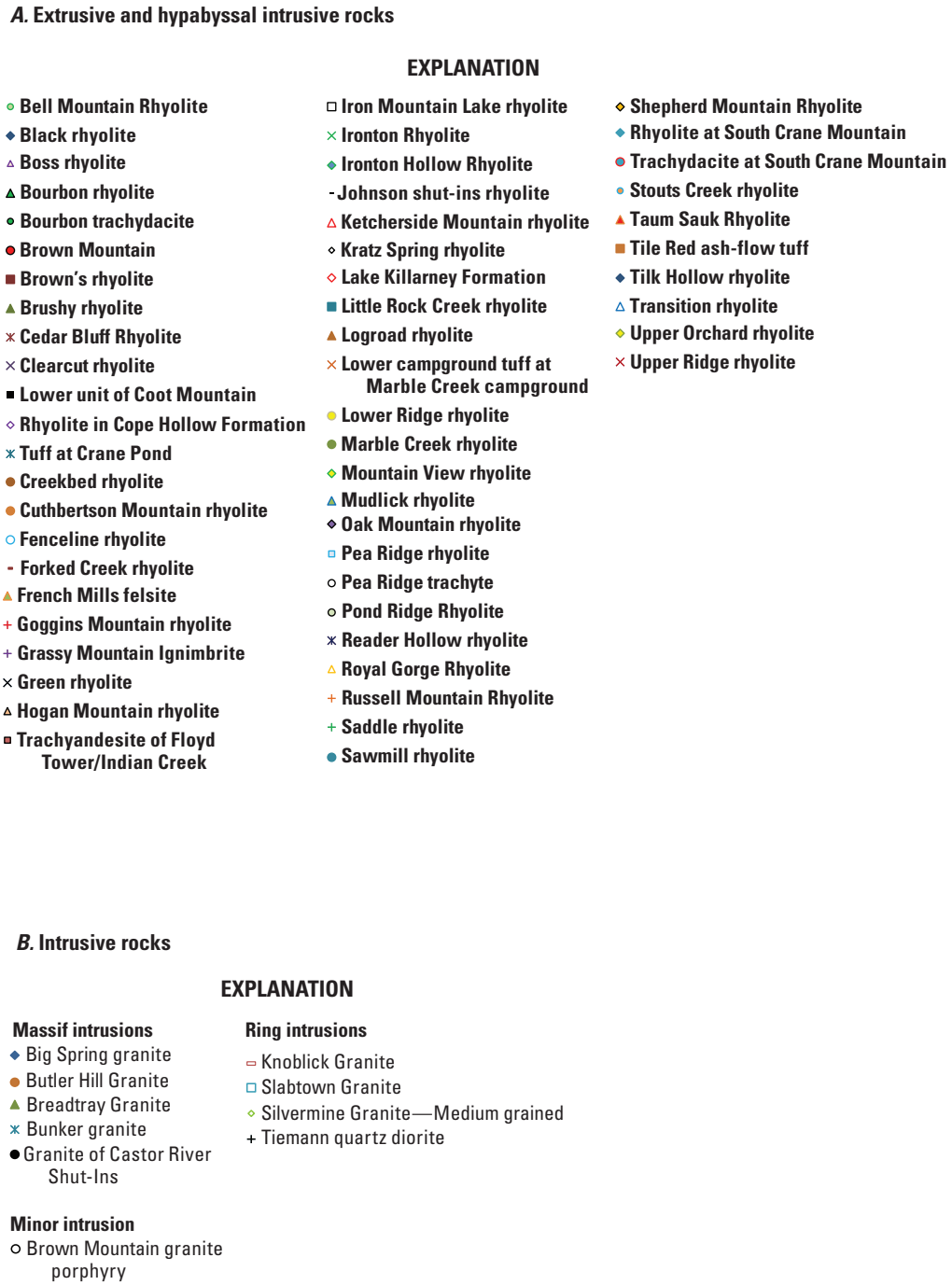

Figure 16. Variation diagrams showing that compositions of 1.48 to 1.45 billion year old igneous rocks in the St. Francois Mountains terrane, southeast Missouri are consistent with their petrogenesis in an intraplate, anorogenic setting. *A*, *B*, From Pearce and others (1984); applicable to rocks with >56 weight percent SiO_2; *C*, *D*, After Whalen and others (1987) showing the range of compositions for typical I (igneous source)-, S (sedimentary source)-, and A (anorogenic)-type igneous rocks with >60 weight percent SiO_2. *E*, *F*, Discriminant diagram after Grebennikov (2014) showing the range of compositions for magmas, with >67 weight percent SiO_2, associated with oceanic islands and continental rifts (field A1) and those associated with intracratonic settings (field A2).—Continued

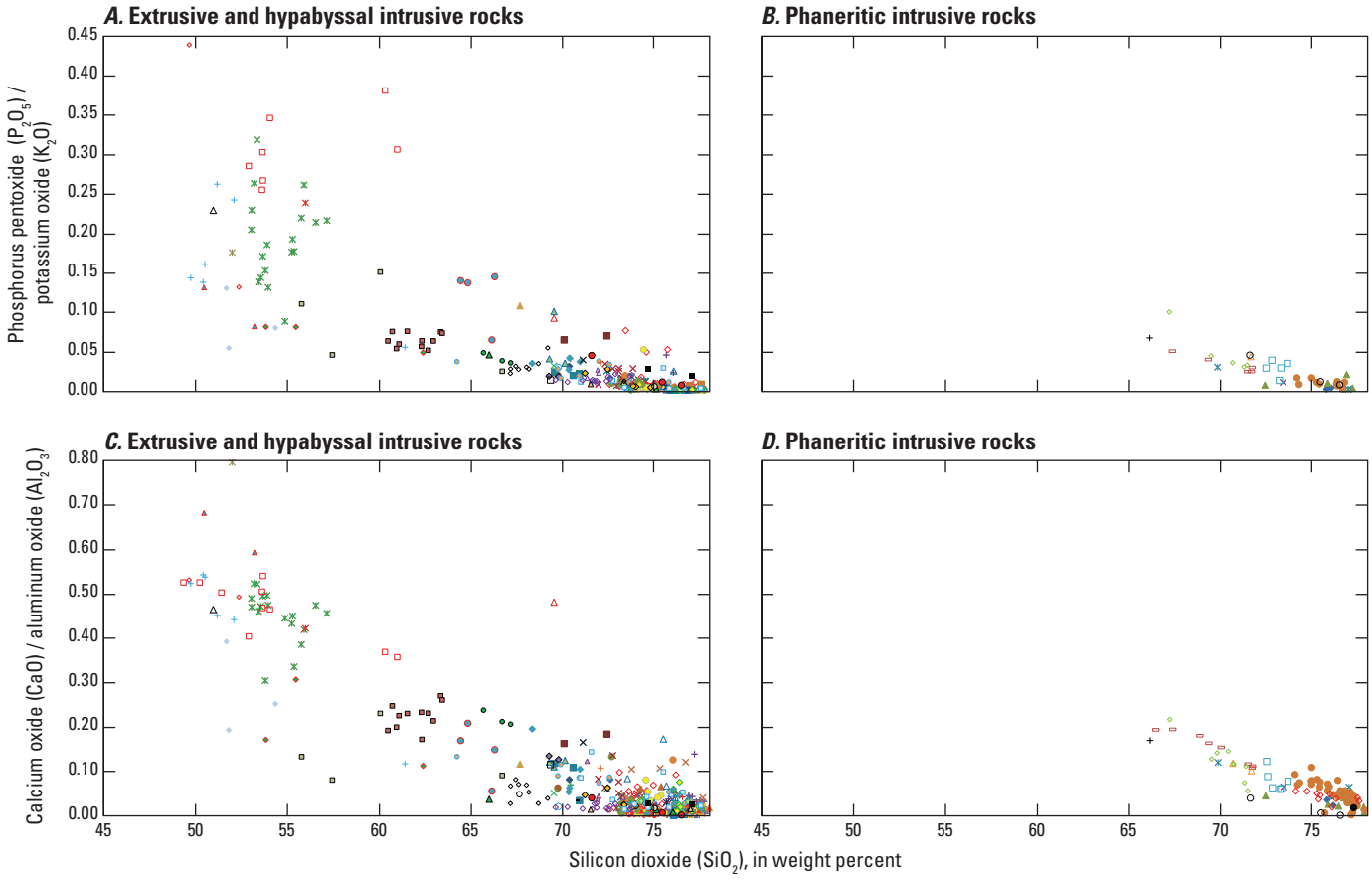

Figure 17. Variation diagrams showing that compositions of igneous rocks in the St. Francois Mountains terrane, southeast Missouri are consistent with primary magmas being variably contaminated by crustal assimilants. A, P_2O_5/K_2O relative to SiO_2 for extrusive and hypabyssal intrusive rocks. B, P_2O_5/K_2O relative to SiO_2 for phaneritic intrusive rocks. C, CaO/Al_2O_3 relative to SiO_2 for extrusive and hypabyssal intrusive rocks. D, CaO/Al_2O_3 relative to SiO_2. for phaneritic intrusive rocks. [P_2O_5, phosphorous pentoxide; K_2O, potassium oxide; SiO_2, silicon dioxide; CaO, calcium oxide; Al_2O_3, aluminum oxide]

A. **Extrusive and hypabyssal intrusive rocks**

EXPLANATION

- Bell Mountain Rhyolite
- Black rhyolite
- Boss diorite
- Boss andesite
- Boss rhyolite
- Boss trachyte
- Bourbon basalt
- Bourbon rhyolite
- Bourbon trachydacite
- Brown Mountain
- Brown's rhyolite
- Brushy rhyolite
- Trachyte host of Camels Hump IOA deposit
- Cedar Bluff Rhyolite
- Clearcut rhyolite
- Lower unit of Coot Mountain
- Basalt in Cope Hollow Formation
- Rhyolite in Cope Hollow Formation
- Tuff at Crane Pond
- Creekbed rhyolite
- Cuthbertson Mountain rhyolite
- Fenceline rhyolite
- Forked Creek rhyolite
- French Mills felsite
- Goggins Mountain rhyolite
- Grassy Mountain Ignimbrite
- Green rhyolite
- Hogan Mountain rhyolite
- Trachyandesite of Floyd Tower/Indian Creek
- Iron Mountain Lake rhyolite
- Ironton Rhyolite
- Ironton Hollow Rhyolite
- Johnson shut-ins rhyolite
- Ketcherside Mountain rhyolite
- Kratz Spring basalt
- Kratz Spring rhyolite
- Kratz Spring trachyte
- Lake Four Winds basalt
- Lake Killarney Formation
- Little Rock Creek rhyolite
- Logroad rhyolite
- Lower campground tuff at Marble Creek campground
- Lower Ridge rhyolite
- Marble Creek rhyolite
- Mountain View rhyolite
- Mudlick rhyolite
- Oak Mountain rhyolite
- Pea Ridge rhyolite
- Pea Ridge trachyte
- Pond Ridge Rhyolite
- Reader Hollow rhyolite
- Royal Gorge Rhyolite
- Russell Mountain Rhyolite
- Saddle rhyolite
- Sawmill rhyolite
- Shepherd Mountain Rhyolite
- Silver Mines basaltic andesite
- Rhyolite at South Crane Mountain
- Trachydacite at South Crane Mountain
- Stouts Creek rhyolite
- Taum Sauk Rhyolite
- Tile Red ash-flow tuff
- Tilk Hollow rhyolite
- Transition rhyolite
- Upper and Lower andesites of Marble Creek campground
- Upper Orchard rhyolite
- Upper Ridge rhyolite

B. **Intrusive rocks**

EXPLANATION

Massif intrusions

- Big Spring granite
- Buford Granite Porphyry
- Butler Hill Granite
- Breadtray Granite
- Bunker granite
- Granite of Castor River Shut-Ins

Minor intrusion

- Brown Mountain granite porphyry

Ring intrusions

- Knoblick Granite
- Slabtown Granite
- Silvermine Granite—Medium grained
- Silvermine Granite—Fine grained
- Stono Granite
- Tiemann quartz diorite

Figure 17. Variation diagrams showing that compositions of igneous rocks in the St. Francois Mountains terrane, southeast Missouri are consistent with primary magmas being variably contaminated by crustal assimilants. A, P_2O_5/K_2O relative to SiO_2 for extrusive and hypabyssal intrusive rocks. B, P_2O_5/K_2O relative to SiO_2 for phaneritic intrusive rocks. C, CaO/Al_2O_3 relative to SiO_2 for extrusive and hypabyssal intrusive rocks. D, CaO/Al_2O_3 relative to SiO_2. for phaneritic intrusive rocks. [P_2O_5, phosphorous pentoxide; K_2O, potassium oxide; SiO_2, silicon dioxide; CaO, calcium oxide; Al_2O_3, aluminum oxide]—Continued

Kratz Spring trachyte, Boss rhyolite, Bourbon rhyolite, Royal Gorge Rhyolite, Ironton Hollow-Cedar Bluff Rhyolite, and Boss granite) has REE dispersion values ≥0.4, which presumably reflects correspondingly less homogeneous magma reservoirs. Within-geologic unit chondrite-normalized REE patterns are essentially parallel, like those for the entire group of representative geologic unit REE patterns, which suggests that within-unit relative REE fractionation was minor. Consequently, evolution of magma reservoirs represented by each of the 1.48 to 1.45 Ga igneous rock units in the St. Francois Mountains terrane involved fractionation processes in which mineral assemblages and their mineral-melt REE distribution coefficients were also relatively invariant.

Among 1.48 to 1.45 Ga igneous rocks in the St. Francois Mountains terrane, chondrite-normalized REE abundances span nearly an entire order of magnitude. Average patterns for individual intrusions are parallel, although total REE content and extent of negative europium anomaly development vary. Consequently, relatively uniform processes controlled the petrogenesis of most of the 1.48 to 1.45 Ga igneous rocks, because relative REE fractionation, as would be depicted by relative pattern rotation, is absent. Absolute REE abundances among these rocks cannot be principally related to simple differentiation processes, fractionation or accumulation of constituent minerals, because total REE and SiO_2 contents do not vary systematically. Consequently, dilution processes associated with variable crustal contaminant assimilation and compositional variations within source melt regions are likely principally responsible for the range of REE abundances characteristic of the 1.48 to 1.45 Ga igneous rocks in the St. Francois Mountains terrane. REE pattern parallelism compatible with REE dilution relations among these rocks requires contaminants with relatively uniform compositions.

The 1.48 to 1.45 Ga Mesoproterozoic igneous rocks in the St. Francois Mountains terrane constitute a significant component of the broadly 1.4 Ga igneous rocks exposed throughout the United States (du Bray and others, 2018a). Globally, petrogenesis of ferroan granitoids involves (1) incompletely mixed mantle- and crust-derived magmas and (2) extensional tectonic settings (Dall'Agnol and others, 2012). Magmatism that yielded the 1.48 to 1.45 Ga large felsic igneous province of the St. Francois Mountains terrane was likewise in agreement with these parameters. The genesis of these igneous rocks was critically dependent on the tectonic setting prevailing during magmatism and the character of the juvenile continental crust domains in which they are hosted. The addition of hundreds of cubic kilometers of Paleoproterozoic juvenile sialic crust southward from the Laurentian core may have been a consequence of a long-lived outboard- (southward-) migrating arc system, coupled with formation and closure of successive backarc basins (Condie, 1982). Alternating subduction and slab roll-back processes, accompanied by addition of basaltic magma into the crust during lithospheric stretching and related decompression melting, may have been responsible for the continental growth manifested by 1.48 to 1.45 Ga igneous rocks across the continental United States in general, and in particular the St. Francois Mountains terrane (du Bray and others, 2018a). These processes are similar to extensional accretionary orogeny as described by Collins (2002). This type of continental augmentation is accompanied by complex extensional tectonics and reflects back-arc processes that provide the thermal energy required by bimodal intracratonic magmatism at variable distance inboard from continental margins (Karlstrom and others, 2001) and contrasts ignificantly with continental growth achieved by accretionary collage processes. Accordingly, 1.48 to 1.45 Ga igneous rocks in the St. Francois Mountains terrane reflect extension-driven continental augmentation and cratonization following supercontinent fragmentation.

Conclusions

The ages of Mesoproterozoic igneous rocks in the St. Francois Mountains terrane of southeast Missouri define older (1.48 to 1.45 billion years old), volumetrically dominant, and younger (1.33 to 1.28 billion years old) magmatic episodes. Magmatism associated with the older episode appears to have been fairly continuous and characterized by a fairly uniform epidocity during approximately 30 million years. Most significantly, intrusive and extrusive rocks associated with the older episode are coeval as are granitoid rocks that form the ring- and massif-type intrusions. A likely genetic association between ore formation at the Pea Ridge iron oxide-apatite ± rare earth element ore deposit and the older episode of Mesoproterozoic magmatism in southeast Missouri is borne out by the coincidence of their ages, between about 1.48 to 1.46 billion years ago and 1.48 to 1.45 billion years ago, respectively.

The 1.48 to 1.45 billion year old igneous rocks in the St. Francois Mountains terrane have somewhat diverse compositions that are diagnostic of the petrogenetic processes responsible for the associated magmatism. In particular, the occurrence of low-degree partial melting of preexisting, intermediate-composition granitoid rock at relatively elevated crustal pressures is in agreement with the abundant ferroan, peraluminous igneous rocks in the St. Francois Mountains terrane. Whether the resulting magmas are calc alkalic or alkali calcic depends on pressure and crustal depth prevailing during magma genesis. More advanced partial melting of crustally derived, intermediate-composition granitoid rocks at lower pressure may have been responsible for the significantly less voluminous, transitionally magnesian to magnesian and peraluminous igneous rocks in this region. Extensive differentiation of tholeiitic basalt may have produced volumetrically less important ferroan but metaluminous magmas in the St. Francois Mountains terrane. The wide-ranging alkalinity among these ferroan but metaluminous rocks may reflect the balance between clinopyroxene relative to plagioclase fractionation, with the more alkalic rocks representing magmas affected by significant clinopyroxene fractionation, at

higher pressure, and the more calcic rocks reflecting relatively greater plagioclase fractionation, at lower pressure conditions. A combination of mantle-derived mafic inputs and more evolved contributions derived by partial melting of juvenile crustal protoliths are likely responsible for the diversity of compositions characteristic of 1.48 to 1.45 billion year old igneous rocks in the St. Francois Mountains terrane. As such, the petrogenesis of these rocks requires multiple, distinct source inputs. Available data are consistent with crustal melting events in an extensional, intracratonic setting that accompanied mantle upwelling and emplacement of tholeiitic basaltic magma at or near the base of the crust. Primary mafic mantle-derived magmas assimilated crustal-derived partial melts. Crystal fractionation operative in mid-crustal magma chambers further modified magma compositions, resulting in significant major and trace element compositional diversity. The resulting, variably mingled and mixed silicate liquids formed variably homogenized storage reservoirs that continued polybaric evolution in reservoirs lodged at various depths in the crust.

References Cited

Aleinikoff, J.N., 2021, SHRIMP U-Pb geochronologic data for zircon and titanite from Mesoproterozoic rocks of the St. Francois Mountains terrane, southeast Missouri, U.S.A.: U.S. Geological Survey data release, https://doi.org/10.5066/P95Q3QC4.

Aleinikoff, J.N., Selby, D., Slack, J.F., Day, W.C., Pillers, R.M., Cosca, M.A., Seeger, C.M., Fanning, C.M., and Samson, I.M., 2016, U-Pb, Re-Os, and Ar/Ar geochronology of rare earth element (REE)-rich breccia pipes and associated host rocks from the Mesoproterozoic Pea Ridge Fe-REE-Au deposit, St. Francois Mountains, Missouri: Economic Geology, v. 111, p. 1883–1914.

Aleinikoff, J.N., Wintsch, R.P., Fanning, C.M., and Dorais, M.J., 2002, U-Pb geochronology of zircon and polygenetic titanite from the Glastonbury Complex, Connecticut, USA: An integrated SEM, EPMA, TIMS and SHRIMP study: Chemical Geology, v. 188, p. 125–147.

Aleinikoff, J.N., Wintsch, R.P., Tollo, R.P., Unruh, D.M., Fanning, C.M., and Schmitz, M.D., 2007, Ages and origin of the Killingworth complex and related rocks, south-central Connecticut: Implications for the tectonic evolution of southern New England: American Journal of Science (Rodgers volume), v. 307, p. 63–118.

Anders, E., and Ebihara, M., 1982, Solar-system abundances of the elements: Geochimica et Cosmochimica Acta, v. 46, p. 2362–2380.

Anderson, J.L., 1983, Proterozoic anorogenic granite plutonism of North America *in* Medaris, L.G., Jr., Byers, C.W., Mickelson, D.M., and Shanks, W.C., eds., Geological Society of America Memoir 161, p. 133–154.

Anderson, J.L., and Bender, E.E., 1989, Nature and origin of Proterozoic A-type granitic magmatism in the southwestern United States of America: Lithos, v. 23, p. 19–52.

Anderson, R.E., 1962, Igneous petrology of the Taum Sauk area, Missouri: St. Louis, Washington University, Ph.D. dissertation, 100 p.

Ayuso, R.A., Slack, J.F., Day, W.C., and McCafferty, A.E., 2016, Geochemistry, Nd-Pb isotopes, and Pb-Pb ages of the Mesoproterozoic Pea Ridge iron oxide-apatite–rare earth element deposit, southeast Missouri: Economic Geology, v. 111, p. 1935–1962.

Baker, J., Peate, D., Waight, T., and Meyzen, C., 2004, Pb isotopic analysis of standards and samples using a ^{207}Pb–^{204}Pb double spike and thallium to correct for mass bias with a double-focusing MC-ICP-MS: Chemical Geology, v. 211, p. 275–303.

Bateman, P.C., 1992, Plutonism in the central part of the Sierra Nevada batholith, California: U.S. Geological Survey Professional Paper 1483, 186 p.

Berry, A.W., Jr., 1970, Precambrian volcanic rocks associated with the Taum Sauk caldera, St. Francois Mountains, Missouri: Lawrence, University of Kansas, Ph.D. dissertation, 146 p.

Bickford, M.E., and Mose, D.G., 1975, Geochronology of Precambrian rocks in the St. Francois Mountains, southeast Missouri: Geological Society of America Special Paper 165, 48 p.

Bickford, M.E., Sides, J.R., and Cullers, R.L., 1981, Chemical evolution of magmas in the Proterozoic terrane of the St. Francois Mountains southeastern Missouri—Field, petrographic, and major element data: Journal of Geophysical Research, v. 86, p. 10365–10386.

Bickford, M.E., Van Schmus, W.R., Karlstrom, K.E., Mueller, P.A., and Kamenov, G.D., 2015, Mesoproterozoic-trans-Laurentian magmatism—A synthesis of continent-wide age distributions, new SIMS U–Pb ages, zircon saturation temperatures, and Hf and Nd isotopic compositions: Precambrian Research, v. 265, p. 286–312.

Black, L.P., Kamo, S.L., Allen, C.M., Davis, D.W., Aleinikoff, J.N., Valley, J.W., Mundil, R., Campbell, I.H., Korsuch, R.J., Williams, I.S., and Foudoulis, C., 2004, Improved $^{206}Pb/^{238}U$ microprobe geochronology by the monitoring of a trace-element-related matrix effect; SHRIMP, ID–TIMS, ELA–ICP–MS and oxygen isotope documentation for a series of zircon standards: Chemical Geology, v. 205, p. 115–140.

Bowring, J.F., McLean, N.M., Bowring, S.A., 2011, Engineering cyber infrastructure for U-Pb geochronology: Tripoli and U-Pb_Redux: Geochemistry, Geophysics, Geosystems, v. 12, no. 6.

Brown, M.V., 1988, Geologic map of the exposed Precambrian rocks, Des Arc NE quadrangle, Iron and Madison Counties, southeast Missouri: U.S. Geological Survey Miscellaneous Field Studies Map MF-2032, scale 1:24,000.

Christiansen, E.H., and McCurry, M., 2008, Contrasting origins of Cenozoic silicic volcanic rocks from the western Cordillera of the United States: Bulletin of Volcanology, v. 70, p. 251–267.

Coble, M.A., Vazquez, J., Barth, A.P., Wooden, J., Burns, D., Kylander-Clark, A., Jackson, S., and Vennari, C.E., 2018, Trace element characterization of MAD-559 zircon reference material for ion microprobe analysis: Geostandards and Geoanalytical Research, v. 42, no. 4, p. 481–497, accessed December 2017, at https://doi.org/10.1111/ggr.12238.

Collins, W.J., 2002, Nature of extensional accretionary orogens: Tectonics, v. 21, p. 6-1–6-12.

Condie, K.C., 1982, Plate tectonics model for Proterozoic continental accretion in the southwestern United States: Geology v. 10, p. 37–42.

Cousens, B.L., Prytulak, Julie, Henry, C.D., Alcazar, Al, and Brownrigg, Tim, 2008, Geology, geochronology, and geochemistry of the Miocene-Pliocene ancestral Cascades arc, northern Sierra Nevada, California and Nevada—The roles of the upper mantle, subducting slab, and the Sierra Nevada lithosphere: Geosphere, v. 4, p. 814–828.

Cullers, R.L., Koch, R., and Bickford, M.E., 1981, Chemical evolution of magmas in the Proterozoic terrane of the St. Francois Mountains, southeastern Missouri 2: Trace element data: Journal of Geophysical Research, v. 86, no. B11, p. 10388–10401.

Dall'Agnol, R., Frost, C.D., and Rämö, O.T., 2012, IGCP Project 510 "A-type granites and related rocks through time"—Project vita, results, and contribution to granite research, *in* Dall'Agnol, R., Frost, C.D., and Rämö, O.T., eds., A-type granites and related rocks through time: Lithos, v. 151, p. 1–16.

Davis, W.J., Pestaj, T., Rayner, N., and McNicoll, V., 2018, Long-term reproducibility of $^{207}Pb/^{206}Pb$ age at the GSC SHRIMP lab based on the GSC Archean reference zircon 1242: 9th International Shrimp Workshop, Korea Basic Science Institute. p. 107.

Day, W.C., Aleinikoff, J.N., du Bray, E.A., and Ayuso, R.A., 2017, Constraints on ages of magmatism and iron oxide-apatite (IOA) and iron oxide-copper-gold (IOCG) mineral deposit formation in the Mesoproterozoic St. Francois Mountains Terrane of southeast Missouri, USA: 14th Society of Geology Applied to Ore Deposits Biennial Meeting, Quebec City, Canada, August 20–23, 2017, p. 854–858.

Day, W.C., Slack, J.F., Ayuso, R.A., and Seeger, C.M., 2016, Regional geologic and petrologic framework for iron oxide ± apatite ± rare earth element and iron oxide copper-gold deposits of the Mesoproterozoic St. Francois Mountains terrane, southeast Missouri, USA: Economic Geology, v. 111, p. 1825–1858.

du Bray, E.A., Day, W.C., and Meighan, C.J., 2018b, Compilation of new and previously published geochemical and modal data for Mesoproterozoic igneous rocks of the St. Francois Mountains, southeast Missouri: U.S. Geological Survey Data Series 1080, 10 p., accessed April 2018, at https://doi.org/10.3133/ds1080.

du Bray, E.A., Holm-Denoma, C.S., San Juan, C.A., Lund, Karen, Premo, W.R., and DeWitt, Ed, 2015, Geochemical, modal, and geochronologic data for 1.4 Ga A-type granitoid intrusions of the conterminous United States: U.S. Geological Survey Data Series 942, 19 p., accessed January 2018, at http://dx.doi.org/10.3133/ds942.

du Bray, E.A., Holm-Denoma, C.S., Lund, Karen, and Premo, W.R., 2018a, Review of the geochemistry and metallogeny of approximately 1.4 Ga granitoid intrusions of the conterminous United States: U.S. Geological Survey Scientific Investigations Report 2017–5111, 34 p., accessed March 2018, at https://doi.org/sir20175111.

du Bray, E.A., and John, D.A., 2011, Petrologic, tectonic, and metallogenic evolution of the Ancestral Cascades magmatic arc, Washington, Oregon, and northern California: Geosphere, v. 7, no. 5, p. 1102–1133.

England, P.C., and Katz, R.F., 2010, Melting above the anhydrous solidus controls the location of volcanic arcs: Nature, v. 467, p. 700–703.

Ewart, A., 1982, The mineralogy and petrology of Tertiary–Recent orogenic volcanic rocks with special reference to the andesitic-basaltic compositional range, *in* Thorpe, R.S., ed., Andesites: New York, John Wiley and Sons, p. 25–87.

Farmer, G.L., Glazner, A.F., and Manley, C.R., 2002, Did lithospheric delamination trigger late Cenozoic potassic volcanism in the southern Sierra Nevada, California?: Geological Society of America Bulletin, v. 114, no. 6, p. 754–768.

Frost, B.R., and Frost, C.D., 2008, A geochemical classification of feldspathic igneous rocks: Journal of Petrology, v. 49, no. 11, p. 1955–1969.

Frost, C.D., Bell, J.M., Frost, B.R., Chamberlain, K.R., 2001, Crustal growth by magmatic underplating: Isotopic evidence from the northern Sherman batholith: Geology, v. 29, no. 6, p. 515–518.

Frost, C.D., and Frost, B.R., 2011, On ferroran (A-type) granitoids; their compositional variability and modes of origin: Journal of Petrology, v. 52, no. 11, p. 39–53.

Gerstenberger, H., Haase, G., 1997, A highly effective emitter substance for mass spectrometric Pb isotope ratio determinations: Chemical Geology, v. 136, no. 3–4, p. 309–312.

Gill, J., 1981, Orogenic andesites and plate tectonics: New York, Springer-Verlag, 390 p.

Gleason, J.D., Marikos, M.A., Barton, M.D., and Johnson, D.A., 2000, Neodymium isotopic study of rare earth element sources and mobility in hydrothermal Fe oxide (Fe-P-REE) systems: Geochimica et Cosmochimica Acta, v. 64, p. 1059–1068.

Granitto, M., du Bray, E.A., Day, W.C., Meighan, C.J., Slack, J.F., and Ayuso, R.A., 2018, Geochemical and modal data for Mesoproterozoic igneous rocks of the St. Francois Mountains, southeast Missouri: U.S. Geological Survey data release, https://doi.org/10.5066/F79W0DSN.

Grebennikov, A.V., 2014, A-type granites and related rocks—Petrogenesis and classification: Russian Geology and Geophysics, v. 55, no. 9, p. 1074–1086.

Green, T.H., 1982, Anatexis of mafic crust and high pressure crystallization of andesite, *in* Thorpe, R.S., ed., Andesites: New York, John Wiley and Sons, p. 465–487.

Guiness, E.A., Arvidson, R.E., Strebeck, J.W., Schultz, K.J., Davies, G.R., and Leff, C.E., 1982, Identification of a Precambrian rift through Missouri by digital image processing of geophysical and geological data: Journal of Geophysical Research, v. 87, no. B10, p. 8529–8545.

Hanson, G.N., 1980, Rare earth elements in petrogenetic studies of igneous systems: Annual Review of Earth and Planetary Sciences, v. 8, p. 371–406.

Harrison, R.W., Lowell, G.R., and Unruh, D.M., 2000, Geology, geochemistry, and age of Mesoproterozoic igneous rocks in the Eminence-Van Buren area: A major structural outlier of the St. Francois Mountains terrane, south-central Missouri [abs.]: Geologic Society of America Abstracts with Programs, v. 32, no. 3, p. A-14.

Harrison, R.W., Orndorff, R.C., and Weary, D.J., 2002, Geology of the Stegall Mountain 7.5-minute quadrangle, Shannon and Carter Counties, south-central Missouri: U.S. Geological Survey Geologic Investigations Series Map I-2767, scale 1:24,000.

Heaman, L.M., 2009, The application of U-Pb geochronology to mafic, ultramafic and alkaline rocks: An evaluation of three mineral standards: Chemical Geology, v. 261, no. 1–2, p. 43–52.

Hildenbrand, T.G., Griscom, A., Van Schmus, W.R., Stuart, W.D., 1996, Quantitative investigations of the Missouri gravity low: A possible expression of a large, Late Precambrian batholith intersecting the New Madrid seismic zone: Journal of Geophysical Research, v. 101, no. B10, p. 21921–21942.

Hildreth, Wes, 2007, Quaternary magmatism in the Cascades—Geologic perspectives: U.S. Geological Survey Professional Paper 1744, 125 p.

Hildreth, W., and Moorbath, S., 1988, Crustal contributions to arc magmatism in the Andes of central Chile: Contributions to Mineralogy and Petrology, v. 98, no. 4, p. 455–489.

Hoffman, P.F., 1989, Speculations on Laurentia's first gigayear (2.0 to 1.0 Ga): Geology, v. 17, no. 2, p. 135–138.

Ireland, T.R., 1995, Ion microprobe mass spectrometry: Techniques and applications in cosmochemistry, geochemistry, and geochronology, *in* Hyman, M., and Rowe, M., eds., Advances in analytical geochemistry, JAI Press, v. 2, p. 1–118.

Ireland, T.R., Williams, I.S., 2003, Considerations in zircon geochronology by SIMS, in: Zircon: Mineralogical Society of America Reviews in Mineralogy and Geochemistry, v. 53, no. 1, p. 215–241.

Irvine, T.N., and Baragar, W.R.A., 1971, A guide to the chemical classification of the common volcanic rocks: Canadian Journal of Earth Sciences, v. 8, no. 5, p. 523–548.

Jackson, S.E., 2008, Calibration strategies for elemental analysis by LA-ICP-MS chap. 11 *of* Laser ablation-ICP-MS in the earth sciences—Current practices and outstanding issues: Mineralogical Association of Canada, Short Course Series, v. 40 p. 169–188.

Jaffey, A.H., Flynn, K.F., Glendenin, L.E., Bentley, W.C., and Essling, A.M., 1971, Precision measurement of half-lives and specific activities of ^{235}U and ^{238}U: Physical Review C, v. 4, no. 5, p. 889–1906.

Jochum, K.P., Weis, U., Stoll, B., Kuzmin, D., Yang, Q., Raczek, I., Jacob, D.E., Stracke, A., Birbaum, K., Frick, D.A., Günther, D., and Enzweiler, J., 2011, Determination of reference values for NIST SRM 610—617 glasses following ISO guidelines: Geostandards and Geoanalytical Research, v. 35, no. 4, p. 397–429.

Karlstrom, K.E., Ahall, K.-I., Harlan, S.S., Williams, M.L., McLelland, J., and Geissman, J.W., 2001, Long-lived (1.8–1.0 Ga) convergent orogeny in southern Laurentia, its extensions to Australia and Baltica, and implications for refining Rodinia: Precambrian Research, v. 111, no. 1–4, p. 5–30.

Kennedy, A.K., Kamo, S.L., Nasdala, L., and Timms, N.E., 2010, Grenville skarn titanite: Potential reference material for SIMS U-Th-Pb analysis: Canadadian Mineralalogist, v. 48, no. 6, p. 1423–1443.

King, E.M., Trzaskus, A.P., and Valley, J.W., 2008, Oxygen isotope evidence for magmatic variability and multiple alteration events in the Proterozoic St. Francois Mountains, Missouri: Precambrian Research, v. 165, no. 1–2, p. 49–60.

Kisvarsanyi, E.B., 1972, Petrochemistry of a Precambrian igneous province, St. Francois Mountains, Missouri: Contribution to Precambrian Geology No. 4, Missouri Geological Survey and Water Resources Report of Investigations no. 51, 96 p.

Kisvarsanyi, E.B., 1980, Granitic ring complexes and hotspot activity in the St. Francois Mountains terrane, midcontinent region, United States: Geology, v. 8, no. 1, p. 43–47.

Kisvarsanyi, E.B., 1981, Geology of the Precambrian St. Francois Mountains terrane southeastern Missouri: Missouri Department of Natural Resources, Division of Geology and Land Survey, Report of Investigations no. 64, 58 p.

Kisvarsanyi, G., and Kisvarsanyi, E.B., 1990, Alkaline granite ring complexes and metallogeny in the Middle Proterozoic St. Francois terrane, southeastern Missouri, USA: Geological Association of Canada Special Paper 38, p. 433–446.

Kisvarsanyi, G., and Proctor, P.D., 1967, Trace element content of magnetites and hematites, southeast Missouri metallogenic province, U.S.A.: Economic Geology, v. 62, no. 4, p. 449–471.

Krogh, T., 1973, A low-contamination method for hydrothermal decomposition of zircon and extraction of U and Pb for isotopic age determinations: Geochemica et Cosmochemica Acta, v. 37, no. 3, p. 485–494.

Le Maitre, R.W., 1989, A classification of igneous rocks and glossary of terms: Oxford, United Kingdom, Blackwell Scientific, 193 p.

Loiselle, M.C., and Wones, D.R., 1979, Characteristics and origin of anorogenic granites: Geological Society of America Abstracts with Programs, v. 11, no. 7, p. 468.

Lowell, G.R., 1976, Petrography of Precambrian rocks in the Hawn State Park area, Ste. Genevieve County, Missouri, *in* Kisvarsanyi, E.B., ed., Studies in Precambrian geology with a guide to selected parts of the St. Francois Mountains, Missouri: Missouri Department of Natural Resources, Contribution to Precambrian Geology 6, Report of Investigations 61, p. 140–148.

Lowell, G.R., 1991, The Butler Hill caldera: A mid-Proterozoic ignimbrite-granite complex: Precambrian Research, v. 51, no. 1–4, p. 245–263.

Lowell, G.R., and Rämö, O.T., 1999, Petrology and geochemistry of the Shepherd Mountain gabbro—Implications for basalt genesis at 1.33 Ga in southeast Missouri [abs.]: Geological Society of America Abstracts with Programs, v. 31, no. 5, p. 32.

Ludwig, K.R., 1980, Calculation of uncertainties of U-Pb isotope data: Earth and Planetary Science Letters, v. 46, p. 212–220.

Ludwig, K.R., 2003, Isoplot/Ex version 3.00, A geochronological toolkit for Microsoft Excel: Berkeley Geochronology Center Special Publication, no. 4, 73 p.

Ludwig, K.R., 2009, Squid 2, version 2.50, A user's manual: Berkeley Geochronology Center, Special Publication, no. 5, 110 p.

Ludwig, K.R., 2012, Isoplot/Ex rev. 3.75—A geochronological toolkit for Microsoft Excel: Berkeley Geochronology Center, Special Publication, no. 5, 75 p.

Macdonald, Ray, Smith, R.L., and Thomas, J.E., 1992, Chemistry of the subalkalic silicic obsidians: U.S. Geological Survey Professional Paper 1523, 214 p.

Matthews, N.E., Vazquez, J.A., Calvert, A.T., 2015, Age of the Lava Creek supereruption and magma chamber assembly at Yellowstone based on $^{40}Ar/^{39}Ar$ and U-Pb dating of sanidine and zircon crystals: Geochemistry, Geophysics, Geosystems, v. 16, no. 8, p. 2508–2528.

Mattinson, J.M., 2005, Zircon U–Pb chemical abrasion ("CA-TIMS") method—Combined annealing and multi-step partial dissolution analysis for improved precision and accuracy of zircon ages: Chemical Geology, v. 220, no. 1–2, p. 47–66.

McLean, N.M., Bowring, J.F., Bowring, S.A., 2011, An algorithm for U-Pb isotope dilution data reduction and uncertainty propagation: Geochemistry, Geophysics, Geosystems, v. 12, no. 6, p. 913–940.

Menuge, J.F., Brewer, T.S., and Seeger, C.M., 2002, Petrogenesis of metaluminous A-type rhyolites from the St. Francois Mountains, Missouri and the Mesoproterozoic evolution of the southern Laurentian margin: Precambrian Research, v. 113, no. 3–4, p. 269–291.

Miyashiro, Akiho, 1974, Volcanic rock series in island arcs and active continental margins: American Journal of Science, v. 274, p. 321–355.

National Institute of Standards, 1992, Certificate of analysis: National Institutes of Standards, 2 p., available at http://67.199.38.241/ProdImages/612.pdf.

Neymark, L.A., Holm-Denoma, C.S., and Moscati, R.J., 2018, In situ LA-ICPMS U–Pb dating of cassiterite without a known-age matrix-matched reference material—Examples from worldwide tin deposits spanning the Proterozoic to the Tertiary: Chemical Geology, v. 483, p. 410–425.

Neymark, L.A., Holm-Denoma, C.S., Pietruszka, A.J., Aleinikoff, J.N., Fanning, C.M., Pillers, R.M., and Moscati, R.J., 2016, High spatial resolution U-Pb geochronology and Pb-isotope geochemistry of magnetite-apatite ore from the Pea Ridge iron oxide-apatite (IOA) deposit, Saint Francois Mountains, SE Missouri, USA: Economic Geology, v. 111, no. 8, p. 1915–1933.

Orndorff, R.C., Harrison, R.W., Weary, D.J., 1999, Geologic map of the Eminence quadrangle, Shannon County, Missouri: U.S. Geological Survey Geologic Investigations Map I-2653, scale 1:24,000.

Paces, J.B., and Miller, J.D., Jr., 1993, Precise U-Pb ages of Duluth Complex and related mafic intrusions, northeastern Minnesota; geochronological insights to physical, petrogenetic, paleomagnetic, and tectonomagnetic processes associated with the 1.1 Ga Midcontinent Rift System: Journal of Geophysical Research B, Solid Earth and Planets, v. 98, no. B8, p. 13997–14013.

Patiño Douce, A.E., 1997, Generation of metaluminous A-type granites by low-pressure melting of calc-alkaline granitoids: Geology, v. 25, p. 743–746.

Paton, C., Hellstrom, J., Paul, B., Woodhead, J., and Hergt, J., 2011, Iolite—Freeware for the visualisation and processing of mass spectrometric data: Journal of Analytical Atomic Spectrometry, v. 26, p. 2508–2518.

Pearce, J.A., Harris, N.B.W., and Tindle, A.G., 1984, Trace element discrimination diagrams for the tectonic interpretation of granitic rocks: Journal of Petrology, v. 25, no. 4, p. 956–983.

Pippin, C.G., 1996, Geology and geochemistry of the Cope Hollow formation and the western St. Francois Mountains, southeastern Missouri: DeKalb, Northern Illinois University, M.S. thesis, 182 p.

Pratt, W.P., Anderson, R.E., Berry, A.W., Jr., Bickford, M.E., Kisvarsanyi, E.B., and Sides, J.R., 1979, Geologic map of exposed Precambrian rocks, Rolla 1° x 2° quadrangle, Missouri: U.S. Geological Survey Miscellaneous Investigations Series Map I-1161, scale 1:250,000.

Rämö, O.T., Boyd, W.W., Vaasjok, M., Cameron, R.L., and Ryckman, D.A., 1994, 1.3 Ga mafic magmatism of the St. Francois Mountains of SE Missouri: Implications for mantle composition beneath mid-continental USA: Mineralogical Magazine, v. 58A, p. 754–755.

Rogers, J.J.W., and Santosh, M., 2002, Configuration of Columbia, a Mesoproterozoic supercontinent: Gondwana Research v. 5, no. 1, p. 5–22.

Rutherford, M.J., and Hill, P.M., 1993, Magma ascent rates from amphibole breakdown: An experimental study applied to the 1980–1986 Mount St. Helens eruption: Journal of Geophysical Research, v. 98, no. B11, p. 19667–19685.

Scharer, U., 2002, The effect of initial ^{230}Th disequilibrium on young U-Pb ages: The Makalu case, Himalaya: Earth and Planetary Science Letters, v. 67, p. 191–204.

Schmitt, A.K., and Zack, T., 2012, High-sensitivity U–Pb rutile dating by secondary ion mass spectrometry (SIMS) with an O_{2^+} primary beam: Chemical Geology, v. 332–333, p. 65–73.

Shand, S.J., 1951, Eruptive rocks: New York, John Wiley, 488 p.

Sides, J.R., 1981, Geology of the Ketcherside Mountain area, southeastern Missouri, and the source of the Grassy Mountain Ignimbrite: Geological Society of America Bulletin, v. 92, no. 1, p. 686–693.

Sides, J.R., Bickford, M.E., Shuster, R.D., and Nusbaum, R.L., 1981, Calderas in the Precambrian terrane of the St. Francois Mountains, southeastern Missouri: Journal of Geophysical Research, v. 86, no. B11, p. 10349–10364.

Skjerlie, K.P., and Johnston, A.D., 1993, Fluid-absent melting behavior of an F-rich tonalitic gneiss at mid-crustal pressures—Implications for the generation of anorogenic granites: Journal of Petrology, v. 34, no. 4, p. 785–815.

Slack, J.F., Corriveau, Louise, and Hitzman, M.W., 2016, A special issue devoted to Proterozoic iron oxide-apatite (±REE) and iron oxide copper-gold and affiliated deposits of southeast Missouri, USA, and the Great Bear magmatic zone, Northwest Territories, Canada—Preface: Economic Geology, v. 111, no. 8, p. 1803–1814.

Stacey, J.S., and Kramers, J.D., 1975, Approximation of terrestrial Pb isotope composition by a two-stage model: Earth and Planetary Science Letters, v. 26, no. 2, p. 207–222.

Stern, R.A., and Amelin, Y., 2003, Assessment of errors in SIMS zircon U-Pb geochronology using a natural zircon standard and NIST 610 glass: Chemical Geology, v. 197, no. 1–4, p. 111–142.

Stern, R.A., Bodorkos, S., Kamo, S.L., Hickman, A.H., and Corfu, F., 2009, Measurement of SIMS instrumental mass fractionation of Pb isotopes during zircon dating: Geostandards and Geoanalytical Research, v. 33, no. 2, p. 145–168.

Stoeser, D.B., and Elliott, J.E., 1980, Postorogenic peralkaline and calc-alkaline granites and associated mineralization of the Arabian Shield, Kingdom of Saudi Arabia, *in* Cooray, P.G., and Tahoun, S.A., eds., Evolution and mineralization of the Arabian-Nubian Shield: Jiddah, King Abdulaziz University, Oxford-New York, Pergamon Press, Institute of Applied Geology Bulletin 3, v. 4, p. 1–23.

Streckeisen, Albert, 1976, To each plutonic rock its proper name: Earth-Science Reviews, v. 12, no. 1, p. 1–33.

Sun, S.-S., and McDonough, W.F., 1989, Chemical and isotopic systematics of oceanic basalts; implications for mantle composition and processes, *in* Saunders, A.D., and Norry, M.J., eds., Magmatism in the ocean basins: Geological Society of London Special Publication 42, p. 313–345.

Sylvester, P.J., 1984, Geology, petrology, and tectonic setting of the mafic rocks of the 1480 Ma old Granite/Rhyolite terrane of Missouri, USA: St. Louis, Washington University, Ph.D. thesis, 588 p.

Sylvester, P.J., 2008, Matrix effects in laser ablation-ICP-MS, chap. 5 *of* Laser ablation-ICP-MS in the earth sciences—Current practices and outstanding issues: Mineralogical Association of Canada, Short Course Series, v. 40, no. 4, p. 67–78.

Tera, F., and Wasserburg, G.J., 1972, U-Th-Pb systematics in three Apollo 14 basalts and the problem of initial Pb in lunar rocks: Earth and Planetary Science Letters, v. 14, no. 3, p. 281–304.

Thomas, W.A., Tucker, R.D., Astini, R.A., and Denison, R.E., 2012, Ages of pre-rift basement and synrift rocks along the conjugate rift and transform margins of the Argentine Precordillera and Laurentia: Geosphere, v. 8, no. 6, p. 1366–1383.

Tolman, C., and Robertson, F., 1969, Exposed Precambrian rocks in southeast Missouri: Missouri Geological Survey and Water Resources, Contribution to Precambrian Geology 1, Report of Investigations 44, 68 p.

Turekian, K.K., and Wedepohl, K.H., 1961, Distribution of the elements in some major units of the Earth's crust: Geological Society of America Bulletin, v. 72, no. 2, p. 175–192.

Van Schmus, W.R., Bickford, M.E., and Turek, A., 1996, Proterozoic geology of the east-central Midcontinent basement: Geological Society of America Special Paper 308, p. 7–31.

Walker, J.A., Pippin, C.G., Cameron, B.I., and Patino, L., 2002, Tectonic insights provided by Mesoproterozoic mafic rocks of the St. Francois Mountains, southeastern Missouri: Precambrian Research, v. 117, p. 251–268.

Watson, E.B., 1979, Zircon saturation in felsic liquids; experimental results and applications to trace element geochemistry: Contributions to Mineralogy and Petrology, v. 70, no. 11, p. 407–419.

Watts, K.E. and Mercer, C.N., 2020, Zircon-hosted melt inclusion record of silicic magmatism in the Mesoproterozoic St. Francois Mountains terrane, Missouri: Origin of the Pea Ridge iron oxide-apatite-rare earth element deposit and implications for regional crustal pathways of mineralization: Geochimica et Cosmochimica Acta, v. 272, p. 54–77.

Wenner, D.B., and Taylor H.P., Jr., 1976, Oxygen and hydrogen isotope studies of a Precambrian granite-rhyolite terrane, St. Francois Mountains, southeastern Missouri: Geological Society of America Bulletin, v. 87, p. 1587–1598.

Wetherill, G.W., 1956, Discordant uranium-lead ages: Transactions American Geophysical Union, v. 37, p. 320–326.

Whalen, J.B., Currie, K.L., and Chappell, B.W., 1987, A-type granites: Geochemical characteristics, discrimination and petrogenesis: Contributions to Mineralogy and Petrology, v. 95, no. 4, p. 407–419.

White, L.T., and Ireland, T.R., 2012, High-uranium matrix effect in zircon and its implications for SHRIMP U–Pb age determinations: Chemical Geology, v. 306–307, no. 4, p. 78–91.

Wiedenbeck, M., Alle, P., Corfu, F., Griffin, W.L., Meier, M., Oberli, F., Von Quadt, A., Roddick, J.C., and Spiegel, W., 1995, Three natural zircon standards for U-Th-Pb, Lu-Hf, trace element and REE analyses: Geostandards Newsletter, v. 19, no., p. 1–23.

Williams, I.S., 1998, U-Th-Pb geochronology by ion microprobe: Reviews in Economic Geology, v. 7, no. 3, p. 1–35.

Williams, I.S., and Hergt, J.M., 2000, U–Pb dating of Tasmanian dolerites: a cautionary tale of SHRIMP analysis of high-U zircon, *in* Woodhead, J.D., Hergt, J.M., and Noble, W.P., eds., Beyond 2000: New Frontiers in Isotope Geoscience: Lorne, Abstract Proceedings, p. 185–188.

Wood, D.A., Joron, J.L., and Treuil, M., 1979, A re-appraisal of the use of trace elements to classify and discriminate between magma series erupted in different tectonic settings: Earth and Planetary Science Letters, v. 45, no. 2, p. 326–336.

Publishing support provided by the Science Publishing Network, Denver Publishing Service Center

For more information concerning the research in this report, contact the
Center Director, USGS Geology, Geophysics, and Geochemistry Science Center
Box 25046, Mail Stop 973
Denver, CO 80225
(303) 236-1800
Or visit Geology, Geophysics, and Geochemistry Science Center website at https://www.usgs.gov/centers/gggsc

ISSN 2330-7102 (online)
https://doi.org/10.3133/pp1866